Numerical Simulation of a Premixed Hydrogen Gas Turbine Combustor

Master Thesis

L.W. Doodeman

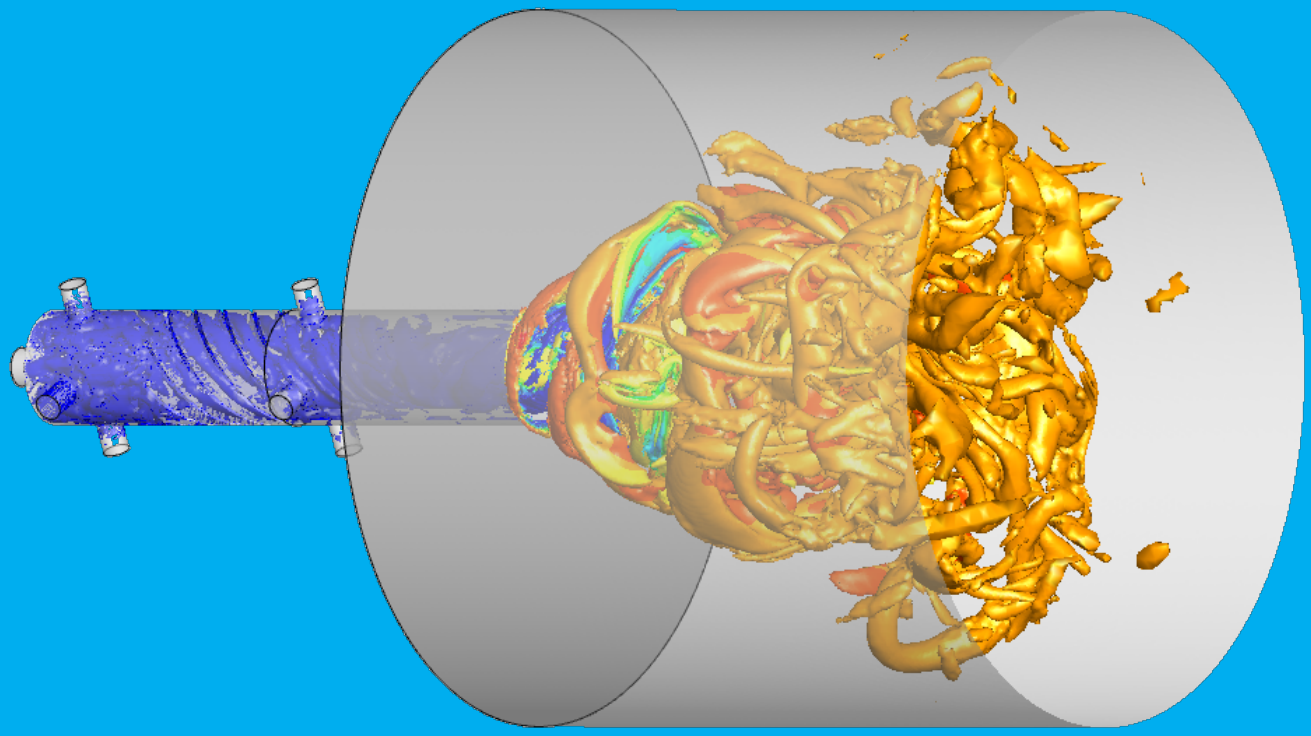

Master of Science
Delft University of Technology
Faculty of Aerospace Engineering
Flight Performance and Propulsion

TU Delft

Numerical Simulation of a Premixed Hydrogen Gas Turbine Combustor

Master Thesis

by

L.W. Doodeman

to obtain the degree of Master of Science
at the Delft University of Technology,
to be defended publicly on Tuesday November 1, 2022 at 14:00.

Student number:	4580915	
Project duration:	November 8th, 2021 - November 1st, 2022	
Thesis Committee:	Dr. ir. I. Langella	TU Delft, supervisor
	Prof. Dr. ir. A. Gangoli Rao	TU Delft, chairman
	Prof. Dr. ir. S. Hickel	TU Delft

This thesis is confidential and cannot be made public until November 1, 2025.

An electronic version of this thesis is available at http://repository.tudelft.nl/.
(24,579 words)

TU Delft

Preface

This master thesis marks the completion of the master Flight Performance and Propulsion. The thesis gave me an opportunity to apply the knowledge I have gained throughout my academic career while also learning a lot more. I would like to express my sincere gratitude to Gioele Ferrante for his daily assistance, whose collaboration I really enjoyed. In addition, I would like to thank my supervisors, Dr. Arvind Gangoli Rao and Dr. Ivan Langella, for providing valuable feedback and inspiration on the project.

L.W. Doodeman
Delft, October 18, 2022

Abstract

Large eddy simulation paradigm is employed to analyse the internal flow field of a lean premixed swirl-stabilized combustor with axial air injection at both non-reacting and reacting conditions for a methane and a methane-hydrogen fuel mixture. The Thickened Flame combustion model with the kinetic mechanism GRI 3.0 and the detailed chemical kinetics solver SAGE available in ConvergeCFD is employed to simulate the flow. An adaptive mesh strategy is used to maximise the mesh resolution in the flame and boundary layer regions. The numerical results are first validated against in-house experimental velocity measurements obtained via particle image velocimetry, and then leveraged to provide further insights on the flow behaviour. Significant reductions in CO_2, CO and NO_x emissions are observed when changing the fuel to the CH_4/H_2 mixture. From a POD analysis is observed that a Precessing Vortex Core is present in both the reacting and non-reacting conditions. Flashback and severe local extinctions are not observed during the simulated time.

Contents

List of Figures

List of Tables

Nomenclature

Greek Symbols

Δ	Subgrid grid size
δ_{ij}	Kronecker delta
δ_l^0	flame thickness
$\dot{\omega}$	Laminar reaction rate
ϵ	Dissipation term
η	Combustion efficiency
η_K	Kolmogorov length scale
$\Gamma(a)$	Gamma function PDF
κ	Von Karman constant
λ	Thermal conductivity
μ_t	Friction velocity
ν	Kinematic viscosity
ν_t	Kinematic Eddy Viscosity
ρ	Density
ρ_u	Unburned density
τ_{ij}^{r}	Anisotropic portion of SGS stress tensor
τ_{ji}	Viscous stress or SGS stress tensor
$\tilde{\tau}_{ij}$	Filtered SGS stress tensor
φ	Equivalence ratio
∇	Prescribed length scale
τ	Turbulent kinetic energy

Non-dimensional Parameters

Da	Damköhler number
Ka	Karlovitz number
Le	Lewis number
Re	Reynolds number

Sc Schmidt number

Sw Swirl number

Roman Symbols

s_t Turbulent flame speed

$\bar{c}_{p,m}$ Molar constant-pressure specific heat of species m

$\bar{h}_m$ Molar specific enthalpy

$\bar{S}_{ij}$ Deformation tensor of the resolved field

$\bar{W}$ Mean reaction rate

$[X_j]$ Molar concentration of species J

$\overline{\mathscr{D}}_\sigma$ Differential operator sigma model

$\widetilde{L}_{ii}$ Trace of the Leonard stress

$\widetilde{L}_{ij}$ Leonard stress

a PDF model parameter

A_s Eigenvalues correlation matrix

B Beta function PDF

b PDF model parameter

c Progress variable

C_s Correlation matrix POD analysis

C_s Smagorinsky model constant

D Molecular diffusion rate

D_t Turbulent diffusivity

E_A Activation energy

e_0 Total energy

G Field variable used in G-equation

G_x Axial flux of the axial momentum

G_θ Axial flux of the angular momentum

G_{ij} Consistent Dynamic Structure matrix

H Enthalpy

k Reaction rate coefficient

k_{fi} Forward rate coefficient SAGE

$K_{f,j}$	Rate of reaction
k_{ri}	Reverse rate coefficient SAGE
k_{res}	Resolved TKE
L	Integral turbulent length scale
m	Total number of LES time steps
P	Multi-dimensional sub-grid PDF
P_{atm}	Atmospheric pressure
q_i	Rate-of-progress variable SAGE
q_j	Heat flux
R	Gas constant
r	Reaction rate
r_0	Outer radius of the annulus
R_h	Axial air injection tube radius
R_n	Mixing tube radius
S	Entropy
S_L	Laminar flame speed
S^*_{ij}	Viscous strain rate
s^0_l	Laminar flame speed
T	Temperature
t	Time
U	Axial velocity component
u'	Turbulent velocity
v_k	Subgrid turbulent viscosity
x	x-coordinate
y^+	Y plus values
Y_k	Mass fraction of species k
Z	Mixture fraction
k_{sgs}	Subgrid kinetic energy

1 Introduction

Hydrogen represents an attractive alternative fuel to tackle the problem of carbon-based emissions reduction in aeronautics. According to various studies, e.g.: [1], hydrogen combustion is among the most promising approaches for powering long-distance flight due to its high energy density, minimal carbon emissions and the possibility of producing it from water electrolysis through renewable energy. Nevertheless, its high flame temperature might cause substantial nitric oxides (NO_x) formation. This can be effectively decreased by using premixed lean-burn technology, taking advantage of hydrogen's wide flammability range to stabilize the flame under very lean conditions [2]. However, the risk of flashback due to the high flame speed and the possibility of instabilities caused by hydrogen's high diffusivity, pose design difficulties [3].

The present work aims to contribute to the development of a lean premixed hydrogen combustor for aeronautical applications with minimal NO_x and carbon emissions. The laboratory-scale swirl stabilised combustor at the TU Delft is numerically simulated. The combustor is composed of an axial swirler issuing into a mixing tube, where the fuel is injected and mixes with air before entering the combustion chamber. To prevent flashback, the stream-wise momentum component is increased by means of axial air injection [4], with the intended effect of achieving control on the stream-wise position of the flame stabilization point. In-house particle image velocimetry (PIV) velocity measurements of both reacting and non-reacting flow with a CH_4/air mixture are available.

Large Eddy Simulation (LES) is used for the numerical analysis of the combustor. In the LES approach, the reacting Navier-Stokes equations are filtered so that the large turbulent scales are resolved, while the effects of the smaller unresolved, sub-grid scale (SGS) motions, are modelled [5]. The capability of LES to accurately predict unsteady reacting flow physical features with an affordable computational cost makes it a suitable tool to analyse the complex swirled and recirculating turbulent flow field inside the combustor. Many combustion models have been proposed in literature to mimic the interaction between turbulence, diffusion and reactions at the subgrid scale, and the reader can find a review in [6]. In the present study, the combustor operates in a turbulent partially premixed regime. Therefore, an accurate prediction of the turbulent mixing processes between fuel and oxydizer is crucial, in order to identify the formation of inhomogeneous mixture spots in the mixing tube. The unclosed turbulence-diffusion-reaction interaction is modelled using the Thickened Flame Model (TFM), which predicts mixing in under resolved flame fronts by including numerical diffusion which artificially thickens the flame [7]. The TFM model is used together with detailed chemistry to properly account for the turbulence-flame interaction in presence of differential diffusion effects, that can arise due to the presence of hydrogen in the fuel stream. In addition, an adaptive mesh refinement strategy based on the flame location and velocity gradient between cells is used to maximise the mesh resolution in the flame and boundary layer regions.

The objective of this work is to shed light on the effects of hydrogen addition on the operational characteristics of lean-burn swirled combustion devices. Numerical simulations of the TUDelft combustor operating with CH_4 under reacting and non-reacting conditions are carried out first. The results are compared to the experimental measurements to validate the numerical model and provide additional insights on the internal turbulent flow field, temperature field, emissions and flame stabilization. The analysis is then extended to another operating set point with the same power setting and air stream mass flow rate, but with a fuel mixture composed by 60% H_2 and 40% CH_4 in volume. A comparison between the two fuel conditions is carried out to assess the effects of hydrogen addition in terms of effectiveness of fuel/oxydiser mixing, flame anchoring and temperature field in relation to emissions level. Furthermore, the effects of the turbulent swirling flow features are analysed, with focus on the description of the Pre-

cessing Vortex Core (PVC) through modal analysis of the predicted velocity fields. Moreover, the presence of flashback and local extinctions is analysed. In summary, the research objective is formulated as follows:

"To **numerically simulate** with a LES model **cold and reacting flow** in a **lean premixed hydrogen gas turbine combustor**, to be able to design a combustor which reduces **NO_x emissions** while maintaining **combustion stability**

A literature review of the relevant subjects was conducted prior to the formulation of this goal. In section 1 the findings of this literature review are presented. Next, is elaborated on the test case and methodology behind the CFD simulations in section 3 and section 4 respectively. Afterwards, will be elaborated on the validity and analysis of the results in section 5. Subsequently, conclusions are drawn in section 6 and recommendations for future research are given in section 7.

2
Theoretical background

The main findings of the literature review can be divided in the relevance of the project, the main physical phenomenon behind the proposed innovation and the modeling approach, illustrated in Fig. 2.1. In the relevance of the project section, the motivation behind hydrogen combustion, the APPU project and the modeling approach is given. Next, the review of the main physical phenomenon includes background information on turbulent combustion and the effects of hydrogen, lean premixed combustion and swirling flow. Subsequently, in the modeling approach section, the turbulence model, the combustion model, and the numerical details are discussed. The section on numerical details discusses meshing, wall models, CFL number and discretization schemes.

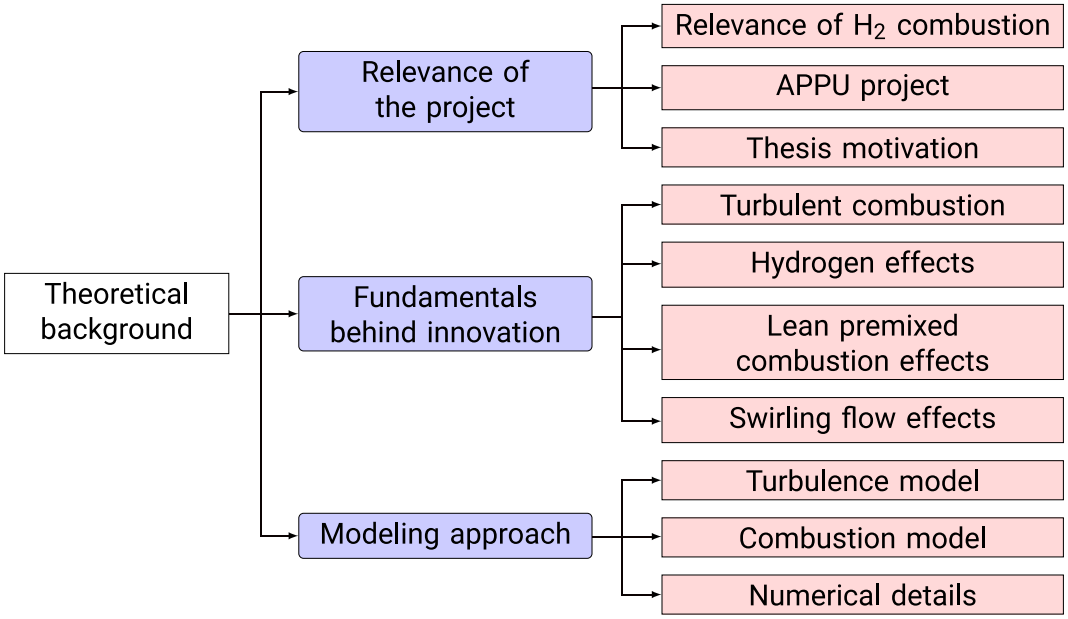

Figure 2.1: Theoretical background overview

2.1. Relevance of the project

2.1.1. The relevance of hydrogen combustion

Currently, aviation accounts for around 3% of the CO_2 emissions globally. The European Aviation industry is committed to reaching net-zero CO_2 emissions for all flights within and departing from Europe before 2050. According to the research of the Netherlands Aerospace Centre (NLR), hydrogen combustion is the most promising approach for powering long-distance flight due to its high energy density and minimal CO and CO_2 emissions [1]. However, the challenge for hydrogen combustion, is that NO_x emissions are still present due to the nitrogen content in air. Because nitrogen formation increases with the combustion temperature and the hydrogen flame temperature is about 100K higher than with kerosene, there is more NO_x emission at the same equivalence ratio [8]. The equivalence ratio is defined as the ratio of the fuel mass flow rate to the air mass flow rate divided by the same ratio under stoichiometric conditions [9]. Stoichiometry is defined as the ratio in which all fuel is burned while there is no excess air [10].

A possible solution towards NO_x reduction is lean premixed combustion. Lean conditions are defined by an equivalence ratio lower than 1, meaning that the deficient reactant is the fuel [11]. One of the major challenges for a lean premixed hydrogen flame include the prevention of instabilities such as flashback

and flame extinction [12]. Flashback is defined as the situation where the flame propagates upstream in the injection unit [13]. Hydrogen is relatively prone to flashback due to its fast reaction rate, that enables a high flame speed [14]. Furthermore, can the lean conditions result in flames that are closer to the extinction limit. However, the higher flammability limit of hydrogen extends the lean blow out (LBO) limit [15], which is defined as the phenomenon of flame extinction due to a value of the fuel to air ratio which is below a certain minimum threshold [16].

2.1.2. APPU project

The present project aims to simulate the processes in the axial swirler and combustor of the Advanced Propulsion and Power Unit (APPU) project, shown in Fig. 2.2. This project aims to address the problem of reducing CO and CO_2 emission. This system is different from a regular auxiliary power unit (APU) that only powers non-propulsive functions of an aircraft [17]. The APPU system is, namely, also providing propulsive power to the open rotor at the aft end of the fuselage in a Boundary Layer Ingestion (BLI) configuration. The open rotor is, due to the increased effective bypass ratio and BLI configuration, more efficient than a traditional turbofan engine [18]. Furthermore, the novel system aims to improve the main engine operating characteristics, as it eliminates the need for power and bleed off-takes of the main engine. Preliminary studies indicate that the realization of the APPU aircraft could reduce CO_2 emissions for a typical 2000 km flight by 20%, and Landing and Take-off (LTO) emissions by 50% [19].

Figure 2.2: APPU project poster [19]

2.1.3. Motivation of the modeling approach

The methods used for numerical modeling of turbulent flow can be divided into three categories, Reynolds Averaged Navier Stokes (RANS), Large Eddy Simulation (LES), and Direct Numerical Simulation (DNS). In RANS modelling, the Navier-Stokes equations are solved for the steady mean flow. This method is relatively computationally cheap, but is not able to capture unsteady and periodic flow phenomena [12]. DNS, on the other hand, resolves all the length and time scales, but due to the time-dependent nature of the Navier-Stokes equations and the wide range of physical scales, especially for large Reynolds numbers, its application is currently limited to relatively simple scientific cases. In LES, a low-pass filter is applied analytically to the Navier Stokes equations and the transport equations for the filtered quantities are computed directly, while the smaller scales, called subgrid scales (SGS), are modeled [20]. Because,

the majority of the turbulent fluctuations are resolved, LES is significantly more accurate than RANS for turbulent flows [21]. LES models are becoming increasingly popular for modeling combustion, due to increasing computational power and their ability to capture unsteady flow features [12].

Combustion modelling is necessary due to the great number of species involved during the reaction [22]. Closing the reaction rate calculations with the Arrhenius equation would introduce problems caused by the high non-linear temperature dependence [23]. Furthermore, the complexity of the problem is increased by the large variety of lengths, velocities and time scales involved [6]. Turbulence-chemistry can therefore have a large effect on the reaction rate [23].

2.2. Physical fundamentals behind innovation

The aim of this chapter is to understand the physical processes underlying the modeling approach and the validation and interpretation of the results. First, the fundamentals of turbulence, combustion and their interaction are described, including the formation of NO_x, the relevance of flame regimes and the phenomenon leading to combustion instabilities. Second, the effects of hydrogen addition are described using differential diffusion and auto-ignition quantities. Finally, the definitions of lean premixed combustion and swirling flow are discussed, along with their effects on emissions and flame stability.

2.2.1. Turbulent combustion

Turbulence

Turbulence refers to the irregular, chaotic motion of flows, where the speed of a fluid fluctuates in both direction and magnitude [24]. Furthermore, it can be considered that turbulence is composed of eddies of various sizes [25]. The energy present in the large-scale eddies is supplied by external energy sources, like the kinetic energy of the mean flow. The fluid motions of these integral length scales depend on the geometry and boundary conditions, making them largely inhomogeneous and anisotropic. In addition, these length scales are long living and contain high energy [26]. However, because large eddies are unstable, they break down and transfer their energy to smaller eddies. This mechanism is called the energy cascade [27]. At the smallest eddy scale, called the Kolmogorov scale, the fluid motions are independent of the geometry and flow direction [28]. The flow is relatively homogeneous and isotropic, and the length scales have a low energy content and a short lifetime [26]. Finally, the energy will be converted to heat by viscous dissipation processes [29].

Combustion

When fuels react through combustion, molecular bounds in the reactants are broken and energy is released. The reactions are triggered for a fuel-oxidizer mixture after a certain activation energy is overcome [30]. Subsequently, the reactants turn via intermediate species into the products [31]. The reaction rate can be described using the reaction rate coefficient k and the concentrations of the reactants $[A]$ $[B]$, as can be seen in Equation 2.1, for the reaction involving species A and B as reactants. The reaction order in relation to the species is represented by m and n [32].

$$r = k[A]^m[B]^n \tag{2.1}$$

Subsequently, the reaction rate coefficient can be described using the modified Arrhenius form, given in Equation 2.2. Where A represents the pre-exponential factor, E_A the activation energy, n the temperature exponent and R the gas constant [33]. Here is illustrated that the reaction rate depends exponentially on the temperature.

$$k = AT^n \exp\left(-E_a/\mathrm{R}T\right) \tag{2.2}$$

NO_x formation

The formation of NO_x emissions can be described mainly through three mechanisms, namely thermal NO_x, prompt NO_x and fuel NO_x. The typical effect of temperature on these mechanisms is illustrated in Fig. 2.3 [34]. Thermal NO_x, also named Zeldovich NO_x, describes the process in which nitrogen is combined with O and OH radicals. The reactions present in this mechanism are exponentially dependent on the temperature, as can be seen in Fig. 2.3. In addition, is the reaction also dependent on the pressure and the residence time [35]. The prompt NO_x mechanism describes the reaction of nitrogen molecules with radicals that are produced as a result of the combustion of hydrocarbons [34]. The third mechanism, called the fuel NO_x, describes the formation of NO_x when nitrogen molecules are present in the fuel [35].

Combustion turbulence interaction

There are several phenomena that cause interactions between turbulent and combustion processes. One of these phenomena include the corrugation of the flame by the large scale eddies ahead of the flame

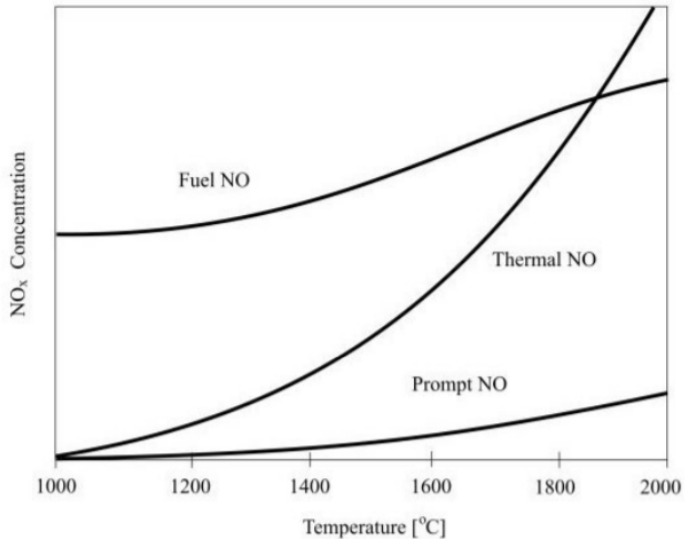

Figure 2.3: Temperature dependency in NO_x formation mechanisms in combustion processes [34]

front. The wrinkling of the flame increases the flame surface area and thereby the flame speed [36] [37]. However, the wrinkling of the flame structure also leads to high flame stretch that could possibly quench the flame [20]. Furthermore, the burnt gases increase the kinematic viscosity, lowering the Reynolds number and thereby leading to re-laminarisation of the flow [20]. However, combustion also leads to an increase in vorticity called flame generated turbulence. The initial magnitude of turbulence determines if a vortex will be enhanced, unmodified or damped due to combustion [12].

Flame regimes

The phenomenology present in turbulent premixed combustion can be classified in multiple regimes. The Damköhler number and the Karlovitz number are often used ratios to describe the phenomenology. The Damköhler number represents the ratio of the turbulent characteristic time scale to the chemical time scale and is given in Equation 2.3. The Karlovitz number describes the ratio of the chemical time scale to the Kolmogorov time scales and is given in Equation 2.4 [38]. In these equations, L represents the integral turbulent length scale, S_L the laminar flame speed, δ_L the laminar flame speed, u' the turbulent velocity and η_K the Kolmogorov length scale. These Damköhler and Karlovitz number have been used for the "Borghi, Peters diagram", given in Fig. 2.4 [39] [40].

$$Da = \frac{L}{\delta_L}\frac{S_L}{u'} \tag{2.3}$$

$$Ka = \left(\frac{\delta_L}{\eta_K}\right)^2 = \left(\frac{u'}{S_L}\right)^{3/2}\left(\frac{\delta_L}{L}\right)^{1/2} \tag{2.4}$$

The regime diagram illustrates that the flamelet assumption is valid for Da>1 and Ka<1. The flamelet assumption states that the flame can be seen as an ensemble of thin, 1-dimensional laminar flames. The turbulent flow is not able to modify the inner structure of the flame, which enables turbulence to be segregated from chemistry. The flamelet regime can be further classified into the wrinkled flame regime, where turbulence is not able to alter the flame structure and the corrugated flame regime, where the smallest eddies are able to enter the preheat zone and thereby form pockets of fresh and burnt gases. The other regime is called the thickened flame regime which is valid for Ka>1. This implies that the Kolmogorov scales are smaller than the flame structure scales what allows them to modify the inner flame structure. This regime can be further classified into the thin reaction zone and the distributed reaction zone. In the thin reaction zone, the eddies can modify the preheat zone but not the reaction zone. In the distributed reaction zone, the inner structure of the reaction zone is also affected by turbulence [12]. Both the thin and divided reaction zones may indicate strong non-linear interactions between turbulence and chemistry, which are difficult to model [41]. However, there was observed that the flamelet assumption could hold up to Karlovitz numbers of around 1000 [42]. Therefore, the regime diagram should only be

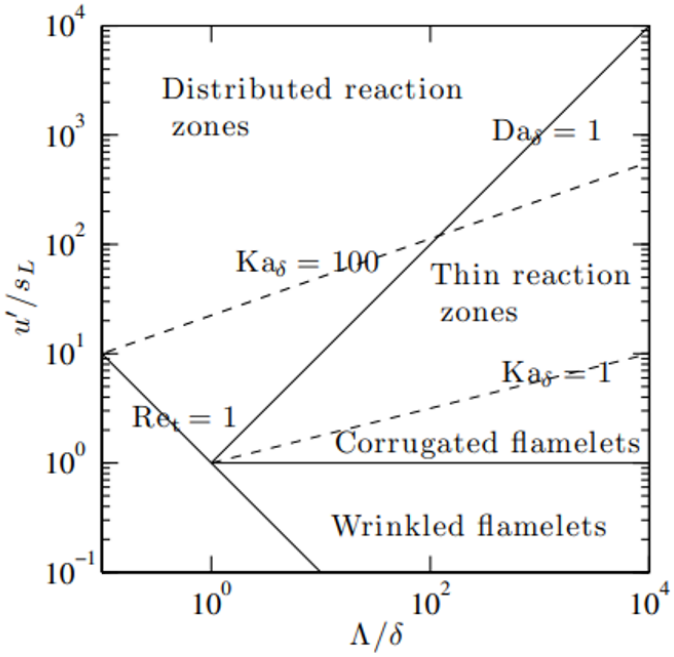

Figure 2.4: "Borghi, Peters regime diagram" [39][40]

used as a rough estimate of the combustion regimes [43].

Combustion instabilities

Combustion instability is defined as the phenomenon of unstable combustion, caused by the unsteady coupling between pressure oscillations and the flame [44]. This section discusses hydrodynamic instabilities, thermoacoustic instabilities, flashback and blow out. Hydrodynamic instabilities are caused by molecular diffusion effects at low Lewis numbers, defined as the ratio between thermal diffusivity and mass diffusivity [45]. At low Lewis numbers, which are encountered in lean hydrogen combustion, the curvature of the flame is amplified, causing an imbalance between heat and species diffusivity, reducing the flame speed, and thereby enhancing hydrodynamic instabilities [46] [47].

Thermoacoustic instability is another form of instability. According to Beita et al. [3] it can be described as “undesirable, large amplitude oscillations of one or more natural acoustic modes of a combustor arising from resonant interactions between oscillatory flow and unsteady heat release processes”. The self-sustaining instabilities can be described using a feedback process. First vortices in the combustor lead to flow perturbations that cause fluctuations in the reaction rates, and thereby oscillations in the heat release. These oscillations induce fluctuations in the acoustic pressure, which lead again to flow perturbations [3]. These instabilities can lead to harmful effects, such as component oscillations, increased heat transfer rates, flashback, and blow out [48].

Flashback is an instability condition where the flame propagates upstream [49]. Flashback can cause serious hardware damage. According to Lieuwen [48], flashback can be caused by the following mechanisms: lower flow velocity compared to the turbulent burning velocity, combustion instabilities, induced turbulence and low velocity in the boundary layer, and combustion-induced vortex breakdown (CIVB). The latter form of flashback is caused by the breakdown of the flow due to the contribution of the flame [50]. For a tubular premix burner without center body, the inner recirculation zone can propagate upstream, carrying the flame tip inside the mixing tube, as can be seen in Fig. 2.5. For the proposed project, CIVB is of particular interest as Fritz et al. [51] discovered that this form of flashback is the most common form of flashback in swirl-stabilized burners with a cylindrical premixing zone .

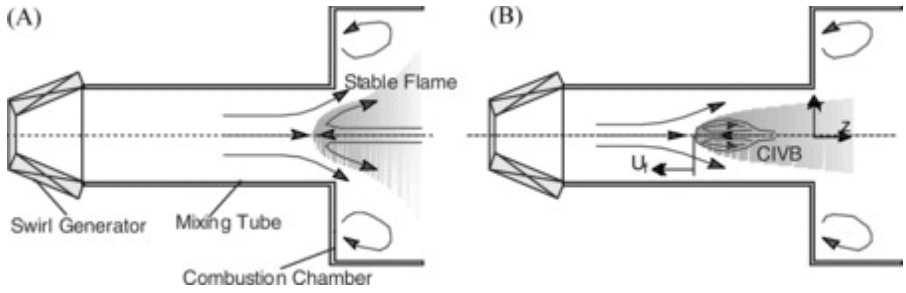

Figure 2.5: Flashback due to CIVB: Fig. A represents a stable flame and Fig. B represents flashback due to CIVB [48]

Blow out is another instability condition that can cause serious harm. Low frequency oscillations at high amplitudes are generated by local extinctions. These oscillations may generate pressure waves that contribute to thermoacoustic feedback loops [52].

Since the experiments will be conducted for the reacting cases, inflow conditions that could cause serious hardware changes shall be prevented. A precessing vortex core (PVC) could be a relevant phenomenon which could lead to instabilities but could still be present in an experimental test without causing serious harm. According to Syred et al. [53], a PVC is a helical coherent structure precessing around the axis of the flow while they spin around their own axis. These structures are located along the shear layer between the jet and the central vortex breakdown bubble [54]. The PVC can significantly affect the flame because it can lead to improved fuel-air and burned-unburned gas mixing and thereby to increased heat release efficiency and reduced NOx emissions. However, the PVC-driven pressure and velocity oscillations can excite the characteristic frequencies of the combustor, leading to possible thermo-acoustic instabilities [55].

2.2.2. Hydrogen effects

During the project, no experimental or numerical data are available for the CH_4/H_2 case. Therefore, understanding the relevant differences between methane and hydrogen is of significant interest for the validation process. Moreover, by comparing the properties with those of kerosene, the impact of the innovation can be evaluated. The important thermophysical and chemical properties of hydrogen, gaseous methane and kerosene are given in Table 2.1. Remarkable differences can be seen, of which the effects are described using differential diffusion in section 2.2.2 and auto-ignition quantities in section 2.2.2.

Property	**Hydrogen**	**Methane**	**Kerosene**
Flammability limits in air (by volume) [56]	4 to 75	4.4 to 16.4	0.7 to 5
Minimum ignition energy in air (mJ) [57]	0.011	0.28	20
Maximum adiabatic flame Temperature in air (K) [58]	2483 [a]	2236 [a]	2286 [a],[b]
Maximum laminar flame speed in air (cm/s)	306 [3] [c]	37.6 [3] [c]	56.8 [59] [d]
Thermal diffusivity (mm^2/s)	153.26 [3] [c]	23.69 [3] [c]	0.08 [60] [a]
Mass diffusivity (mm^2/s)	78.79 [3] [c]	23.98 [3] [c]	6 [61] [e]
Molar mass (kg/kmol)	2.02 [62]	16.04 [62]	≈ 140 [63] [64]
LHV (MJ/Kg)	119.96 [62]	50.05 [62]	43.0 [65]

Table 2.1: Properties of hydrogen, methane and kerosene, [a] At 298 K and 1 atm, [b] Decane, [c] At 293 K and 1 atm, [d] Jet-A fuel at 403 and 1 atm K, [e] At 300 K and 1 atm

Differential diffusion effects

Hydrogen has very high diffusivity coefficients, affecting the turbulent flame speed, heat release rate, and burning rate [66]. The flame speed of hydrogen is significantly higher than that of hydrocarbon flames,

resulting in an increased flashback propensity and a shift of the unstable region to lower air flow rates and equivalence ratio's when compared to methane [67] [68]. In addition, Fig. 2.6 shows that for the same equivalence ratio, the flame speed is higher for hydrogen flames, resulting in more NO_x emissions [8]. Furthermore, because of the lower minimum ignition energy of hydrogen compared to that of hydrocarbon fuels and a larger flammability limit, this results in a faster burning rate, increasing the thermodynamic efficiency [69]. This efficiency is defined as the ratio between the energy in the fuel and the energy converted into work [70]. Moreover, the higher molecular distribution of hydrogen has a beneficial effect on the uniformity of the mixture and thus on the combustion efficiency, which is defined as the ratio of the chemical energy in the fuel to the energy converted into heat [71].

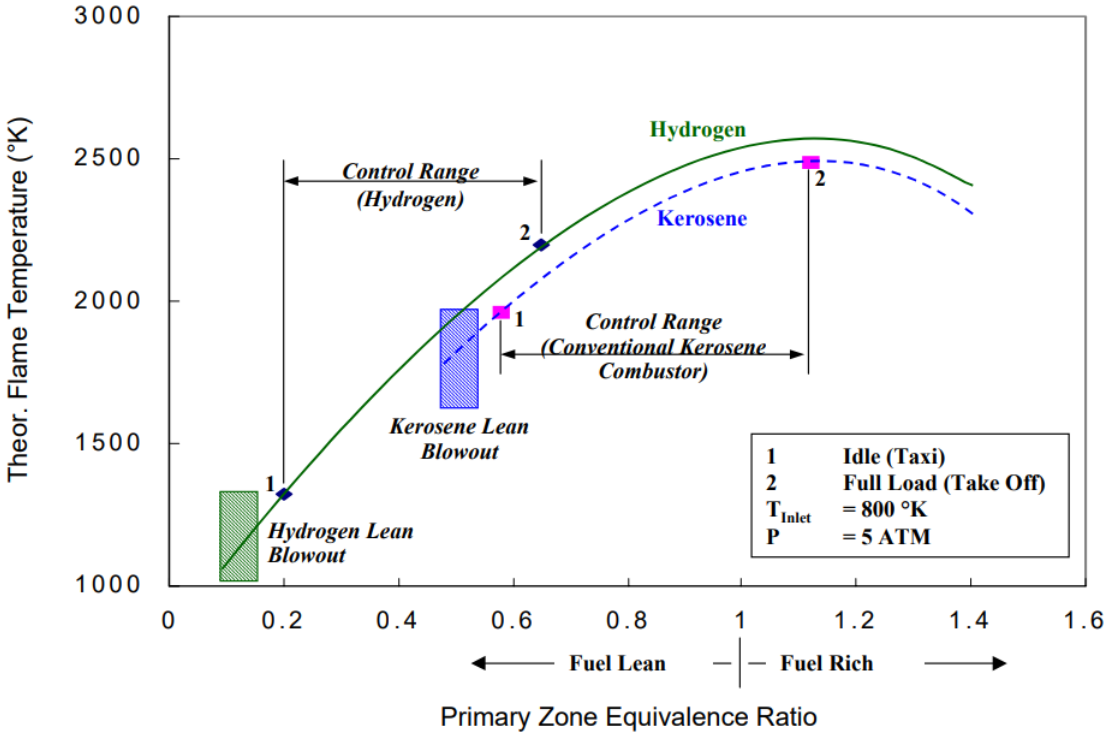

Figure 2.6: Temperature characteristics of hydrogen and kerosene combustion [8]

Auto-ignition effects

The higher flammability limits result in an extended lean blow out limit, as can be seen in Fig. 2.6 [72]. This is partly due to the higher strain resistance of hydrogen [3]. Hence, the extended LBO limit has a decreasing effect on the generated pressure waves, which cause thermoacoustic instabilities [52]. Furthermore, Lieuwen et al. [73] claim that because the hydrogen content in a methane-hydrogen mixture increases, the auto-ignition potential also rises due to the noticeably reduced ignition delay time. The ignition delay time is defined as the required time for spontaneous ignition at a given condition. Fig. 2.7 shows that increasing the hydrogen content significantly shortens the ignition time for methane hydrogen mixtures.

2.2.3. Lean premixed combustion effects

The objective of lean premixed combustion can be described as decreasing emissions, while maintaining proper flame stability. In the section below the definitions of lean and premixed combustion are given. Subsequently, the effects of these conditions on the NO_x emissions and flame instabilities are examined.

Definition of lean premixed combustion

To determine how much fuel is present in the reactants, the equivalence ratio is used. The equivalence ratio is determined using Equation 3.5, where X indicates the mole fraction and stoic the stoichiometric

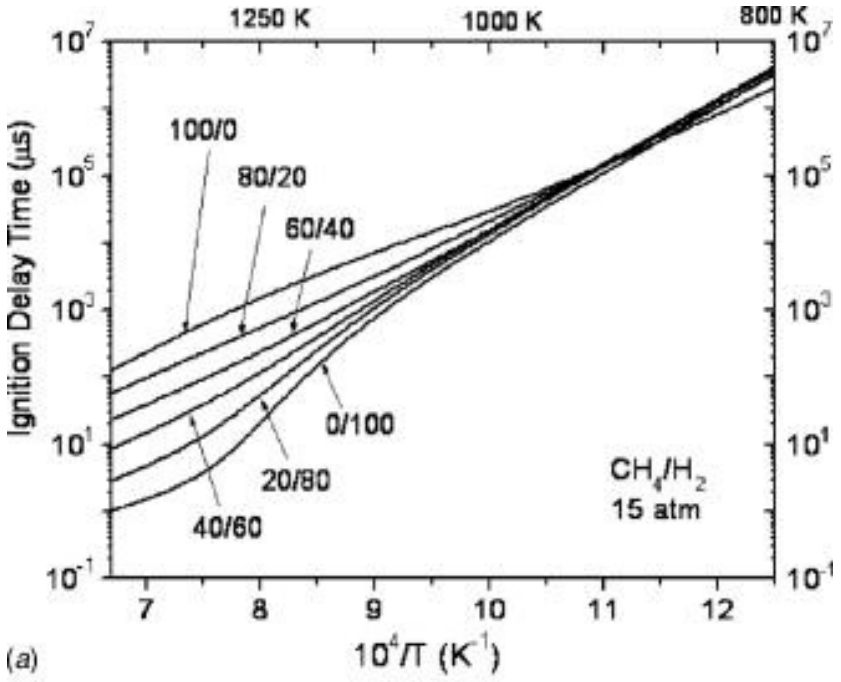

Figure 2.7: Effect of hydrogen content in methane mixture at $P = 15$ atm and $\phi = 0.4$ [73]

conditions [74]. Applying this equation to a mixture of hydrogen and methane results in Equation 2.6 [75]. When the equivalence ratio is smaller than 1, the mixture is called lean and when the equivalence ratio is higher than 1, the mixture is called rich. Premixed combustion is defined as the condition where the fuel and the oxidizer are premixed before combustion [76].

$$\varphi = \left[(X_{\text{fuel}}) / X_{O_2} \right] / \left[(X_{\text{fuel}}) / X_{O_2} \right]_{\text{stoich.}} \tag{2.5}$$

$$\varphi = \left[\left(X_{CH_4} + X_{H_2} \right) / X_{O_2} \right] / \left[\left(X_{CH_4} + X_{H_2} \right) / X_{O_2} \right]_{\text{stoich.}} \tag{2.6}$$

Effects on emissions and stability

The lower flame temperature in lean combustion drastically reduces NO_x production due to thermal NO_x formation [2]. For hydrogen combustion, the adiabatic flame temperature peaks slightly closer to the rich side of the stoichiometric value, as can be seen in Fig 2.6 [8]. Unfortunately, with ultra lean combustion, non-combustible mixture pockets can enter the combustion zone. This can lead to local extinctions, causing oscillations at high amplitudes that can trigger thermoacoustic instabilities [77].

Premixed combustion could allow better control of the combustion process, reducing fuel-rich pockets that lead to higher flame temperatures and thus spikes in NO_x emissions. In addition, premixed combustion improves the heat and mass transfer of a gas mixture [78], leading to a higher combustion efficiency compared to unpremixed combustion [12]. Another advantage of premixed combustion is the shortened flame length, allowing a shorter combustion chamber design [78]. The disadvantage of premixed combustion is the collection of large amounts of premixed reactants, which without a proper premixer can ignite in an uncontrolled explosion. Furthermore, in the case of partially premixed mixtures, a higher degree of premixing leads to a higher burn rate of hydrogen, expanding the flammability limits of the mixture. This makes the system less prone to extinction, but on the other hand makes it more vulnerable to upstream flame movement, raising the reaction zone temperature, which can lead to combustion induced vortex breakdown [79]. As discussed in section 2.2.1, this type of instability can increase the flashback propensity.

2.2.4. Swirling flow effects

Preliminary results indicated the significant effect of swirl on the flow field, making the swirl number an important quantity for validation purposes. First, the definition of the swirl number is discussed. Then the effect of the swirl number on NO_x emissions and flame stability is described.

Definition of the swirl number

The effective swirl number is a dimensionless number which is defined as the ratio of the axial flux of the angular momentum G_θ to the outer radius of the annulus r_o, multiplied with the axial flux of the axial momentum G_x, as shown in Equation 2.7.

$$Sw_0 = \frac{G_\theta}{r_o G_x} \tag{2.7}$$

The axial flux of the angular momentum and axial momentum are defined in Equation 2.8 and Equation 2.9. Here represents U the axial velocity component, W the tangential velocity component and ρ the fluid density [80].

$$G_\theta = \int_0^R (Wr)\rho U 2\pi r\, dr \tag{2.8}$$

$$G_x = 2\pi \int_0^R \left(\rho U^2 r\right) dr \tag{2.9}$$

In the proposed thesis, the swirl number can be varied by adjusting the amount of axial air injection and using a swirler whose swirler vanes can be positioned at different angles.

Effects on emissions and stability

The value of the effective swirl number can be a distinguishing parameter for the presence of a recirculation zone, which promotes mixing, retains hot products and radicals and contributes to the anchoring of the flame [80]. As the local axial velocity in the recirculation zone is slowed down, the residence time increases, resulting in a more stable and complete combustion process [81]. The increased flame stability results in lower temperature peaks, leading to a reduction of NO_x [82]. Furthermore, due to the inner recirculation zone the flame becomes less attached to the burner rim, reducing the boundary layer flashback propensity [83]. According to the research of Dellenback et al. [84] and Guo et al. [85] a recirculation bubble is formed when the swirl number is larger than 0.4 for a flow undergoing an axisymmetric sudden expansion at a Reynolds number of 100,000. However, higher swirl strength also increases the reaction at the front, raising the temperature what has an increasing effect on NO_x emissions and could potential lead to Combustion Induced Vortex Breakdown [79]. Also, the risk of flashback is increased as the inner recirculation zone enhances upstream flame propagation [72].

2.3. Modeling approach

This section provides background information on the various aspects of the modelling approach. Subsequently, the implementation of the models is described in section 4.

2.3.1. Turbulence modeling

Since RANS models are not capable of capturing correct turbulence chemistry interactions and unsteady and periodic flow phenomena, while DNS models are still limited to relatively simple cases, LES models are examined for the proposed thesis. This section first explains the foundation of LES models, followed by the fundamentals of the SGS model that is used in the study.

Fundamentals of LES

The Navier-Stokes equations are the fundamental governing equations used in fluid mechanics. They are based on the conservation of mass, momentum, and energy. For a compressible fluid, they are given in Equations 2.10a, 2.10b and 2.10c, respectively [86].

$$\frac{\partial \rho}{\partial t} + \frac{\partial}{\partial x_j}\left[\rho u_j\right] = 0 \tag{2.10a}$$

$$\frac{\partial}{\partial t}\left(\rho u_i\right) + \frac{\partial}{\partial x_j}\left[\rho u_i u_j + p\delta_{ij} - \tau_{ji}\right] = 0 \tag{2.10b}$$

$$\frac{\partial}{\partial t}\left(\rho e_0\right) + \frac{\partial}{\partial x_j}\left[\rho u_j e_0 + u_j p + q_j - u_i \tau_{ij}\right] = 0 \tag{2.10c}$$

The viscous stress τ_{ji} is given in Equation 2.11 for a Newtonian fluid. The δ_{ij} represents the Kronecker delta and can be described by Equation 2.12 [87].

$$\tau_{ij} = 2\mu S^*_{ij} \tag{2.11}$$

$$\delta_{ij} \equiv \begin{cases} 0 & \text{for } i \neq j \\ 1 & \text{for } i = j \end{cases} \tag{2.12}$$

Furthermore, the viscous strain rate S^*_{ij} and the heat flux q_j are given in Equations 2.13 and 2.14. The e_0 represents the total energy and λ the thermal conductivity [88].

$$S^*_{ij} \equiv \frac{1}{2}\left(\frac{\partial u_i}{\partial x_j} + \frac{\partial u_j}{\partial x_i}\right) - \frac{1}{3}\frac{\partial u_k}{\partial x_k}\delta_{ij} \tag{2.13}$$

$$q_j = -\lambda \frac{\partial T}{\partial x_j} \tag{2.14}$$

Since solving all length and time scales of the Navier-Stokes equation requires too much computational power, modeling is required for the described setup. The filtering operation of the mass, momentum and energy Navier Stokes equations in LES models leads to Equation 2.15a, Equation 2.15b and Equation 2.15c respectively [89]. The quantities denoted with a bar on top are convoluted with a filter.

$$\frac{\partial \rho}{\partial t} + \rho \cdot \nabla \overline{u} = 0 \tag{2.15a}$$

$$\frac{\partial \overline{u}}{\partial t} + \overline{u} \cdot \nabla \overline{u} = -\frac{1}{\rho}\nabla \bar{p} + \nu \nabla^2 \overline{u} - \nabla \cdot \tau \tag{2.15b}$$

$$\frac{\partial}{\partial t}\left(\rho e_0\right) + \rho e_0 \nabla u + p \nabla u + \nabla \cdot q = \nabla u \cdot \tau \tag{2.15c}$$

The subgrid scale (SGS) tensor is represented by τ, which incorporates the effects of the unresolved scales. The equation defining the SGS tensor is given in Equation 2.16 [89]. As the term $\overline{u_i u_j}$ is unclosed, modeling is required to determine the SGS tensor [90].

$$\tau_{ij} = \overline{u_i u_j} - \bar{u}_i \bar{u}_j \tag{2.16}$$

SGS models

Typical SGS closure models include Zero- and One-Equation models. In Zero-Equation models, no transport equation is solved, but an equation is used to calculate the subgrid stress tensor. By adding a transport equation for One-Equation models, more physical processes are considered, such as the convection, production and dissipation of subgrid kinetic energy. This leads to a more accurate modelling of the anisotropic effects that occur during the combustion process. However, the addition of an extra transport equation, leads to a slight increase in computational effort [91]. The One-Equation model used in this project is the Dynamic Structure model which uses a dynamic approach to determine the subgrid kinetic energy term of the momentum equations [92].

2.3.2. Combustion modeling

As the flame thickness is usually thinner than the smallest resolved scale, combustion is a SGS phenomenon in LES [12]. According to Pope, the accuracy of LES models have a first order dependency on the rate-controlling processes which have to be modelled [5]. Moreover, it can be deduced from the Arrhenius equation, given in Equation 2.2, that the temperature has a strong non-linear effect on the reaction rate. An accurate description of all processes using the Arrhenius equation requires solving the smallest time and length scales, which makes the problem stiff. Modelling is therefore required due to the available computational resources [93] [23].

Moreover, a large number of species are often involved in the reaction, increasing the urge of computational modelling [22]. According, to the San Diego University, the detailed mechanism of hydrogen combustion involves 57 species in 268 reactions [94]. Furthermore, as significant density changes are present in combustion processes, it is advisable to use a density weighted average called Favre filtering. This enables the decoupling of terms involving density and transported variables [12]. For example, the Favre-averaged velocity describes the fluid mass that is transported in the flow [95] [96].

The Thickened Flame model (TF) and the SAGE model are discussed below. Since the models use a presumed probability density function (PDF), the working principle behind a PDF is described first.

Probability density function

A probability density function is used in combustion models to provide information on the mean and variance of thermochemical quantities when the flame is not completely resolved [97]. An example of an application of a PDF is given in Equation 2.17 for the filtered reaction rate $\overline{\dot{\omega}}_k$ of species k. Here it can be observed that the reaction rate is a function of the laminar reaction rate $\dot{\omega}_k$ and the PDF P, incorporating the mean and variance. The PDF is only a function of the temperature T and the composition space Y, which is represented by species mass fractions [12]. It is possible to describe the mass fractions of species by using only the progress variable c and the mixture fraction Z [98]. The progress variable c is a method of describing combustion processes by assigning a value of 0 to unburnt gases and 1 to burnt gases [99]. Two major methods exist for determining a PDF in a fluctuating flow field. In a transported PDF a balance equation is solved for determining the PDF and in a presumed PDF the shape of the PDF is presumed [100].

$$\overline{\dot{\omega}}_k = \int P(\mathbf{Y}, T)\dot{\omega}_k(\mathbf{Y}, T)\mathrm{d}\mathbf{Y}\mathrm{d}T \tag{2.17}$$

A presumed PDF estimates the occupation of a turbulent flame for each cell. Using the mean and variance, a distribution for averaged quantities, such as the mixture fraction and progress variable can be made, taking into account turbulent effects of the flow [100]. The shape of a PDF can be determined with distribution functions such as the beta and the delta function. A beta function describes a distribution whose shape depends on the average and variance of the considered variable x. The shape parameters a and b are estimated using the sample mean $\bar{x}$ and sample variance s^2, noticeable in Equation 2.18 and Equation 2.19.

$$a = \bar{x}\left[\frac{\bar{x}(1-\bar{x})}{s^2-1}\right] \quad (2.18) \qquad b = (1-\bar{x})\left[\frac{\bar{x}(1-\bar{x})}{s^2-1}\right] \quad (2.19)$$

Subsequently, the model parameters are used in the PDF of the beta distribution, given in Equation 2.20. The beta function $B(a,b)$ is calculated using the gamma function $\Gamma(a)$, the equations that describe the beta and the gamma function are given in Equation 2.21 and Equation 2.22 [101].

$$f(x;a,b) = \frac{1}{B(a,b)}x^{a-1}(1-x)^{b-1} \quad (2.20)$$

$$B(a,b) = \frac{\Gamma(a)\Gamma(b)}{\Gamma(a+b)} \quad (2.21) \qquad \Gamma(a) = \int_{t=0}^{\infty} t^{a-1}\mathrm{e}^{-t}\,\mathrm{d}t \quad (2.22)$$

A delta function is defined as having infinite magnitude at a specified time and zero magnitude at all the other times, while the area under the magnitude time curve is unity. In Equation 2.23 and Equation 2.24 the function properties are demonstrated [102].

$$\begin{aligned}\delta(t-\alpha) &= \infty \quad t=\alpha \\ &= 0 \quad t\neq\alpha\end{aligned} \quad (2.23) \qquad \int_{-\infty}^{\infty}\delta(t-\alpha)\,dt = 1 \quad (2.24)$$

An advantage of using PDF models is that spatially unresolved information about the mean and variances of scalars can be retrieved from the statistics incorporated by the PDF, at low computational costs compared to detailed chemistry [103].

Thickened flame approach

In a detailed chemistry solver, like the SAGE model discussed below, a minimum of five cells across the flame are required to determine the laminar flamespeed. To prevent an under prediction of the laminar flamespeed as a result of an unresolved flame, either the cell size must decrease or the flame needs to be artificially thickened [104]. In this model the flame is resolved by artificially thickening the flame by decreasing the thermal diffusivity and increasing the pre-exponential constant [105]. To identify the reaction zone, a flame sensor based on a reference flame is used to ensure that the thickening factor only affects the flame region [106]. Furthermore, to ensure that the flame propagating speed is unaffected by the flame thickening, the diffusivity and reaction rate are multiplied with an efficiency function to correct the flame wrinkling [7]. The relationships between the laminar flame speed s_l^0, the molecular diffusion rate D, the mean reaction rate $\bar{W}$ and the flame thickness δ_l^0 are given in Equation 2.25 and Equation 2.26 [7].

$$s_l^0 \propto \sqrt{D\bar{W}} \quad (2.25) \qquad \delta_l^0 \propto \frac{D}{s_l^0} \quad (2.26)$$

This method is capable of analysing the complex behaviour of quenching, ignition and swirl stabilized flames [79]. However, increasing the flame thickness leads to a change in the interaction between chemistry and turbulence. While this factor is accounted for by the efficiency factor, it can still lead to inaccuracies [7].

Sage

In the SAGE model, the reaction rates for each reaction are computed using the Arrhenius equation. The net production rate $\dot{\omega}_j$ of the species j is presented in Equation 2.27. For determining ν_{ji}, the stoichiometric coefficients of the reactants and products are used, represented by ν''_{ji} and ν'_{ji}, as can be seen in Equation 2.28.

$$\dot{\omega}_j = \sum_{i=1}^{I}\nu_{ji}q_i \quad (2.27) \qquad \nu_{ji} = \nu''_{ji} - \nu'_{ji} \quad (2.28)$$

Then, using Equation 2.29, the rate-of-progress variable q_i is determined. The molar concentration of species J is represented by $[X_j]$. The forward and reverse rate coefficients are represented by k_{fi} and k_{ri}.

$$q_i = k_{fi} \prod_{j=1}^{J} [X_j]^{\nu'_{ji}} - k_{ri} \prod_{j=1}^{J} [X_j]^{\nu^*_{ji}} \tag{2.29}$$

The forward rate coefficient is determined with the Arrhenius equation, visible in Equation 2.2. For determining the reverse rate coefficients, Equations 2.30 and 2.31 are used. P_{atm} represents the atmospheric pressure, R the ideal gas constant, T the temperature, S the entropy and H the enthalpy.

$$k_{ri} = \frac{k_{fi}}{K_{ci}} \tag{2.30}$$

$$K_{i,c} = K_{i,p} \left(\frac{P_{atm}}{RT} \right)^{\sum_{m=1}^{M} \nu_{mi}} \exp\left(\sum_{m=1}^{M} \nu_{m_i} \frac{S^0_m}{R} - \frac{\Delta H^0_i}{RT} \right) \tag{2.31}$$

The governing equations for mass and energy for constant volume combustion are given in Equation 2.32 and Equation 2.33. Where $\bar{h}_m$ and $\bar{c}_{p,m}$ represent the molar specific enthalpy and molar constant-pressure specific heat of species m [107].

$$\frac{d[X_m]}{dt} = \dot{\omega}_m \tag{2.32}$$

$$\frac{dT}{dt} = \frac{V \frac{dP}{dt} - \sum_m \left(\bar{h}_m \dot{\omega}_m \right)}{\sum_m \left([X_m] \, \bar{c}_{p,m} \right)} \tag{2.33}$$

The combustion-turbulence interaction, affects the commutation error caused by the spatial filtering in a LES model, since temperature fluctuations have a significant effect on the mixing rate. To account for these fluctuations, a transported PDF can be applied. The SAGE chemistry model accounts for the spatial distribution of species and temperature, making it an accurate model for emission modelling. The major disadvantage of the model is the expensive computational effort required [108].

2.3.3. Numerical details

Besides turbulence and combustion models, the quality of an LES simulation also depends on temporal and spatial discretization [109]. The effects of the wall models and CFL numbers on the discretization will be discussed in the sections 2.3.4 and 2.3.5. Then, in section 2.3.6 will be elaborated on the discretization schemes that will be used during the proposed project. Finally, the criteria for validating the mesh quality will be discussed in section 2.3.7.

2.3.4. Wall models

Wall models are used because there is often not enough resolution near the wall to correctly resolve the viscous sublayer [110]. The wall models available in Converge CFD consist of the Law-of-the-Wall model and the Werner and Wengle model. To determine the correct wall model, it is relevant to analyze the y^+ values of the simulation. The y^+ value is used as an indication of how fine the mesh is near the wall. It is a non-dimensional variable which is demonstrated in Equation 2.34. The y variable describes the distance from the wall till the first cell adjacent from the wall, u_τ the friction velocity and ν the kinematic velocity [111].

$$y^+ = \frac{y u_\tau}{\nu} \tag{2.34}$$

The Law-of-the-Wall model uses a logarithmic curve fit of a turbulent boundary layer to determine the shear speed u_τ. When the y^+ value is greater than 11.05, the shear speed is determined with Equation 2.35 and with Equation 2.36 when the y^+ value is less than 11.05. In these equations $U_{i,\,\text{tang}}$ represents the tangential velocity, κ the Von Kármán constant and E a constant.

$$u_\tau = \frac{\left|U_{i,\,\text{tang}}\right|}{\left(\frac{1}{\kappa}\ln\left(E\frac{\rho u_\tau y}{\mu}\right)\right)} \tag{2.35}$$

$$u_\tau^2 = \frac{\mu U_{i,\text{tang}}}{\rho y} \tag{2.36}$$

The Werner and Wengle model is not dependent on the y^+, but on the condition given in Equation 2.37. The values of the constants A and B are respectively 8.3 and $\frac{1}{7}$

$$\left|U_{i,\,\text{tang}}\right| \leq \frac{\mu}{2\rho y} A^{\frac{2}{1-B}} \tag{2.37}$$

If the condition is satisfied, the shear speed is calculated using Equation 2.38, otherwise it is calculated by Equation 2.39.

$$u_\tau = \sqrt{\frac{\mu\left|U_{i,\,\text{tang}}\right|}{\rho y}} \tag{2.38}$$

$$u_\tau = \sqrt{\left[\frac{1-B}{2}A^{\frac{1+B}{1-B}}\left(\frac{\mu}{\rho y}\right)^{1+B} + \frac{1+B}{A}\left(\frac{\mu}{\rho y}\right)^{B}\left|U_{i,tang}\right|\right]^{\frac{2}{1+B}}} \tag{2.39}$$

2.3.5. CFL number

According to Laney [112], the full numerical domain of dependence should contain the physical domain of dependence. This condition can be evaluated with the CFL number, which is defined as the characteristic velocity U multiplied by the time step Δt of the numerical model divided by the minimum spacing of a cell Δx, as can be seen in Equation 2.40 [112].

$$\text{CFL} = U\frac{\Delta t}{\Delta x} \tag{2.40}$$

2.3.6. Discretization schemes

Discretization is required to determine the values at the cell faces with the values at the cell centroids [113]. In ConvergeCFD one can choose between a first-order upwind scheme and a second-order central scheme. The first order upwind scheme determines with the direction of the mass flux at the centroids of the cells which centroid value is used at the cell faces. This scheme is less accurate compared to a second-order scheme, but more stable, especially for convection dominated flows. In the second-order central scheme, the value at the cell faces is determined by interpolating between neighboring centroids. The scheme is very accurate but unbounded, which can lead to oscillations in the flow field [113]. It is decided to use the second-order scheme while investigating if the stability of the solution is satisfied.

2.3.7. Validating mesh quality

For the non-reactive case, the Pope's Criterium, devised in 2000, stated that the grid size should be chosen in a way that 80% of the TKE should be resolved [25]. Four years later, Matheou and Chung, refined the criteria by stating that to reliably predict average statistics, at least 90% of the TKE must be resolved [114]. The resolved TKE is calculated with Equation 2.41, where u' is determined with the averaged velocity minus the local velocity.

$$k_{res} = \frac{u'^2 + v'^2 + w'^2}{2} \tag{2.41}$$

However, the Pope's criteria should be treated with care as it is not applicable in areas of the domain where the flow is quasi-laminar. Validating the mesh with the Pope's criteria close to the wall is therefore not very convincing, as the turbulent fluctuations are zero at the wall and in the laminar layer next to the wall, which is called the laminar sublayer [115]. Furthermore, for the reactive case, should be aimed at a cell width of the same size of the flame thickness [116] [117].

3
Methodology: Test case

In this chapter the methodology leading to the geometry and operating conditions is discussed. First the geometry is described in section 3.1. Second, will be elaborated on the operating conditions used in this project in section 3.2. At last, the details about the PIV measurements is given in section 3.3.

3.1. Geometry

The laboratory-scale combustor designed at the TU Delft [118], illustrated in Fig. 3.1, is simulated in the present study. The design comprises an axial swirler with a geometric swirl number of 1.1, defined as in the following paragraph. A mixing tube with a radius $R = 12$ mm and a length of 60 mm is present downstream of the swirler to ensure fuel/air mixing before issuing into the cylindrical combustion chamber. The total air mass flow rate is split into a part injected axially into the mixing tube and a part entering the swirler through four radial ports. The methane/hydrogen fuel is injected in the mixing tube through four radial ports with a diameter of 5.5 mm. The ratio between the combustion chamber and mixing tube diameter, often defined as confinement ratio, is equal to 6. The expansion of the cross section combined with the flow swirl causes a characteristic flow pattern with the formation of an outer recirculation zone (ORZ) and a central recirculation zone (CRZ) over which the flame stabilises, as illustrated in Fig. 3.1. Fuel and air are at a temperature of 288 K before entering the swirler. The combustion chamber is operated at atmospheric pressure. The relevant dimensions of the investigated swirler are summarized in Table 3.1

The geometric swirl number describes the angles at which the vanes of the swirler are positioned. It should be equal to the effective swirl number immediately after the trailing edge of the swirler vanes. For axial swirlers, the geometric swirl number can be approximated with a modification of Equation 2.7, by using Equation 3.1 and Equation 3.2. This assumption is valid when the vanes are very thin and the axial velocity distribution is constant over the radius. In these equations, ϕ represents the vane angle, which is the angle between the axial direction and the tangential direction of the vanes. R_n and R_h are the mixing tube radius and the axial air injection tube radius respectively [80].

$$G'_\theta = 2\pi\rho v_{ax}^2 \tan(\phi)\frac{R_n^3 - R_h^3}{3} \tag{3.1}$$

$$G'_x = \pi R^2 \rho v_{ax}^2 \tag{3.2}$$

3.2. Operating conditions

The reacting flow fields resulting from the methane and methane/hydrogen blends are compared at the same power output, air mass flow rates and axial air percentage (AAI). The power output of the combustor, calculated based on the fuel mass flow rate, fuel Lower Heating Value (LHV) and density [76], is set

Table 3.1: Dimensions of the investigated combustor

Description	Value	Units	Description	Value	Units
Combustion chamber length	380	mm	Mixing tube length	60	mm
Combustion chamber diameter	148	mm	Mixing tube diameter	24	mm
Fuel ports diameter	5.5	mm	Swirler air ports diameter	5.5	mm
AAI port diameter	8	mm	Nr. swirler vanes	8	[-]
Blockage factor swirler	0.324	[-]	Geometric swirl number	1.1	[-]

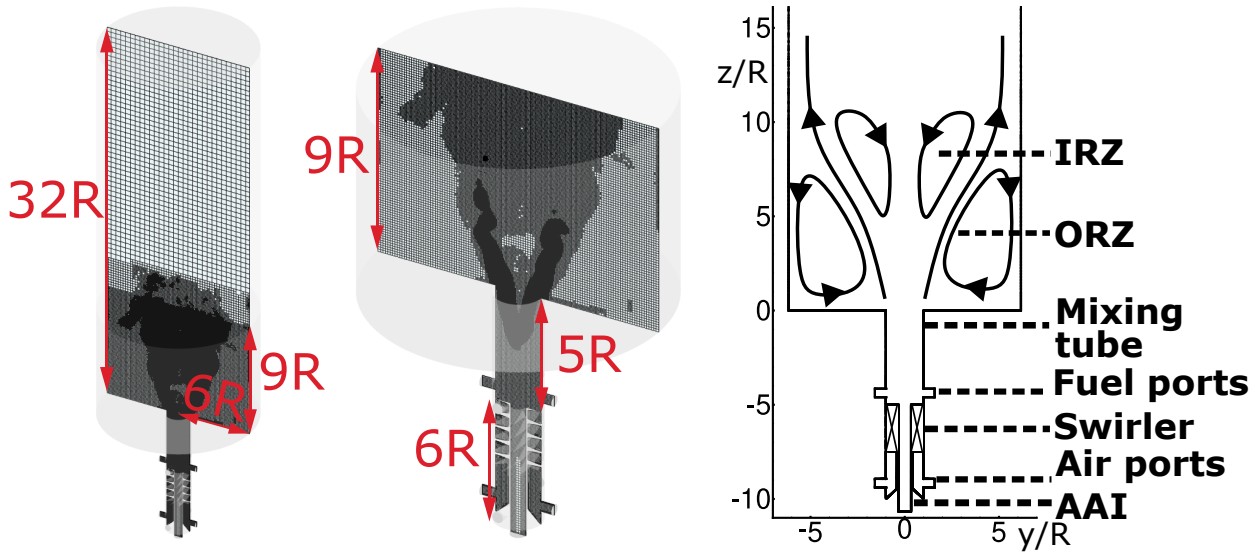

Figure 3.1: Sketch of combustor and mesh (reacting case) used for the LES. R is the radius of the mixing tube

to 11 kW. The density is determined with the ideal gas law [119]. The fuel mass flow rate, in normal litre per minute, is calculated with Equation 3.3. In this equation, η represents the combustion efficiency. The power is expressed in Kw and the LHV in MJ/KG. The combustion efficiency is assumed to be 0.99 [120]. To convert litre per minute to kg per second, Equation 3.4 is used. The amount of axial air injection is defined as percentage of the total air massflow rate and is set to 5%. The value of the total mass flow rate is $\dot{m}_a = 5.061$ g/s.

$$\dot{m} = \frac{Power}{\rho LHV\eta} \cdot 60 \tag{3.3}$$

$$\dot{m}_{kg/s} = \frac{\dot{m}_{nlpm}}{1000 \cdot 60} \cdot \rho \tag{3.4}$$

The hydrogen blend mixture is composed by 40% methane and 60% hydrogen in volume, and the fuel massflow rate is adjusted to match the same power output as for the methane-only case. Subsequently, to calculate the mass fractions, the overall chemical reactions for the combustion process are required. The stoichiometric chemical reaction for both test cases are given below.

Methane combustion

$$CH_4 + 2\,(O_2 + 3.76\,N_2) \Rightarrow CO_2 + 2H_2O + 7.52\,N_2$$

Hydrogen methane blend combustion

$$0.4CH_4 + 0.6H_2 + 1.1(O_2 + 3.76N_2) \Rightarrow 0.4CO_2 + 1.4H_2O + 4.136N_2$$

The equivalence ratio can subsequently be calculated by multiplying the stoichiometric air-to-fuel

Table 3.2: Operating conditions of the investigated combustor

Property	Value	Units	Property	CH_4 Value	CH_4/H_2 Value	Units
Power	11	kW	H2 Mole fraction	0	0.6	-
Air mass flow rate	5.06E-03	kg/s	Fuel mass flow	2.22E-04	1.82E-04	kg/s
AAI%	5	%	Equivalence ratio	0.75	0.70	-
Inflow temperature	288	K				
Outflow pressure	101325	Pa				

(AFR_{stoich}) with the ratio of the fuel mass flow and the air mass flow, as described in Equation 3.5.

$$\phi = \left(\frac{Y_F}{Y_{O_2}}\right)^{-1}_{stoich} \cdot \frac{Y_F}{Y_{O_2}} \tag{3.5}$$

This mixture results in an overall equivalence ratio of 0.7, which is lower than the 0.75 for the methane-only case. It is thus not obvious a priori what the effect of hydrogen addition on thermochemical characteristics and emissions will be. The operating conditions are given in Table 3.2.

3.3. PIV

The in-house experimental data consists of the velocity field on the combustor mid-plane for both non-reacting and reacting conditions (100% methane fuel only). The data is obtained using Particle Image Velocimetry (PIV) of a planar cross section of the center plane of the combustor and TiO_2 seeds. The camera used in the experimental campaign is the LaVision Imager sCMOS CLHS. The measuring window ranges till 200 mm downstream of the combustor inlet [118]. The high spatial resolution of the camera consist of 2560x2160 pixels that are 6.5x6.5 in size. The temporal resolution can be described by a minimum exposure time of 15 μs and frame rate of 50fps. The temporal resolution should be of minor relevance for the accuracy of the experiment, as Bell et al. [121] achieved an error of less than 0.25% when measuring a premixed methane flame using a temporal resolution of 19 μs. Furthermore, 15-20 particles were included in the interrogation window during the experimental campaign, in line with Keane and Adrian's recommendation [122] to include at least 10-20 particles for combustion applications.

4
Methodology: Modeling approach

The methodology of the LES simulations is presented in this chapter. First the details of the Dynamic Structure LES model are described in section 4.1. Next, the implementation of the TFM and SAGE chemistry models is discussed in section 4.2. Subsequently, numerical details are given in section 4.3, including the meshing strategy, and temporal and spatial discretization. Section 4.4 then describes the modelling approach for the additional OpenFoam simulation that serves as validation for the non-reacting CH4 case. Finally, section 4.5 describes the post-processing methods that require explanation.

4.1. LES details

The Favre-filtered Navier Stokes equations including conservation of mass, momentum and energy are solved in the LES paradigm. A set of Favre-filtered transport equations is solved for each chemical species involved in the combustion process within the thickened flame model approach, to be described in the next paragraph. In the Dynamic Structure model, for determining the subgrid stress, the Germano Identity is employed. This is a self-consistency condition for downscaling model parameters from the resolved scale to the unresolved scale [123]. A test filter which is almost twice the size of the original filter is used to find how these different scales are connected. The connection between the subfilter-scale stress tensor $\tilde{\tau}_{ij}$, the resolved stress, called the Leonard stress $\widetilde{L}_{ij}$, and the SGS stress tensor τ_{ij} is given in Equation 4.1.

$$\tilde{\tau}_{ij} = \widetilde{L}_{ij} + \tau_{ij} \tag{4.1}$$

Subsequently, the sub-grid scale (SGS) stresses τ_{ij} in the filtered, momentum equations are closed with Equation 4.2. The trace of the Leonard term L_{ii} is defined as the sum of the eigenvalues of a tensor [124]. The subgrid kinetic energy k_{sgs} is computed using a transport equation, given in Equation 4.3 [92]. Here, ϵ represents the dissipation term and ν_k the subgrid turbulent viscosity.

$$\tau_{ij} = \widetilde{L}_{ij}\left(\frac{2k_{\text{sgs}}}{\widetilde{L}_{ii}}\right) \tag{4.2}$$

$$\frac{\partial k_{\text{sgs}}}{\partial t} + \bar{u}_i\frac{\partial k_{\text{sgs}}}{\partial x_i} = -\tau_{ij}\frac{\partial \bar{u}_i}{\partial x_j} - \epsilon + \frac{\partial}{\partial x_i}\left(\frac{\nu_k}{\sigma_k}\frac{\partial k_{\text{sgs}}}{\partial x_i}\right) \tag{4.3}$$

Since the value of the subgrid-scale kinetic energy adapts itself, a low value is imposed as initial condition to prevent diverging behaviour of the energy equation [92]. In consultation with the help desk of ConvergeCFD an initial intensity of 0.002 fraction. A value for the Smagorinsky constant (C_S) and the viscosity coefficient (C_k) is required. The C_S dynamically adapts in the model and a higher C_S results in more viscosity and thereby larger damping, causing the solution to converge more easily [125]. A value of $C_S = 1.0$ is set. Furthermore, Liu et al. [126] recommended a C_k of 0.5 for the Dynamic Structure model.

Furthermore, the filtered diffusion terms in all scalar equations are modelled using a gradient hypothesis, and a subgrid Schmidt number (Prandtl number in the case of the enthalpy equation) of 0.7 is chosen. The turbulence-combustion interaction modelling at the subgrid level is discussed next.

4.2. Combustion model

As discussed in section 2.3.2, the thickened flame model is employed in the present study for the closure of the filtered reaction rates in the species equations. In this study, the flame thickening factor F is

determined by increasing its value until five or more cells are present across the flame front [104]. Subsequently, the thickened flame front can be resolved and stiffness of the problem caused by the broad range of time scales and strong gradients is eliminated [7]. To identify the reaction zone, a flame sensor is used to ensure that the thickening factor only affects the flame region [106]. The Jaravel's flame sensor is used, taking into account the reaction rate and mass fraction of the fuel [127]. To ensure that the flame propagating speed is unaffected by the flame thickening, the diffusivity and reaction rate are multiplied with an efficiency function to correct the flame wrinkling [7]. The reaction rates for all the species including NO and NO_2 are computed using the multi-step kinetic mechanism GRI 3.0 [128], incorporated in the detailed chemical kinetic solver SAGE [107]. To solve the ordinary differential equations (ODE) present in the SAGE model there is decided to use the CVODE dense solver, which is recommended when the total number of species is less than 100 [129]. The CVODE dense solver is a backward differentiation method (BDF). The solver uses a small timestep as the initial timestep. Subsequently, to increase the time step a first order weighted average of data from prior time steps is employed, while certain limiters like the CFL value are used to limit the maximum size of the timestep [130]. To reduce the computational effort, the temperature is only resolved when the temperature change across a timestep is larger than 2 Kelvin. Moreover, the CVODES dense solver calculates the Jacobian matrix of the ODE system analytically rather than numerically [131].

Furthermore to reduce the computational cost, an adaptive zoning method is applied. Cells are grouped based on their thermodynamic state. In this project the equivalence ratio and temperature are used [132]. In literature most often a bin size of 5 K for temperature and 0.05 for equivalence ratio is used [133] [134] [135]. However, since NO_x emissions are of special interest in this study, it was decided to use a bin size of 2.5 K and 0.01 for the equivalence ratio.

4.3. Numerical details

The LES equations are resolved using the Pressure-Implicit with Splitting of Operators (PISO) algorithm for the pressure-velocity coupling available in the commercial software ConvergeCFD [104] [136]. A minimum of 2 and a maximum of 9 iterations are used to solve the velocity and pressure fields through a predictor-corrector strategy, with a convergence criterion based on density. An external loop is used to solve for the energy, species and other passives transport equations. A variable time step is used to guarantee a CFL number smaller than 0.5 everywhere in the domain. The temporal terms are discretized using an implicit Euler scheme, while second order central schemes are used for all the convective terms except for the subgrid kinetic energy transport equation, where an upwind scheme is used. No blended scheme or limiters are used.

Boundary conditions are assigned as follows. A flat velocity profile is specified at the inlets according to the mass flow rates from the experimental data, while a zero-gradient condition is given at the outlet. At the walls the boundary layer is not entirely resolved within the computational grid, therefore wall functions are used along with the non-slip condition. Both the Werner and Wengle model [137] and the Law of the Wall model [138] were tested in preliminary simulations, discussed in section 5. Temperature is assigned at the inlet using data from the experiments, and adiabatic condition is assumed at the walls. All scalars are zero at the inlet except for oxygen, nitrogen and fuel, which are specified according to their respective mass-flow rates. A zero-gradient condition is used for all scalars at the outlet and on the wall, except for the subgrid kinetic energy, which is zero at the walls.

The mesh has been setup using the adaptive mesh refinement approach available in ConvergeCFD. A baseline mesh with a typical cell size of 5 mm in all directions is used for initialisation purposes. Subsequently, the mesh is refined based on sub-grid scale (SGS) velocity, wall distance values and the TFM thickening factor [139]. The SGS values refine where the gradient of a field variable between two cells is higher than a certain threshold. The SGS value is derived from the first term of an infinite series expansion [140]. Since, the software is able to output the SGS field values, the criteria can be defined a posteriori.

The mesh is refined when the SGS value is greater than 1E-07 for the TFM factor and 1E-03 for the

velocity. In addition, refinement is applied when the Yplus value is greater than 15. The maximum refinement level corresponds to a cell width which is 16 times smaller than the original cell width for the SGS criteria and 64 times smaller for the Yplus value. The total number of cells is limited to 6M cells with a max cell size in the flame front of 0.3 mm and of 1.25 mm in the region of interest (up to a downstream location of $9R$ in the combustion chamber). At the wall, the height of the first cell is limited to a maximum $y^+ = 15$, ensuring that it entirely contains the viscous sublayer. A typical mesh at a generic time step is shown in Fig. 3.1, it can be seen how the mesh gets refined near the wall, and in the regions where the flame front is expected. The Pope's criterion [25], discussed in section 2.3.7 was used to evaluate the mesh quality in preliminary simulations.

Each simulation is run for five flow-through times, defined as the time required for the flow to develop through the domain until a steady average mass flow rate at an axial location of z = 0.11 m (9R) is reached. Two flow-through times are used to guarantee the steady state and three to collect the statistics. All simulations were run on the TU Delft HPC12 internal cluster using between 128-480 cores in parallel. This resulted in about $1.9 \cdot 10^5$ CPU hours per simulation on a wall-clock using 2.3 GHz AMD processors.

4.4. OpenFoam non-reacting simulation

For validation purposes, a non-reacting CH_4 simulation was carried out using a custom solver based on rhoPimpleFoam, available in OpenFoam. The One-Equation kEqn turbulence model [141] was employed. The mesh is inspired by the mesh depicted in Fig. 3.1. It is refined in the swirler, mixing tube, near the wall and around the flame front before gradually becoming coarser downstream. The unstructured mesh involves 14.5M tetrahedral cells with a max cell size of 2 mm in the region of interest (up to a downstream location of $9R$ in the combustion chamber). The time step is set to $3 \cdot 10^{-7}$s, leading to a CFL number between 0.3 and 0.35. The LES equations are resolved using a combination of PISO and Semi-Implicit Method for Pressure-Linked Equations (SIMPLE), called PIMPLE [142]. Three inner loops are used to solve the pressure and velocity and two outer loops for the scalars. The 2_{nd} order Gauss Linear scheme is used for the diffusion terms and a blend between Gauss linear and upwind is used for the TKE and enthalpy. The temporal terms are discretized using an implicit Euler scheme. The kqRWallFunuction wall function is used to provide a zero-gradient boundary condition for the TKE between the wall and the first cell [143].

4.5. Post-Processing methods

The results are analysed using Tecplot 360. The software relies on a finite volume concept in which the velocity field varies linearly within the face of a given cell, including those that share a physical wall [144]. For automatic extraction of data that is not necessarily cell-centred, Tecplot macros have been designed by the author of this report, which can be stored in Tecplot's working directory so that they are loaded on start-up. An example of such a macro is placed in the Appendix. The analyses that require explanation are described in the sections below.

4.5.1. Swirl number

The analysis of the development of the effective swirl number in the mixing tube validates the intended geometric swirl number and serves as a crucial indicator of the flow field and mixing efficiency [80], as described in section 2.2.4. Since the cell size is not uniform along a cross section, the axial flux of the angular momentum (Equation 2.8) and the axial momentum (Equation 2.9) are rewritten to Equation 4.4 and Equation 4.5.

$$G_\theta = \sum \left(v_{\tan} r \rho v_{ax} \text{cellwidth}^2 \right) \tag{4.4}$$

$$G_x R = \sum \left(\rho v_{ax}^2 \text{cellwidth}^2 r \right) \tag{4.5}$$

4.5.2. Unmixedness

At fuel-lean conditions, there are significant correlations between the degree of unmixedness, the presence of instabilities [145], and NOx emissions [146]. The degree of unmixedness in the flame region is therefore analysed according to the method of Li et al. [146]. The difference in cell size is taken into account by arranging the cells in the mixing tube in bins according to their radius so that the bins have the same cross-sectional area. The equivalence ratio, averaged in space and time, is calculated from the mean values of each bin. The standard deviation of the equivalence ratio is used as a parameter for unmixednesss determined by comparing the temporal mean of each bin with the spatial and temporal mean equivalence ratio.

4.5.3. POD analysis

The complex turbulent swirled dynamics in the combustor might hinder the presence of a PVC. Therefore a proper orthogonal decomposition (POD) method is used in this work to analyse the LES dataset with the Snapshot method, developed by Sirovich [147]. In this method the flow is decomposed into a set of deterministic functions capturing portions of the total kinetic energy (TKE) of the flowfield. A correlation matrix (C_s) is computed as

$$C_s = \frac{1}{m-1} V V^T \tag{4.6}$$

where V is the velocity matrix in Y-direction and m is the total number of considered LES time steps [148]. The degree of correlation between the velocity fluctuations in Y-direction at various locations can subsequently be assessed by determining the eigenvalues (A_S) of the correlation matrix. Therefore, it is possible to relate these eigenvalues to the coherent structures found in a flow. By ordering the eigenvalues on size, the temporal modes are sorted based on their contribution to the TKE [148]. To compute the spatial coefficients (Φ_s) of the modes the transported Y-velocity matrix is projected onto the temporal modes A_s as

$$\Phi_s = V^T A_s. \tag{4.7}$$

5
Results and Analysis

This chapter presents and analyzes the results by first discussing the sensitivity analysis performed to build the final model in section 5.1. Second, in section 5.2, the non-reactive and reactive cases of CH_4 are validated with the PIV data. Finally, the effects of H_2 addition are analyzed in section 5.3.

5.1. Sensitivity analysis

A preliminary sensitivity analysis using different turbulence models and mesh sizes is carried out for the non-reacting CH_4/air case. Time averaged axial velocity $\langle \tilde{W} \rangle$ profiles are computed and compared with the experimental data along the radial direction in the combustion chamber at different stream-wise locations z, with $z = 0$ corresponding to the outlet of the mixing tube. The simulation is repeated using three different meshes composed of 3, 6 and 12 million elements respectively, combined with two turbulence models: the dynamic structure model (DS) and the Smagorinsky model (Smag). The distribution of the cells across the three different meshes is depicted in Fig. 5.2. In Fig. 5.1 can be seen that the predicted velocity field does not exhibit a strong dependence on the chosen mesh. Thus, the 6M elements mesh is retained for the following analysis, after having verified that the Pope's criterion is satisfied everywhere in the domain for the CH_4 reacting case, as shown in Fig. 5.3. Results obtained with different turbulence models are also very similar, with a relative error of the peak velocity that remains below 3% at any axial point. Since the dynamic structure model is suited for anisotropic turbulence effects that may arise in the reacting case [149], the latter is used from now on to carry out the LES.

To examine the distinction between the Werner and Wengle wall model [137] and the Law of the Wall model [138], another preliminary analysis is conducted. In Fig. 5.4, the mean axial velocities at the first cell from the wall, on the $x = 0$ plane and for $y > 0$, are shown for both models along the axial direction in the mixing tube. Similar mean axial velocities are obtained, but the Werner and Wengle model is computationally more efficient and is therefore used in this work.

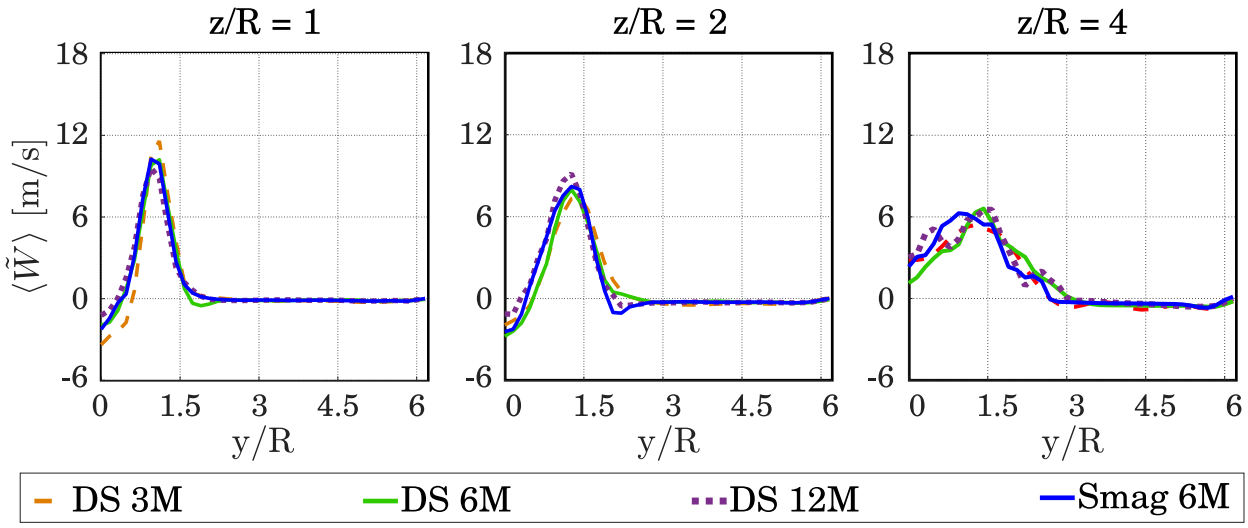

Figure 5.1: Radial profiles of mean axial velocity at different streamwise locations obtained from non-reacting methane/air LES, for different mesh size and two turbulence models: Dynamic Structure model (DS) and Smagorinsky model (Smag)

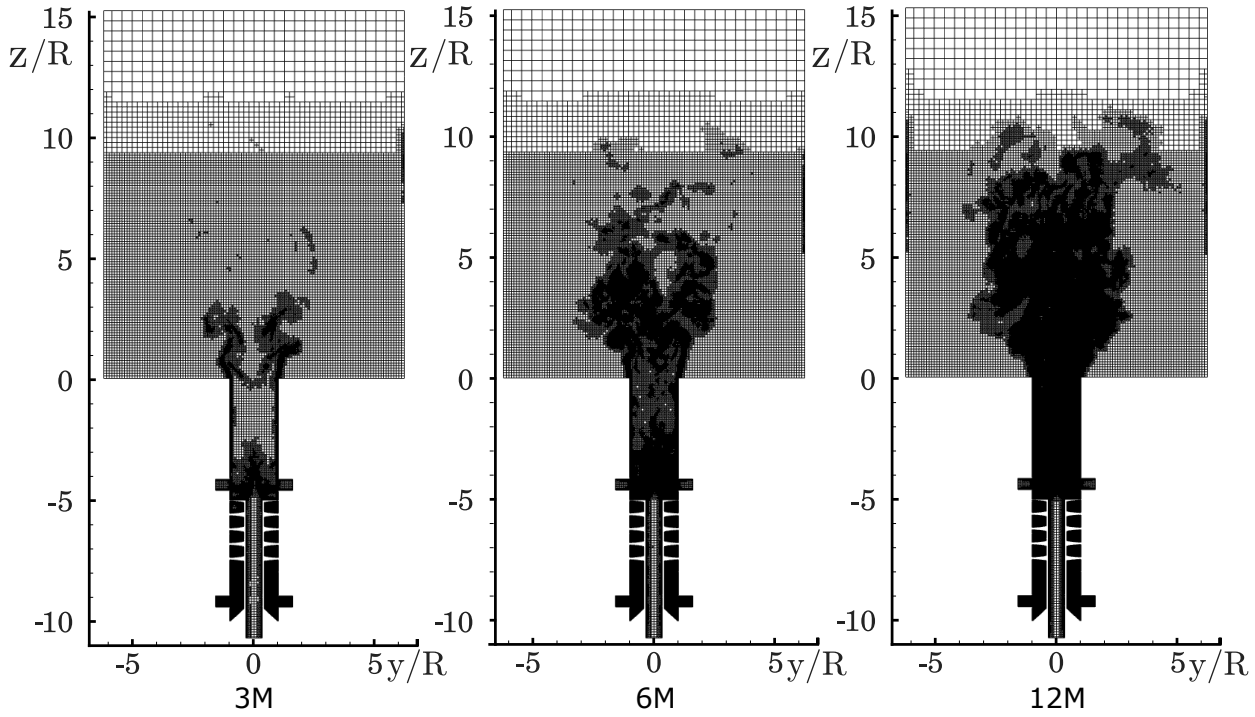

Figure 5.2: Meshes containing 3M cells (left), 6M cells (middle) and 12M cells (right) on the $x = 0$ plane till $z/r = 15$

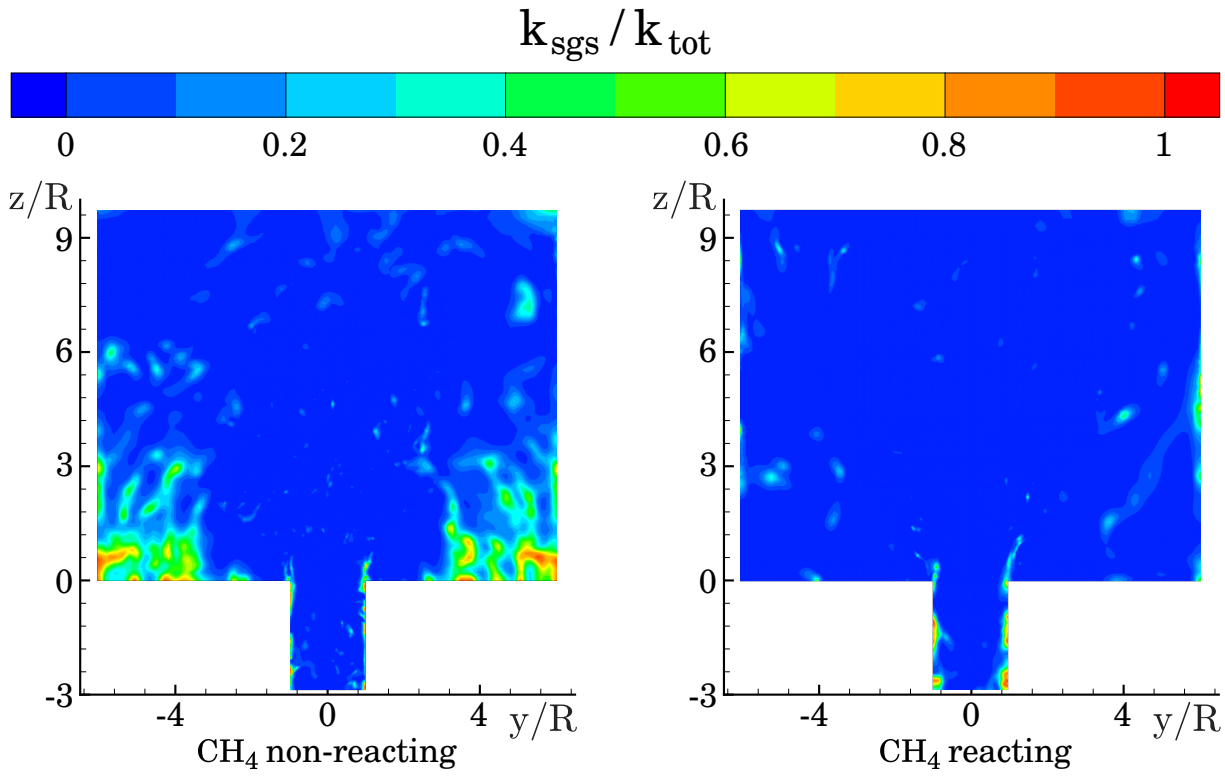

Figure 5.3: Pope's criterion: cell values of the subgrid to total turbulent kinetic energy from methane/air LES

Finally, a sensitivity analysis on the imposed CFL number is carried out. Fig. 5.5 illustrates the time-averaged axial velocity profiles for the CFL values of 0.3, 0.5, and 0.7 for various axial locations z in the combustion chamber on the $x = 0$ plane. The flow field does not exhibit a strong dependence on the imposed CFL numbers for the non-reacting CH4 simulation. A CFL number of 0.5 is chosen, following the recommendations of Xiao et al. [150] for a premixed swirl lean burner.

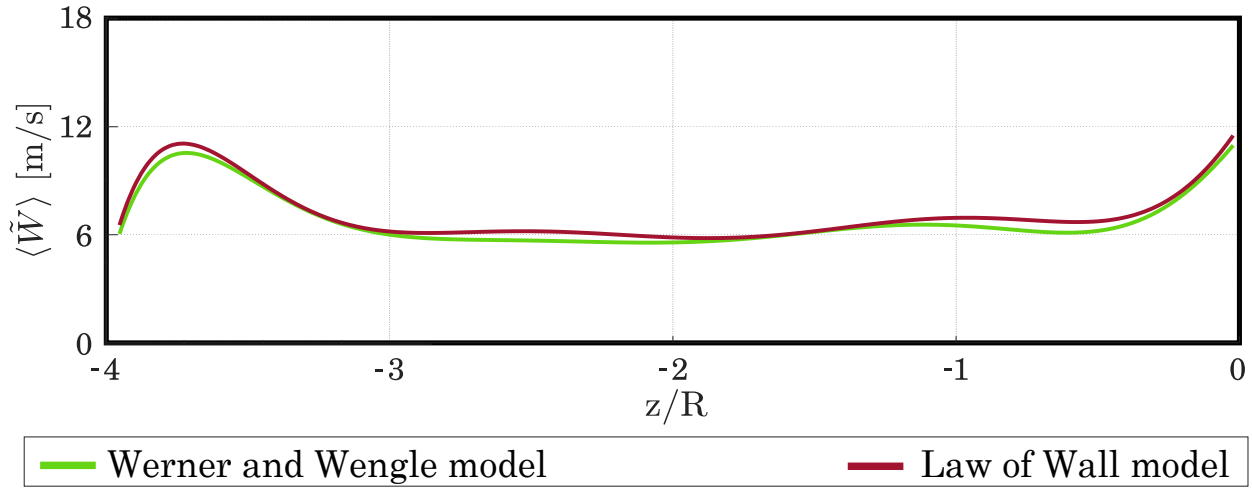

Figure 5.4: Axial profile of mean axial velocity at the first cell in the mixing tube from non-reacting methane/air LES

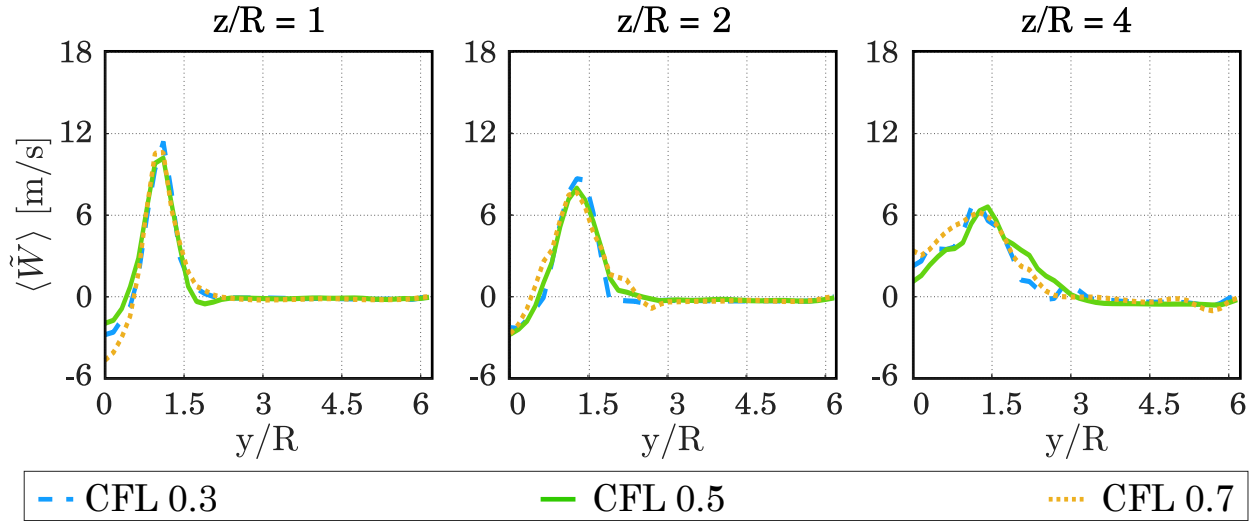

Figure 5.5: Radial profiles of mean axial velocity at different streamwise locations obtained from non-reacting methane/air LES, for different CFL numbers

5.2. Validation

The averaged axial velocity profiles, obtained from the Converge simulations, are compared with data from the experiments in Fig. 5.6 for both non-reacting and reacting (100% CH_4 fuel only) cases. For the non-reacting case, the value of the velocity peak appears to be predicted fairly well; nevertheless, its predicted position in the radial direction is underestimated due to a difference in the spreading rate of the jet. The averaged axial velocity contours in the plane $x = 0$ are shown in Fig. 5.7 for the non-reacting case, which also includes the OpenFoam simulation. It shows that the larger opening of the jet in the experimental case is related to a larger inner recirculation zone extending to $z/R = 4$ with a stronger backflow velocity. It is further noted that the radial location and magnitude of the jet are consistent in the OpenFoam and Converge simulations.

A strong sensitivity of the spreading jet on the outlet boundary conditions was observed in the experimental campaign for the non-reacting case. Given the similarities between the Converge and the OpenFoam simulation, it might be a good idea to revisit the boundary conditions in a later study. Since such a sensitivity was not observed for the reacting simulations, no further investigation is conducted in this project, also considering the relatively good match between LES and measurements in the reacting case, to be discussed next.

Comparisons between LES and experimental radial profiles of mean axial velocity for the reacting case shown in Fig. 5.6, indicate that the LES is able to predict the velocity peak and its radial location with good

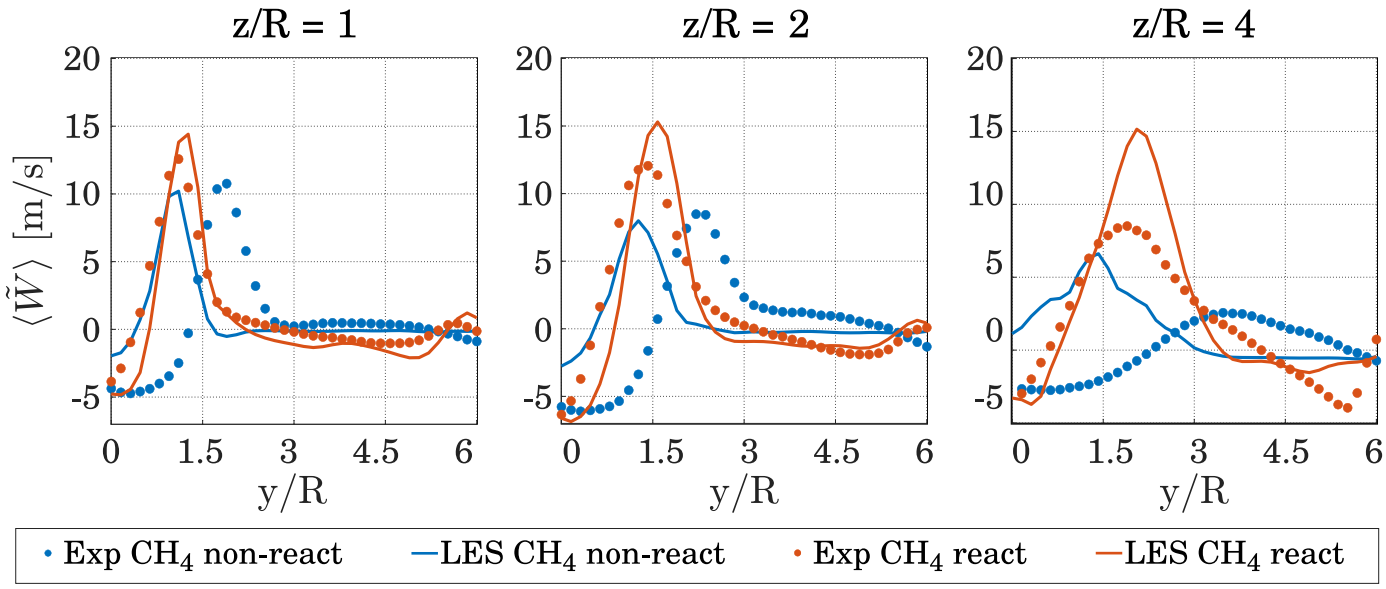

Figure 5.6: Comparison mean axial velocity profiles obtained from LES (solid lines) and experiments (symbols) at various axial locations, for the CH_4 non-reacting and reacting cases

accuracy up to a downstream coordinate $z = 2R$. Further downstream, the LES still predicts the correct location of the peaks and overall velocity behaviour, indicating a correct spreading rate as compared to experiments; however, it over-predicts the peak velocity value at $z = 4R$. This over-prediction of the peak velocity could be caused by insufficient mixing in the SGS model [151], or to the presence of an exhaust confinement in the experimental case [152].

Due to the above analysis, we conclude that the LES predicts with relatively good accuracy the reacting flow field. Since velocity gradients increase due to the heat release from the flame, these comparisons further suggest that the correct flame shape and position is captured, although quantitative investigations on temperature and species could not be performed as this data was not available from experiments. Because of the above reasons, the LES setup with TFM and detailed chemistry is further used for the investigations in the next sections.

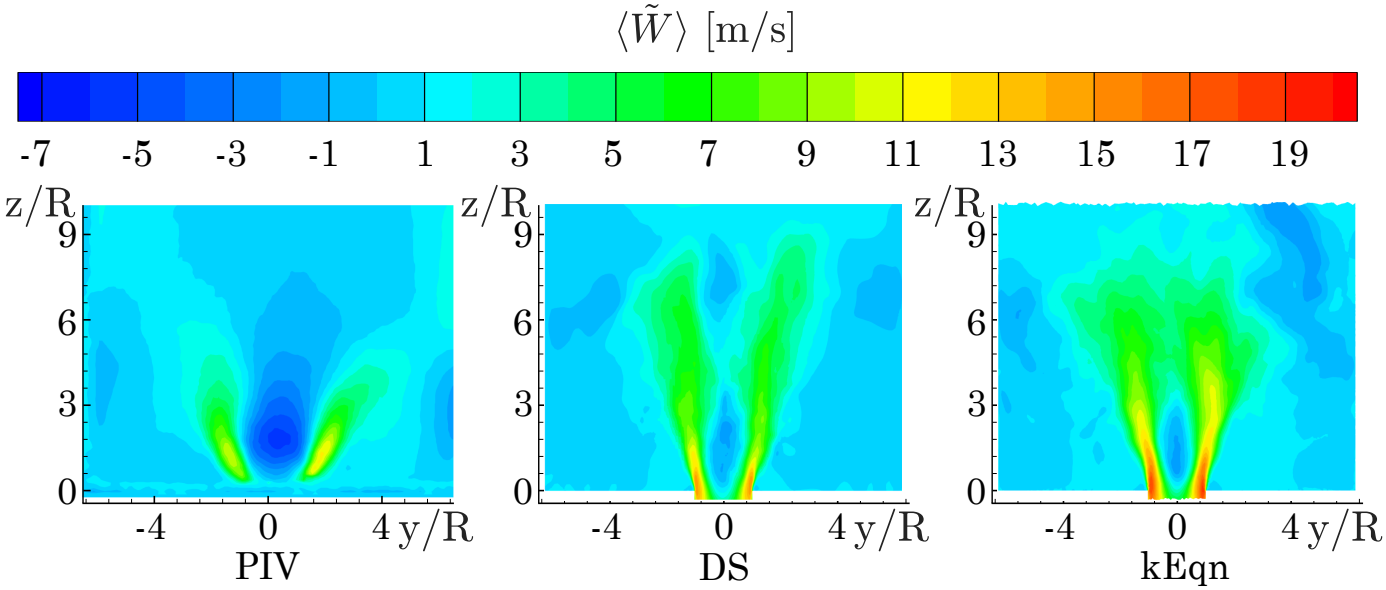

Figure 5.7: Velocity contour plot non-reacting CH_4 case, experiments (left), Converge simulation (centre) and OpenFoam simulation (right)

5.3. Hydrogen blend simulations

The effects of H_2 addition in the fuel stream are investigated in this section for both non-reacting and reacting cases. Mean axial velocity radial profiles at different streamwise locations are shown in Fig. 5.8. Overall, the addition of hydrogen shows little effect on the velocity field in the non-reacting case. Although this was somewhat expected (the fuel/air mixture is lean), this assessment was worth it given the high diffusivity and low density of hydrogen, and its possible effect on mixing properties. In the reacting case, the addition of H_2 results in a higher maximum velocity of the jet and in a shift of the peak closer to the axis ($y/R = 0$). This is due to a more upstream location of the flame anchoring point, which can be observed in Fig 5.10. The mixing tube bounds the momentum increase in the radial direction, favouring the stream-wise momentum increase. In addition, the jet exhibits a wider opening jet angle in the reacting cases, which is the result of the combined effects of heat release and lower density of the products, which lead to an increased velocity in the normal direction of the M-shaped flame.

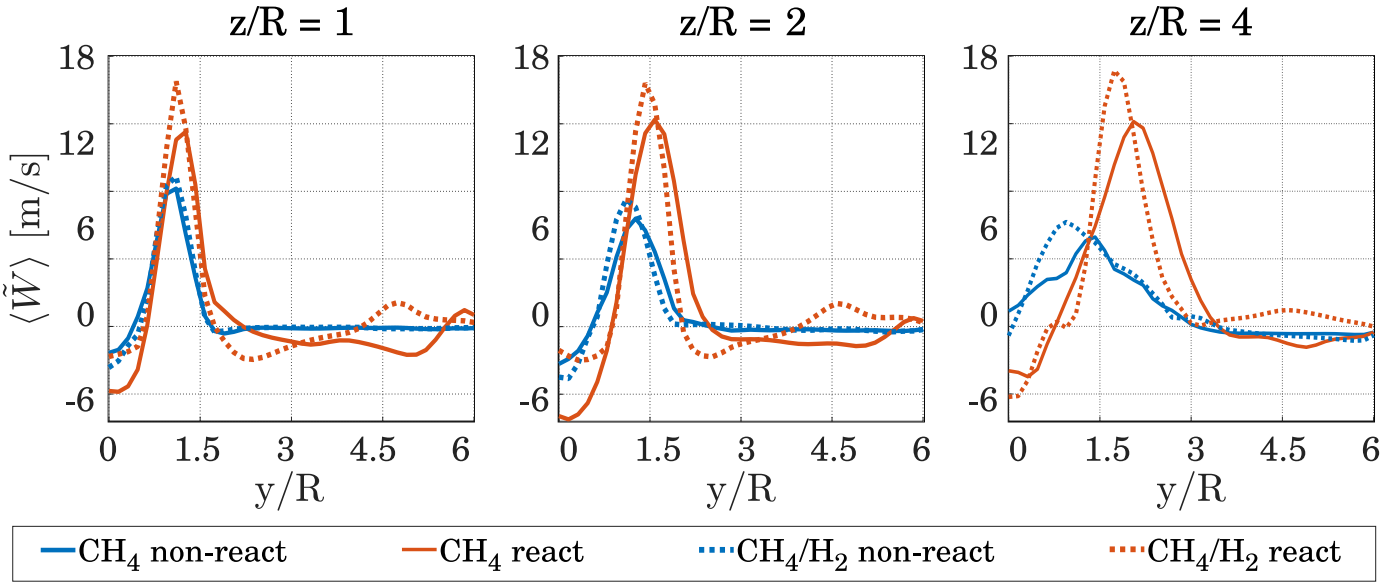

Figure 5.8: Mean axial velocity profiles from the LES for different fuel mixtures (reacting and non-reacting) are compared at different streamwise locations

To better understand the flow in the combustion chamber, the evolution of swirl number SW, equivalence ratio ϕ, and its standard deviation σ through the mixing tube are further investigated in Fig. 5.9. The effective swirl number corresponds to the geometric swirl number of 1.1 at the swirler outlet. This effective swirl number increases in the mixing tube first to then decrease quickly at $z/R \approx -4.5$. This decrease is due the reduction of irregularities in the radial and tangential directions as the flow evolves in the mixing tube, consistently to previous studies [153]. In addition, it is aided by the fuel injection between $z/R = -4.1$ and $z/R = -4.6$. In turn, this affects the viscous dissipation and radial flow divergence, thus the axial flux of angular momentum [154]. The resulting effective swirl number at the mixing tube outlet remains 0.77 for both the non-reacting cases, and it decreases to 0.61 and 0.57 respectively for the CH_4-only and the CH_4/H_2 blend reacting cases. This decrease as compared to the non-reacting case is caused by the increased axial velocity at the combustion chamber inlet [154], and this increase is of larger amount in the hydrogen blend case as was observed for Fig. 5.6. Also, the higher effective swirl number of the reacting CH_4 mixture results in a wider opening of the jet as compared to the CH_4/H_2 reacting case, which is visible in Fig 5.8 [155]. These differences could affect the mixedness of the flow downstream, causing variation of equivalence ratio in the flame region with a direct effect on the emission [4, 156].

The level of unmixedness in the flame region is therefore quantified using the method of Li et al [146]. By looking at the mean behaviour of equivalence ratio Φ and its standard deviation σ in Fig 5.9, one can notice that, while the mixture becomes substantially leaner when hydrogen is added to the mixture, no significant change occurs in terms of σ. This suggests that any change in emissions, to be analysed later,

has to be attributed to variation in mean equivalence ratio, rather than turbulent mixing.

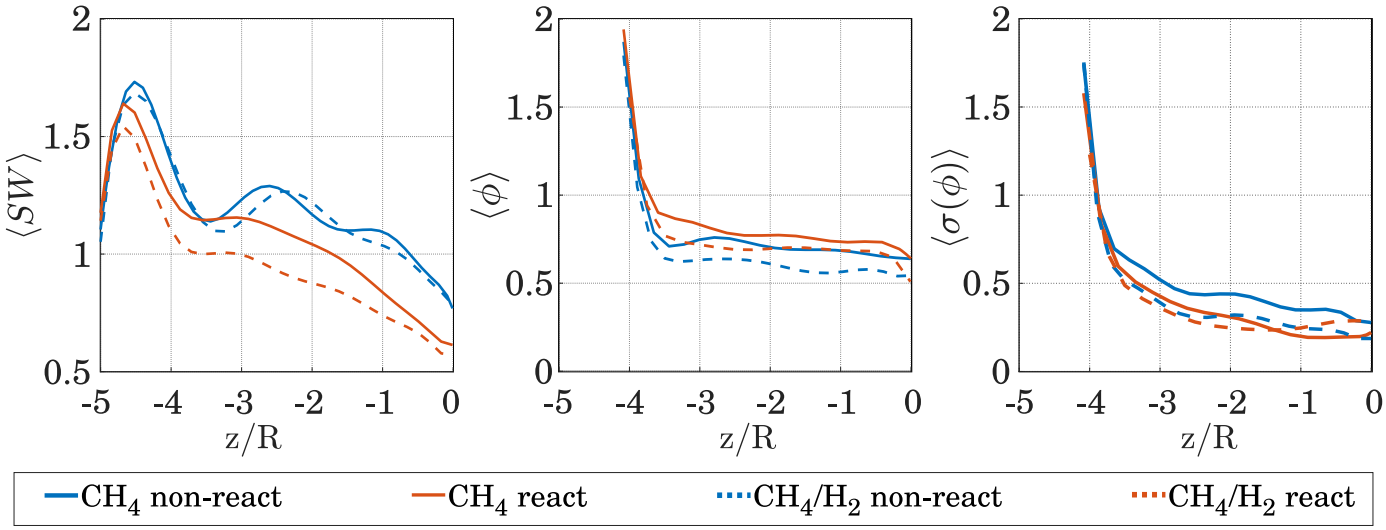

Figure 5.9: Axial profiles of mean swirl number (left), equivalence ratio (centre) and its variance (right) in the mixing tube ahead of the combustor chamber. The region near the combustor entrance, indicated by the dashed rectangle is zoomed out in the top-right of the figures for clarity

Further insights on the flow field behaviour between methane-only and hydrogen blend cases can be provided by looking at the mean temperature field in Fig 5.10. The main observation is that temperature is in general significantly higher in the CH_4 case, which is somewhat counter-intuitive. Nevertheless, lower temperatures in the hydrogen blend case are mainly driven by the overall leaner mixture in this case. This observation is consistent with flamelet calculations using CHEM1D [157], where the adiabatic flame temperature is $1924K$ for CH_4 at $\phi = 0.75$ and $1895K$ for the CH_4/H_2 mixture at $\phi = 0.70$. This result has profound implications in the design of new-generation combusting devices employing swirl-stabilised flame systems. The above result, suggests that when operating at the same power, the use of hydrogen can be beneficial in terms of NO_x emissions due to the lower temperatures, at least for the configuration investigated. A more quantitative assessment on emissions is thus presented next.

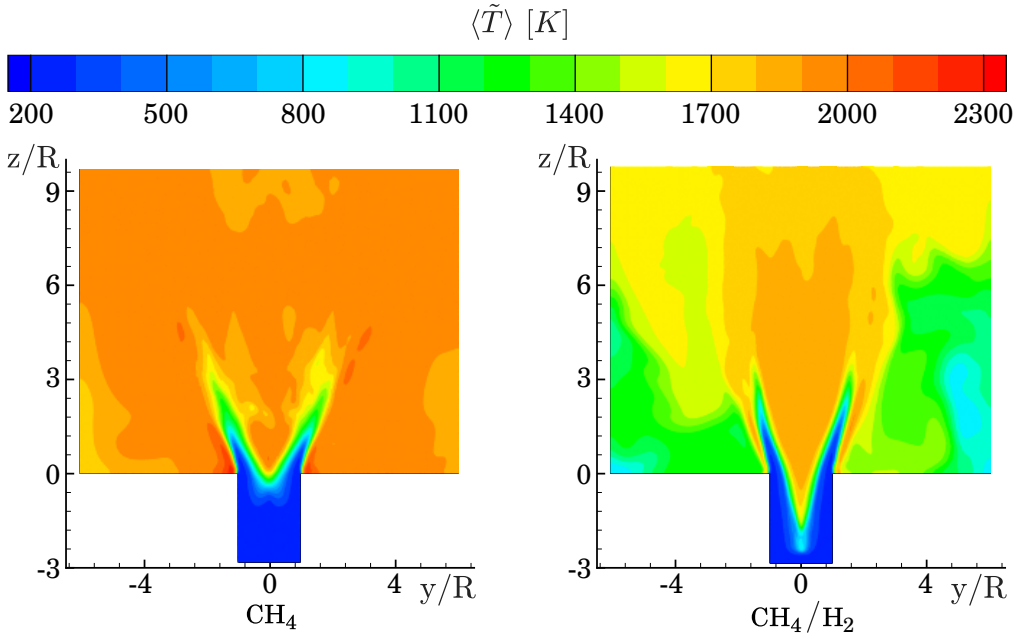

Figure 5.10: Midplane contours of mean temperature from LES for the methane-only and hydrogen enriched cases

5.3.1. Emissions insights

In Table 5.1, the mean mass fraction of CO_2, CO and NO_x at the combustor outlet plane are given. The addition of hydrogen to the fuel results in a decrease in CO_2 and CO, as one would expect with a fuel mixture containing fewer carbon atoms. Moreover, consistently with the decrease of temperature peaks, an overall decrease of 88% of NO is observed. This is an important observation, since the use of hydrogen in lean burn combustors has to be assessed from the same power setting as done in this work.

Table 5.1: Computed mass fraction of species at the outlet plane

Species	CH4	CH4/H2	Difference %
CO2	0.113	0.080	-27%
CO	6.75E-04	3.05E-05	-95%
NO	4.91E-05	6.03E-06	-88%

5.3.2. Stability insights insights

Pressure oscillations and heat release fluctuations caused by PVC may act as drivers for thermoacoustic instabilities [158]. The precession of a PVC is indicated by a spatial phase shift of 90° between two modes [159]. The eigenvalue of the spectrum of the POD modes represents the contribution of the PVC to the total fluctuating kinetic energy. According to this criterion, it can be determined that a PVC is present for both fuel mixtures for both the non-reactive and reactive CH_4 and $CH4/H_2$ cases, see Fig 5.11 and Fig 5.12. This is also in agreement with the study of Dellenback et al. considering the effective swirl number at the combustor inlet [84]. When hydrogen is added to the fuel the modes associated to the PVC tends to interest a more downstream location in the combustor. This behaviour may be associated to a later development of the helicoidal structure of the PVC, which may be caused by the increased flame wrinkling [160] and/or the lower effective swirl number at the combustor outlet [84].

From the TKE and frequency analysis of the POD analysis can be concluded that the TKE and the frequency are in the same order of magnitude for the non-reacting cases. Consistency in the simulation can be inferred from these macro features, which remain essentially the same. Furthermore, it is observed that the TKE increases for the reacting cases. This may indicate the presence of flame generated turbulence [12].

No flashback was observed during the simulation time when hydrogen was added to the mixture. On the other hand, from the temperature profiles in Fig 5.10 it can be seen that, for the CH_4/H_2 mixture, the flame has significantly moved upstream and within the mixing tube. This flame anchoring position is not ideal from practical perspectives as flashback could still be triggered at later times.

Blowout is analysed qualitatively in this project with the contour plots of the OH mass fraction and progress variable. The instantaneous OH mass fraction profiles in the plane x=0 are shown in Fig. 5.7, here the white contour line denotes 25% of the maximum OH mass fraction. No holes in the OH mass fraction profiles are observed, indicating that no severe local extinctions are present in either mixture. Furthermore, the thermochemical state of the mixture is described using the progress variable which is zero for the unburned reactants and 1 for the fully burned mixture. It is defined using the sum of the CO_2

Table 5.2: Turbulent kinetic energy (TKE) (in plane x: 0 m, y: -0.07 – 0.07 m, z: 0–0.1 m) and frequency of PVC from POD for the CH_4 and CH_4/H_2 LES cases. NR is non reacting and R is reacting

	CH_4 non-react	CH_4/H_2 non-react	CH_4 react	CH_4/H_2 react
Frequency [Hz]	253	257	377	217
TKE [m$\hat{2}$/s&2]	8726	9512	24051	23200

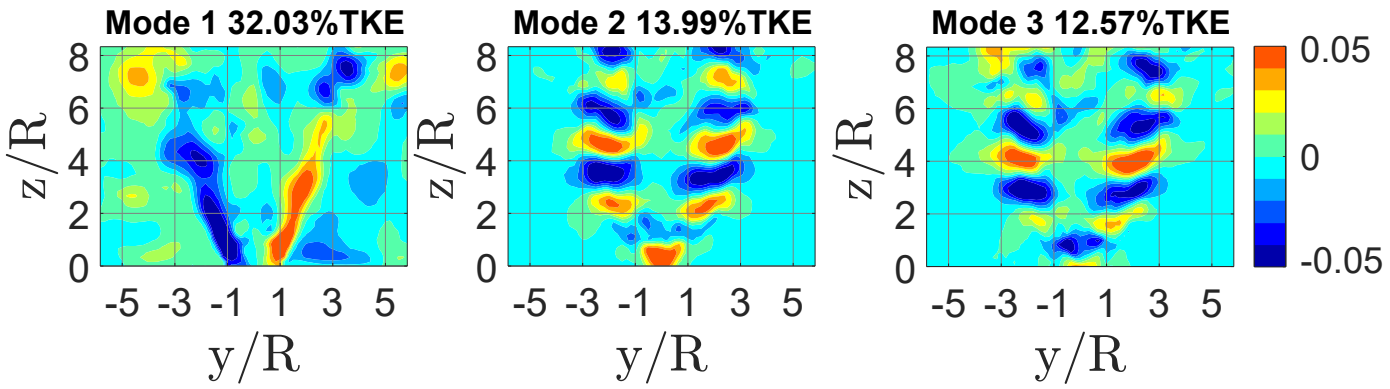

Figure 5.11: Midplane contours of the first three POD modes for the CH4 reacting case

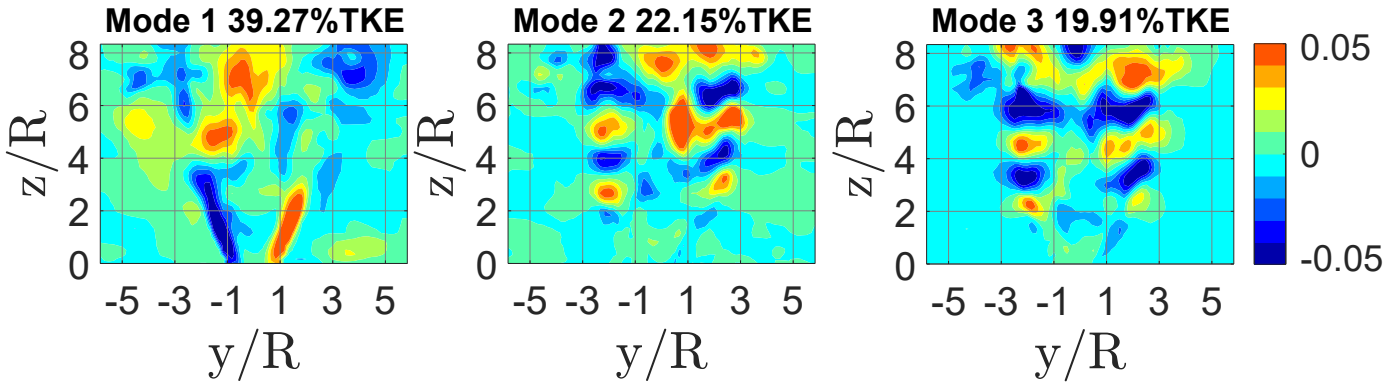

Figure 5.12: Midplane contours of the first three POD modes for the CH4/H2 reacting case

and H_2O mass fractions divided by the sum of the mass fractions of CO_2 and H_2O at the same equivalence number for a burned mixture computed using CHEM1D [161]. No spatial discontinuities can be seen in Fig. 5.15, which would suggest breaks in the reaction rate.

An attempt is made to describe the inner structure, and physical behaviour of the flame using the Borghi-Peters diagram [43]. The flame is filtered by blanking out cells with a progress variable smaller than 0.8 or larger than 0.95 [162]. In addition, the cells with a value of the TFM sensor which is lower than 0.001 are blanked, since the TFM sensor includes the reaction rate, as described in section 4.2. The data visible in the regime diagrams are taken from the time steps shown in Fig. 5.15. In general Kolmogorov eddies can enter reaction regions for $Ka > 100$, leading to local extinctions [163]. In Fig. 5.13, can be seen that it is not expected that severe local extinctions are present, especially in the CH_4/H_2 case. In addition, the Borghi diagram indicates that the flame is more laminar in the CH_4/H_2 mixture, as there are more scatterings in the region of lower Reynolds numbers. This observation corresponds to the flame fronts displayed in Fig. 5.15.

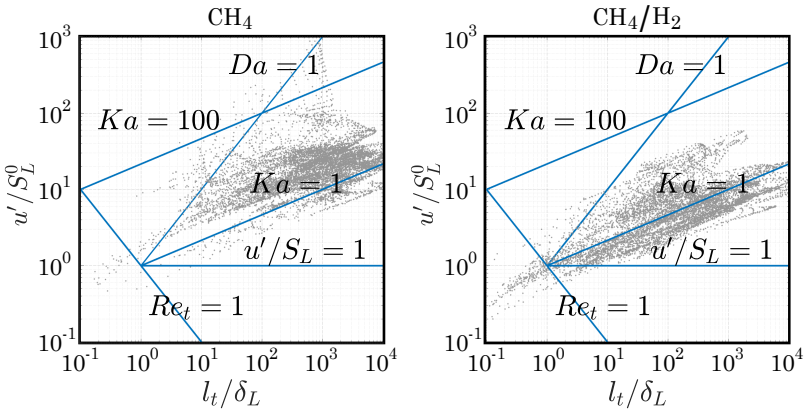

Figure 5.13: Borghi diagram, CH_4 (left), CH/H_2 (right)

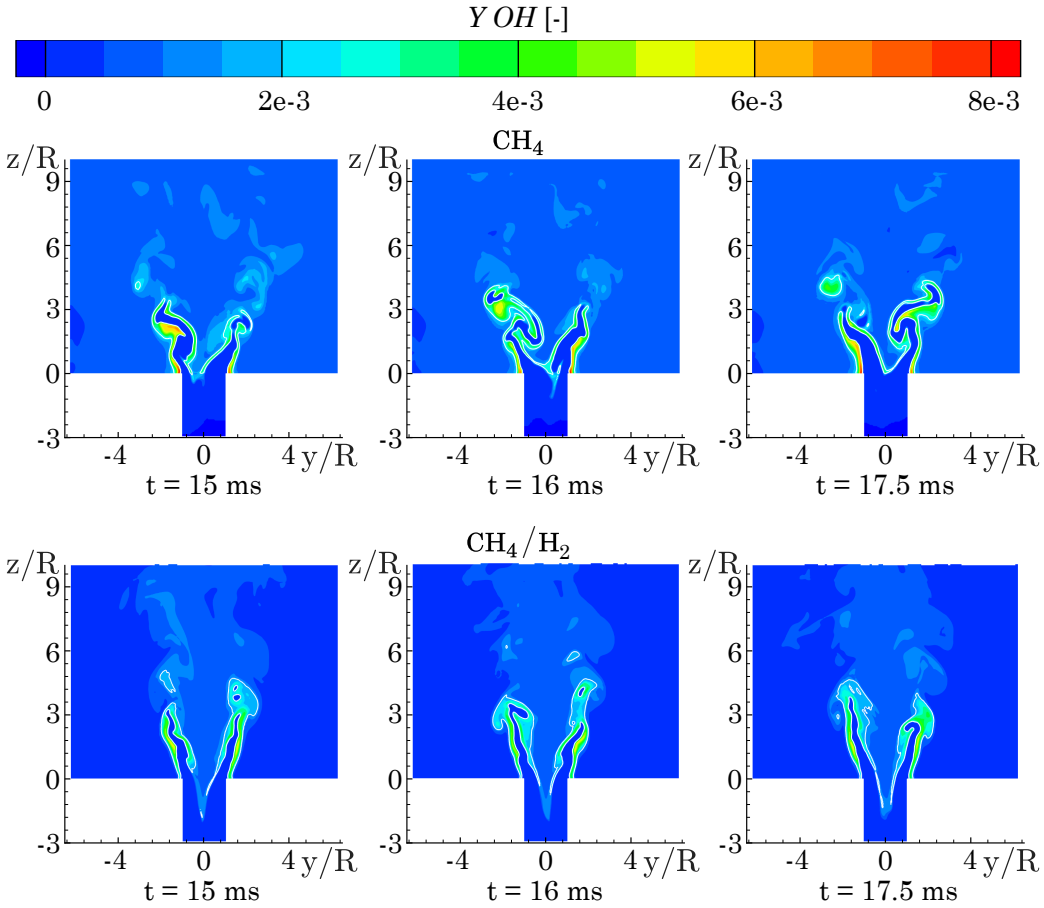

Figure 5.14: Mass fraction of OH contour, CH_4 (upper), CH_4/H_2 (lower)

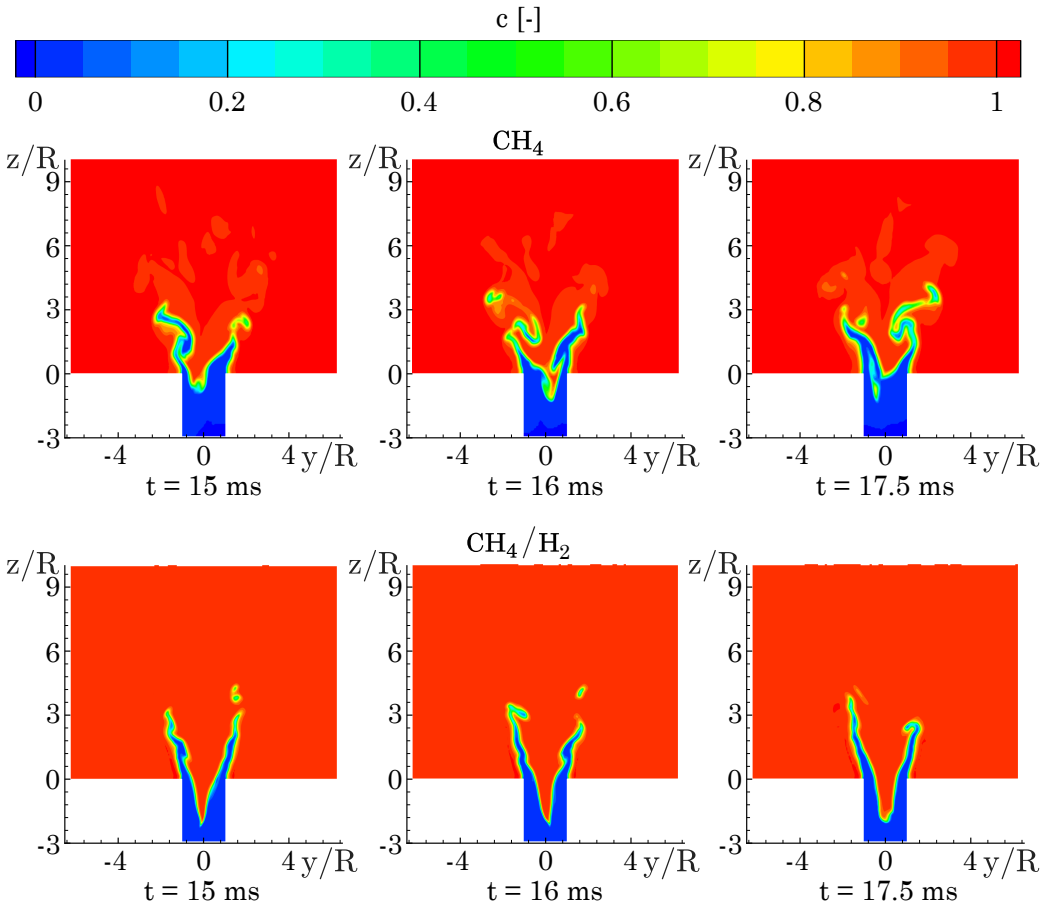

Figure 5.15: Normalized progress variable c, CH_4 (upper), CH_4/H_2 (lower)

6
Conclusion

As emission regulations to combat global warming become more stringent, the aviation industry is looking for propulsion and energy alternatives to conventional gas turbine engines. Hydrogen combustion is the most promising approach for powering long-haul flights, but significant NO_x emissions could arise. A possible solution to the problem of increased NO_x emissions is lean premixed combustion. Furthermore, a swirl-stabilised flow that creates recirculation zones can be used to provide sufficient flame stability while reducing NO_x emissions. Axial air injection is used to counteract the increased flashback propensity of the inner recirculation zone.

Methane and a hydrogen enriched methane mixtures have been studied in this work using LES paradigms and detailed chemistry with a thickened flame approach. Results have been first validated for the methane-only case against experimental measurements of axial velocity, showing that the LES is able to predict the reacting flow field with good accuracy. The effects of hydrogen addition on the emissions and flame stability have then been analysed. Results indicate that, when keeping the power constant, CO emissions decrease by 95% and NO emissions by 88% in mass fraction. These significant reductions are observed to be driven by the fact that the flame burns locally at leaner equivalence ratios, implying lower local temperatures. The POD analysis of the fluctuating velocity field in the y-direction indicates the presence of a precessing vortex core (PVC) in the flow. Finally, although no flashback was observed in the LES as consequence of the addition of hydrogen, the flame was observed to stabilise significantly upstream as compared to the methane-only case. This suggests that further research is needed in order to develop safe-operating burners fuelled with hydrogen or hydrogen blends. Furthermore, it can be qualitatively observed that the number of severe local extinctions is limited, especially in the CH_4/H_2 mixture.

7
Recommendations

This chapter evaluates the study and identifies areas of improvement. Recommendations are also made for future research that could complement this study. The goal of future research is a more accurate model and a better combustion design that produces fewer emissions yet is stable enough.

7.1. Research reflection and improvement

This section discusses analyses that would contribute to the project's objective without changing the geometry or operating conditions, but were not given the necessary priority to be carried out due to time constraints.

- **Refine mesh where the Pope's criterion is not satisfied**
  Evaluation of the mesh of the non-reacting CH_4 simulation using Pope's criterion shows that the ratio of the subgrid kinetic energy to the total kinetic energy is not under 0.2 everywhere. Since the velocity in this area is very low and therefore refinement here was not expected to significantly affect the flow, it was decided to continue using the mesh. However, for future studies, uncertainty about the validity of the flow field decreases when this area is refined.

- **Flame transfer function for stability analysis**
  To better understand the phenomenon leading to instability, it is important to know how the flame responds to flow disturbances, which is characterised by the flame transfer function. This relates fluctuations in velocity, pressure or equivalence ratio to fluctuations in heat release for a specific burner geometry [164] [165]. Several models exist that link the output of the flame transfer function to predictions about the frequency of combustion instabilities. However, since determining the transfer function of a particular burner is challenging [166], it was decided to prioritise elsewhere.

- **Quantitative assessment of local extinctions**
  An examination of the scatter plots of temperature versus mixing fraction allows a more quantitative analysis of local extinctions. As the temperature decreases at a point of extinction, scatters with temperatures significantly lower than the adiabatic flame temperature for a given mixing fraction indicate local extinctions [167]. Due to uncertainties that emerged during the analysis, possibly caused by an incorrect determination of the mixture fraction according to Bilger's definition [168] and uncertainties regarding the calculated adiabatic flame temperature for the mixture of CH_4/H_2 using CHEM1D, it was determined that a quantitative evaluation of the local extinctions was not worth the time investment. The Borghi diagram and the contour plots of the OH mass fraction and progress variable already show that there were no severe local extinctions in either mixture.

7.2. Recommendations and next steps

This section contains recommendations for further work that contributes to the objective of the project. It is divided into suggestions to improve model accuracy and suggestions to optimise geometry or operating conditions.

7.2.1. Potential model improvements

Since the mass flow across axial slices is consistent with the experimental results, the effective swirl number is consistent with the geometric swirl number and the axial velocity fields of the OpenFoam simula-

tion are similar to the Converge CFD simulations, there may be uncertainty about the exhaust pressure in the combustion chamber. Numerically, the meshes in the downstream part of the combustion chamber may not be fine enough to accurately represent the effect of the exhaust pressure. Furthermore, because of the curved exhaust pipe in the experiments, the exhaust pressure may be different from the atmospheric pressure. Whether the difference is experimental or numerical could be determined by sensitivity analysis of the meshes in the downstream part of the combustor and testing different exhaust pressure values. Moreover, it would be useful to measure the exhaust pressure in the experiments.

7.2.2. Potential design improvements

The design modifications, together with their justifications, are presented as individual adjustments to the geometry and operating conditions of the project. Due to the complexity of the effects, it is difficult to predict a priori which combination of design changes would lead to lower emissions at stable combustion.

- **Higher percentage H_2 in the fuel**
  Significant reductions in CO_2, CO and NO are observed when changing the fuel to 60% H2 and 40% CH4 in volume, while flashback or severe local extinctions did not occur in the simulated model. Therefore, it would be interesting to see how a higher concentration of hydrogen in the fuel affects emissions and stability. For higher hydrogen contents, the location of the flame should be evaluated, since it is already located in the mixing tube. It may be necessary to lengthen the mixing tube or increase the amount of axial air injection to prevent dangerous expansion of the flame upstream in the mixing tube.

- **Higher effective swirl number**
  As a weak recirculation zone is observed, it is possible that a higher effective swirl number may better retain hot products and radicals, reducing NO and CO concentrations [169]. However, a higher effective swirl number may also cause the flame to move further upstream, increasing the flashback propensity [79]. Furthermore, a higher swirl number can make the flame more sensitive to thermoacoustic vibrations [170].

- **Smaller axial air injection tube**
  For the same AAI mass flow, a smaller AAI tube diameter would yield a larger axial velocity component but with a smaller radius, which could reduce the degradation of the effective swirl number in the mixing tube [4]. Therefore, this design change could lead to a more intense recirculation zone without increasing the flashback propensity.

- **Dilution holes in mixing tube**
  At higher concentrations of hydrogen in the fuel mixture, the boundary layer flashback propensity could increase [171]. Dilution holes in the mixing tube reduces the equivalence ratio near the wall, resulting in reduced burning velocities and thereby reducing the risk of boundary layer flashback [4]. The location of the dilution holes is important because the injected flow and the flow in the mixing tube mix significantly, making the dilution effect decrease rapidly as the distance between the flame and the injection site increases [172].

Bibliography

[1] E van der Sman et al. *Destination 2050: A Route to Net Zero European Aviation*. 2021.

[2] Eun Seong Cho and Suk Ho Chung. "Improvement of flame stability and NOx reduction in hydrogen-added ultra lean premixed combustion". In: *J. Mech. Sci. Technol.* 23.3 (2009), pp. 650–658. ISSN: 1738494X. DOI: 10.1007/s12206-008-1223-x.

[3] Jadeed Beita et al. "Thermoacoustic Instability Considerations for High Hydrogen Combustion in Lean Premixed Gas Turbine Combustors: A Review". In: *Hydrogen* 2.1 (2021), pp. 33–57.

[4] Thoralf G Reichel. "Flashback prevention in lean-premixed hydrogen combustion". PhD thesis. 2017.

[5] Stephen B Pope. "Ten questions concerning the large-eddy simulation of turbulent flows". In: *New J. Phys.* 6.1 (2004), p. 35.

[6] Denis Veynante and Luc Vervisch. "Turbulent combustion modeling". In: *PECS* 28.3 (2002), pp. 193–266.

[7] O. Colin et al. "A thickened flame model for large eddy simulations of turbulent premixed combustion". In: *PoF* 12.7 (2000), pp. 1843–1863. DOI: 10.1063/1.870436. URL: https://doi.org/10.1063/1.870436.

[8] Joseph Brand et al. "Potential use of hydrogen in air propulsion". In: *AIAA International Air and Space Symposium and Exposition: The Next 100 Years*. 2003, p. 2879.

[9] Paul Palies. *Stabilization and Dynamic of Premixed Swirling Flames: Prevaporized, Stratified, Partially, and Fully Premixed Regimes*. Academic Press, 2020.

[10] Carmen J Giunta. "What's in a name? amount of substance, chemical amount, and stoichiometric amount". In: *J. Chem. Educ.* 93.4 (2016). ACS Publications, pp. 583–586.

[11] Derek Dunn-Rankin. *Lean combustion: technology and control*. Academic Press, 2011.

[12] Ivan Langella. "Large eddy simulation of premixed combustion using flamelets". PhD thesis. University of Cambridge, 2016.

[13] Paul Palies. *Stabilization and Dynamic of Premixed Swirling Flames: Prevaporized, Stratified, Partially, and Fully Premixed Regimes*. Academic Press, 2020.

[14] Bidhan Dam, Norman Love, and Ahsan Choudhuri. "Flashback propensity of syngas fuels". In: *Fuel* 90.2 (2011), pp. 618–625.

[15] Evatt R Hawkes and Jacqueline H Chen. "Direct numerical simulation of hydrogen-enriched lean premixed methane–air flames". In: *Combust Flame*. 138.3 (2004), pp. 242–258.

[16] Pieter DePape and Igor Novosselov. "Model-based approach for combustion monitoring using real-time chemical reactor network". In: *J. Combust.* 2018 (2018).

[17] Francisco José Jiménez-Espadafor Aguilar and José Antonio Vélez Godiño. "Innovative power train configurations for aircraft auxiliary power units focused on reducing carbon footprint". In: *Aerosp Sci Technol* 106 (2020), p. 106109.

[18] Panagiotis Giannakakis et al. "Fuel burn evaluation of a turbo-electric propulsive fuselage aircraft". In: *AIAA Propulsion and Energy 2019 Forum*. 2019, p. 4181.

[19] *The Appu Project*. 2020. URL: https://www.tudelft.nl/lr/appu.

[20] Thierry Poinsot and Denis Veynante. *Theoretical and Numerical Combustion*. 2011.

[21] Yang Zhiyin. “Large-eddy simulation: Past, present and the future”. In: *CJA* 28.1 (2015), pp. 11–24.

[22] Irvin Glassman, Richard A Yetter, and Nick G Glumac. *Combustion*. Academic press, 2014.

[23] C Pantano and S Sarkar. “A subgrid model for nonlinear functions of a scalar”. In: *PoF* 13.12 (2001), pp. 3803–3819.

[24] Stanley Corrsin. “Turbulent flow”. In: *AmSci* 49.3 (1961), pp. 300–325.

[25] Stephen B Pope and Stephen B Pope. *Turbulent flows*. Cambridge university press, 2000.

[26] Stefan Hickel. *06 LES*. 2021. URL: https://brightspace.tudelft.nl/d2l/le/content/397950/viewContent/2274110/View.

[27] Tomio Okawa et al. “Fundamentals for power engineering”. In: *Fundamentals of Thermal and Nuclear Power Generation*. Elsevier, 2021, pp. 77–226.

[28] Lamyaa A El-Gabry, Douglas R Thurman, and Philip E Poinsatte. *Procedure for determining turbulence length scales using hotwire anemometry*. National Aeronautics and Space Administration, Glenn Research Center, 2014.

[29] Sergey V Simonenko, Vyacheslav B Lobanov, et al. “The application of the generalized differential formulation of the first law of thermodynamics for evidence of the tidal mechanism of maintenance of the energy and viscous-thermal dissipative turbulent structure of the Mesoscale oceanic eddies”. In: *J. Mod. Phys.* 9.03 (2018), p. 357.

[30] Chemistry LibreTexts. *Radical Reactions*. Sept. 2021. URL: https://chem.libretexts.org/Bookshelves/Organic_Chemistry/Organic_Chemistry_(McMurry.

[31] Stephen R Turns et al. *Introduction to combustion*. Vol. 287. McGraw-Hill Companies New York, NY, USA, 1996.

[32] Hassan El Bari et al. “Kinetics models of methane production from anaerobic digestion”. In: *Clean Energy and Resources Recovery*. Elsevier, 2021, pp. 271–294.

[33] William H. Green. *Combustion chemistry*. 2014.

[34] S Zandaryaa and A Buekens. “Control of nitrogen oxides”. In: *Pollution Control Technologies* 2 (2014).

[35] David Stansel et al. “Gas Turbine Emissions Improvements by Advances in Design, Analysis, Materials, Manufacturing, and Control Technology”. In: *Proceedings of the 47th Turbomachinery Symposium*. Turbomachinery Laboratory, Texas A&M Engineering Experiment Station. 2018.

[36] H Kolla et al. “Scalar dissipation rate modeling and its validation”. In: *Combust. Sci. Technol.* 181.3 (2009), pp. 518–535.

[37] Arnaud Trouvé. “The production of premixed flame surface area in turbulent shear flow”. In: *Combust Flame*. 99.3-4 (1994), pp. 687–696.

[38] Vladimir A Sabelnikov and Andrei Nikolaevich Lipatnikov. “Bifractal nature of turbulent reaction waves at high Damköhler and Karlovitz numbers”. In: *PoF* 32.9 (2020), p. 095118.

[39] R Borghi. “On the structure and morphology of turbulent premixed flames”. In: *Recent advances in the Aerospace Sciences*. Springer, 1985, pp. 117–138.

[40] N. Peters. “Laminar flamelet concepts in turbulent combustion”. In: *Symposium (International) on Combustion* 21.1 (1988). Twenty-First Symposuim (International on Combustion), pp. 1231–1250. ISSN: 0082-0784. DOI: https://doi.org/10.1016/S0082-0784(88)80355-2. URL: https://www.sciencedirect.com/science/article/pii/S0082078488803552.

[41] Philipp Trisjono et al. “Modeling turbulence–chemistry interaction in lean premixed hydrogen flames with a strained flamelet model”. In: *Combust Flame*. 174 (2016), pp. 194–207.

[42] Srikant Srinivasan and Suresh Menon. “Linear eddy mixing model studies of high Karlovitz number turbulent premixed flames”. In: *Flow Turbul. Combust.* 93.2 (2014), pp. 189–219.

[43] M Düsing, A Sadiki, and J Janicka. “Towards a classification of models for the numerical simulation of premixed combustion based on a generalized regime diagram”. In: *CTMOFQ* 10.1 (2006), pp. 105–132.

[44] KR Sreenivasan and S Raghu. “The control of combustion instability: A perspective”. In: *Curr. Sci.* (2000), pp. 867–883.

[45] K Harstad and J Bellan. “The Lewis number under supercritical conditions”. In: *Int. J. Heat Mass Transf.* 42.6 (1999), pp. 961–970.

[46] Moshe Matalon. “Flame dynamics”. In: *Proc Combust Inst.* 32.1 (2009), pp. 57–82.

[47] Forman A Williams and Joseph F Grcar. “A hypothetical burning-velocity formula for very lean hydrogen–air mixtures”. In: *Proc Combust Inst.* 32.1 (2009), pp. 1351–1357.

[48] Tim Lieuwen et al. “Burner development and operability issues associated with steady flowing syngas fired combustors”. In: *Combust. Sci. Technol.* 180.6 (2008), pp. 1169–1192.

[49] Ahsan Choudhuri. *Effects of combustion-induced vortex breakdown on flashback limits of syngas-fueled gas turbine combustors*. Tech. rep. Univ. of Texas at El Paso, TX (United States), 2011.

[50] M Kröner, J Fritz, and T Sattelmayer. “Flashback limits for combustion induced vortex breakdown in a swirl burner EC] ASME Turbo Expo 2002: Power for Land”. In: *Sea, and Air* (2002), pp. 413–422.

[51] Jassin Fritz, Martin Kröner, and Thomas Sattelmayer. “Flashback in a swirl burner with cylindrical premixing zone”. In: *Turbo Expo: Power for Land, Sea, and Air*. Vol. 78514. American Society of Mechanical Engineers. 2001, V002T02A021.

[52] S Daniele, P Jansohn, and Konstantinos Boulouchos. “Experimental investigation of lean premixed syngas combustion at gas turbine relevant conditions: lean blow out limits, emissions and turbulent flame speed”. In: *Proceedings of 32nd Annual Meeting of the Italian Section on the Combustion Colloquia*. The Combustion Institute Pittsburgh, PA. 2009.

[53] Nicholas Syred. “A review of oscillation mechanisms and the role of the precessing vortex core (PVC) in swirl combustion systems”. In: *PECS* 32.2 (2006), pp. 93–161.

[54] Maarten Vanierschot, Mustafa Percin, and BW Van Oudheusden. “Double helix vortex breakdown in a turbulent swirling annular jet flow”. In: *Phys. Rev. Fluids* 3.3 (2018), p. 034703.

[55] A Gorbunova et al. “Precessing vortex core in a swirling wake with heat release”. In: *Int. J. Heat Fluid Flow* 59 (2016), pp. 100–108.

[56] *Gases - Explosion and Flammability Concentration Limits*. URL: https://www.engineeringtoolbox.com/explosive-concentration-limits-d_423.html (visited on 02/22/2022).

[57] *Minimum Ignition Energy*. URL: https://marinechemistassociation.com/wp-content/uploads/2018/09/ (visited on 02/22/2022).

[58] *Adiabatic Flame Temperatures*. URL: https://www.engineeringtoolbox.com/adiabatic-flame-temperature-d_996.html (visited on 02/22/2022).

[59] Charles L Keesee, Bing Guo, and Eric L Petersen. “Laminar Flame Speed Measurements of Kerosene-Based Fuels Accounting for Uncertainties in Mixture Average Molecular Weight”. In: *J. Eng. Gas* 143.4 (2021).

[60] Hideo Watanabe. “Thermal Conductivity and Thermal Diffusivity of Sixteen Isomers of Alkanes: C n H2 n+ 2 (n= 6 to 8)”. In: *J. Chem. Eng. Data.* 48.1 (2003), pp. 124–136.

[61] Isidoro Martinez. *Thermal data - Mass diffusivity data*. URL: http://webserver.dmt.upm.es/~isidoro/dat1/ (visited on 02/23/2022).

[62] Sara McAllister, Jyh-Yuan Chen, and A Carlos Fernandez-Pello. “Thermodynamics of combustion”. In: *Fundamentals of combustion processes*. Springer, 2011, pp. 15–47.

[63] Victor P Zhukov, Vladislav A Sechenov, and Andrey Yu Starikovskiy. “Autoignition of kerosene (Jet-A)/air mixtures behind reflected shock waves”. In: *Fuel* 126 (2014), pp. 169–176.

[64] Fang Wang et al. “Numerical research on kerosene/air rotating detonation engines under different injection total temperatures”. In: *Aerosp Sci Technol* 103 (2020), p. 105899.

[65] *Fuels Higher and Lower Calorific Values*. URL: https://www.engineeringtoolbox.com/fuels-higher-calorific-values-d_169.html (visited on 06/14/2022).

[66] A. Lipatnikov and J. Chomiak. “Turbulent flame speed and thickness: Phenomenology, evaluation, and application in multi-dimensional simulations”. In: *PECS* 28 (Dec. 2002), pp. 1–74. DOI: 10.1016/S0360-1285(01)00007-7.

[67] Fabien Halter et al. “Characterization of the effects of pressure and hydrogen concentration on laminar burning velocities of methane–hydrogen–air mixtures”. In: *Proc Combust Inst.* 30.1 (2005), pp. 201–208.

[68] Karrar S Hasan, Wisam A Abd Al-wahid, and HHS Khwayyir. “Flashback and combustion stability in swirl burners”. In: *IOP Conference Series: Mater. Sci. Eng.* Vol. 928. 2. IOP Publishing. 2020, p. 022045.

[69] Chenglong Tang, Yingjia Zhang, and Zuohua Huang. “Progress in combustion investigations of hydrogen enriched hydrocarbons”. In: *Renewable Sustainable Energy Rev.* 30 (2014), pp. 195–216.

[70] Marc Ross. “Fuel efficiency and the physics of automobiles”. In: *Contemp. Phys.* 38.6 (1997), pp. 381–394.

[71] Bruce G Miller. “Clean coal technologies for advanced power generation”. In: *Clean Coal Engineering Technology* 7 (2011), pp. 251–300.

[72] Thoralf G. Reichel, Steffen Terhaar, and Oliver Paschereit. “Increasing Flashback Resistance in Lean Premixed Swirl-Stabilized Hydrogen Combustion by Axial Air Injection”. In: *J. Eng. Gas* 137.7 (July 2015). ISSN: 0742-4795.

[73] Tim Lieuwen et al. “Fuel flexibility influences on premixed combustor blowout, flashback, autoignition, and stability”. In: *J. Eng. Gas* 130.1 (2008).

[74] James G Speight. *Handbook of industrial hydrocarbon processes*. Gulf Professional Publishing, 2019, pp. 421–463.

[75] Evatt R Hawkes and Jacqueline H Chen. “Direct numerical simulation of hydrogen-enriched lean premixed methane–air flames”. In: *Combust Flame.* 138.3 (2004), pp. 242–258.

[76] Jurgen Warnatz et al. *Combustion*. Springer, 2006.

[77] C Angelberger et al. “Large eddy simulations of combustion instabilities in premixed flames”. In: *Proc. of the Summer Program*. Citeseer. 1998, pp. 61–82.

[78] Zhiguo Qu et al. “Premixed combustion in a porous burner with different fuels”. In: *Combust. Sci. Technol.* 187.3 (2015), pp. 489–504.

[79] Ashoke De and Sumanta Acharya. “Parametric study of upstream flame propagation in hydrogen-enriched premixed combustion: Effects of swirl, geometry and premixedness”. In: *Int. J. Hydrog. Energy* 37.19 (2012), pp. 14649–14668.

[80] Chigier N. Beer J. “M. and Chigier, NA, Combustion Aerodynamics”. In: *Appl. Sci. Publ. LTD* (1972).

[81] Seonghyeon Seo. *Parametric study of lean premixed combustion instability in a pressurized model gas turbine combustor*. The Pennsylvania State University, 1999.

[82] Zhi X Chen et al. “Large Eddy Simulation of a dual swirl gas turbine combustor: flame/flow structures and stabilisation under thermoacoustically stable and unstable conditions”. In: *Combust Flame*. 203 (2019), pp. 279–300.

[83] Nicholas Syred et al. “Effect of inlet and outlet configurations on blow-off and flashback with premixed combustion for methane and a high hydrogen content fuel in a generic swirl burner”. In: *Applied energy* 116 (2014), pp. 288–296.

[84] PA Dellenback, DE Metzger, and G_P Neitzel. “Measurements in turbulent swirling flow through an abrupt axisymmetric expansion”. In: *AIAA journal* 26.6 (1988), pp. 669–681.

[85] Baoyu Guo, Tim AG Langrish, and David F Fletcher. “Simulation of turbulent swirl flow in an axisymmetric sudden expansion”. In: *AIAA journal* 39.1 (2001), pp. 96–102.

[86] *Navier-Stokes equations*. 2012. URL: https://www.cfd-online.com/Wiki/Navier-Stokes_equations.

[87] Eric W Weisstein. *Kronecker delta*. Wolfram Research, Inc., 2002.

[88] Charles H Forsberg. *Heat transfer principles and applications*. Academic Press, 2020.

[89] C. Meneveau. “Turbulence: Subgrid-Scale Modeling”. In: *Scholarpedia* 5.1 (2010). revision #153312, p. 9489. DOI: 10.4249/scholarpedia.9489.

[90] Maurits H. Silvis et al. *A nonlinear subgrid-scale model for large-eddy simulations of rotating turbulent flows*. 2019. arXiv: 1904.12748 [physics.flu-dyn].

[91] Christopher Rutland. “Large-eddy simulations for internal combustion engines - A review”. In: *IInt. J. Engine Res.* 12 (Oct. 2011). DOI: 10.1177/1468087411407248.

[92] Eric Pomraning. “Development of Large Eddy Simulation Turbulence Models”. PhD thesis. Dec. 2000. DOI: 10.13140/2.1.2035.7929.

[93] Santanu De et al. *Modeling and simulation of turbulent combustion*. Springer, 2018.

[94] UCSD. *Chemical-Kinetic Mechanisms for Combustion Applications, San Diego Mechanism web page, Mechanical and Aerospace Engineering (Combustion Research)*. 2014.

[95] F Moukalled, L Mangani, and M Darwish. “Turbulence Modeling”. In: *The Finite Volume Method in Computational Fluid Dynamics*. Springer, 2016, pp. 693–744.

[96] Sanjiva K Lele. “Turbulence in compressible flows”. In: *Advanced Approaches in Turbulence*. Elsevier, 2021, pp. 399–481.

[97] Brian Edward Launder, Neil D Sandham, et al. *Closure strategies for turbulent and transitional flows*. Cambridge University Press, 2002.

[98] L Tian and RP Lindstedt. “Evaluation of reaction progress variable-mixture fraction statistics in partially premixed flames”. In: *Proc Combust Inst.* 37.2 (2019), pp. 2241–2248.

[99] Dominique Laurence and Wolfgang Rodi. *Engineering Turbulence Modelling and Experiments-4*. Elsevier, 1999.

[100] S Mukhopadhyay, JA Van Oijen, and LPH De Goey. “A comparative study of presumed PDFs for premixed turbulent combustion modeling based on progress variable and its variance”. In: *Fuel* 159 (2015), pp. 728–740.

[101] S. Sinharay. “Continuous Probability Distributions”. In: *International Encyclopedia of Education (Third Edition)*. Ed. by Penelope Peterson, Eva Baker, and Barry McGaw. Third Edition. Oxford: Elsevier, 2010, pp. 98–102. ISBN: 978-0-08-044894-7. DOI: https://doi.org/10.1016/B978-0-08-044894-7.01720-6. URL: https://www.sciencedirect.com/science/article/pii/B9780080448947017206.

[102] SC Gupta. “Delta function”. In: *IEEE Transactions on Education* 1 (1964), pp. 16–22.

[103] Daniel Lee, Eric Pomraning, and Christopher J Rutland. “LES modeling of diesel engines”. In: *SAE Transactions* (2002), pp. 2566–2578.

[104] Erik Tylczak. *Models on top of Models: Thickened flames in converge - converge CFD Software*. July 2020. URL: https://convergecfd.com/blog/models-on-top-of-models-thickened-flames-in-converge.

[105] Denis Veynante. “Large Eddy Simulations of Turbulent Combustion”. In: *Turbulence and Interactions*. Ed. by Michel Deville, Thien-Hiep Lê, and Pierre Sagaut. Berlin, Heidelberg: Springer Berlin Heidelberg, 2009, pp. 113–138. ISBN: 978-3-642-00262-5.

[106] Ludovic Durand and Wolfgang Polifke. “Implementation of the thickened flame model for large eddy simulation of turbulent premixed combustion in a commercial solver”. In: *Turbo Expo: Power for Land, Sea, and Air*. Vol. 47918. 2007, pp. 869–878.

[107] PK Senecal et al. “Multi-dimensional modeling of direct-injection diesel spray liquid length and flame lift-off length using CFD and parallel detailed chemistry”. In: *SAE transactions* (2003), pp. 1331–1351.

[108] Alessandro Di Mauro et al. “Modelling Aspects in the Simulation of the Diffusive Flame in A Bluff-Body Geometry”. In: *Energies* 14.11 (2021), p. 2992.

[109] Francesca di Mare, Robert Knappstein, and Michael Baumann. “Application of LES-quality criteria to internal combustion engine flows”. In: *Comput Fluids* 89 (2014), pp. 200–213.

[110] Lionel Temmerman et al. “Investigation of wall-function approximations and subgrid-scale models in large eddy simulation of separated flow in a channel with streamwise periodic constrictions”. In: *Int J Heat Fluid Flow* 24.2 (2003), pp. 157–180.

[111] Salim Mohamed Salim, M Ariff, and Siew Cheong Cheah. “Wall y+ approach for dealing with turbulent flows over a wall mounted cube”. In: *Prog. Comput. Fluid Dyn.* 10.5-6 (2010), pp. 341–351.

[112] Culbert B Laney. *Computational gasdynamics*. Cambridge university press, 1998.

[113] Hrvoje Jasak. *Error analysis and estimation for the finite volume method with applications to fluid flows*. Imperial College London (University of London), 1996.

[114] Georgios Matheou and Daniel Chung. “Large-eddy simulation of stratified turbulence. Part II: Application of the stretched-vortex model to the atmospheric boundary layer”. In: *JAS* 71.12 (2014), pp. 4439–4460.

[115] G Boudier, LYM Gicquel, and TJ Poinsot. “Effects of mesh resolution on large eddy simulation of reacting flows in complex geometry combustors”. In: *Combust Flame*. 155.1-2 (2008), pp. 196–214.

[116] Michael A Liberman et al. “Self-acceleration and fractal structure of outward freely propagating flames”. In: *PoF* 16.7 (2004), pp. 2476–2482.

[117] Valeria Di Sarli, Almerinda Di Benedetto, and Gennaro Russo. “Large Eddy Simulation of transient premixed flame–vortex interactions in gas explosions”. In: *Chem. Eng. Sci.* 71 (2012), pp. 539–551.

[118] van den Bergh A. *Design and test of a swirl-stabilized methane combustor with axial air injection*. Tu Delft, 2022. URL: https://repository.tudelft.nl/islandora/object/uuid:5262b98f-bf7d-481d-b2ff-e2816d3c9e12?collection=education.

[119] George B. Arfken et al. “chapter 25 - KINETIC THEORY”. In: *University Physics*. Ed. by George B. Arfken et al. Academic Press, 1984, pp. 460–473. ISBN: 978-0-12-059860-1. DOI: https://doi.org/10.1016/B978-0-12-059860-1.50030-8. URL: https://www.sciencedirect.com/science/article/pii/B9780120598601500308.

[120] Herbert IH Saravanamuttoo, Gordon Frederick Crichton Rogers, and Henry Cohen. *Gas turbine theory*. Pearson education, 2001.

[121] JB Bell et al. “Numerical simulation of a laboratory-scale turbulent V-flame”. In: *PNAS* 102.29 (2005), pp. 10006–10011.

[122] Richard D Keane and Ronald J Adrian. “Optimization of particle image velocimeters. I. Double pulsed systems”. In: *MST* 1.11 (1990), p. 1202.

[123] Charles Meneveau. “Turbulence: Subgrid-scale modeling”. In: *Scholarpedia* 5.1 (2010), p. 9489.

[124] Liqun Qi. “Eigenvalues and invariants of tensors”. In: *J. Math. Anal. Appl.* 325.2 (2007), pp. 1363–1377.

[125] Francesco Picano and K Hanjalić. “Leray-α regularization of the Smagorinsky-closed filtered equations for turbulent jets at high Reynolds numbers”. In: *Flow Turbul. Combust.* 89.4 (2012), pp. 627–650.

[126] Xinlei Liu et al. “A comparative numerical investigation of reactivity controlled compression ignition combustion using Large Eddy Simulation and Reynolds-Averaged Navier-Stokes approaches”. In: *Fuel* 257 (2019), p. 116023.

[127] Cedric Mehl, Shuaishuai Liu, and Olivier Colin. “A strategy to couple thickened flame model and adaptive mesh refinement for the LES of turbulent premixed combustion”. In: *Flow Turbul. Combust.* 107.4 (2021), pp. 1003–1034.

[128] M Frenklach et al. *Gri-mech: An optimized detailed chemical reaction mechanism for methane combustion. topical report, september 1992-august 1995*. Tech. rep. SRI International, Menlo Park, CA (United States), 1995.

[129] Abdurrahman Imren. “A Detailed Error Quantification Analysis of Extrapolation-Based Stiff ODE Solvers for Combustion CFD”. In: *Flow Turbul. Combust.* (2022), pp. 1–32.

[130] A Imren and DC Haworth. “On the merits of extrapolation-based stiff ODE solvers for combustion CFD”. In: *Combust Flame*. 174 (2016), pp. 1–15.

[131] Kirk J Vanden and Paul D Orkwis. “Comparison of numerical and analytical Jacobians”. In: *AIAA journal* 34.6 (1996), pp. 1125–1129.

[132] A Babajimopoulos et al. “A fully coupled computational fluid dynamics and multi-zone model with detailed chemical kinetics for the simulation of premixed charge compression ignition engines”. In: *Int. J. Engine Res.* 6.5 (2005), pp. 497–512.

[133] Nimal Naser et al. “On the effects of fuel properties and injection timing in partially premixed compression ignition of low octane fuels”. In: *Fuel* 207 (2017), pp. 373–388.

[134] Nour Atef et al. “Numerical investigation of injector geometry effects on fuel stratification in a GCI engine”. In: *Fuel* 214 (2018), pp. 580–589.

[135] Joohan Kim et al. “Numerical investigation of a fueled pre-chamber spark-ignition natural gas engine”. In: *IInt. J. Engine Res.* 23.9 (2022), pp. 1475–1494.

[136] Raad I Issa. “Solution of the implicitly discretised fluid flow equations by operator-splitting”. In: *J. Comput. Phys.* 62.1 (1986), pp. 40–65.

[137] H Werner and H Wengle. “Large-eddy simulation of turbulent flow over and around a cube in a plate channel”. In: *Turbulent shear flows 8*. Springer, 1993, pp. 155–168.

[138] Peter Bradshaw and George P Huang. “The law of the wall in turbulent flow”. In: *Proc. Math. Phys. Eng. Sci. P ROY SOC A-MATH PHY* 451.1941 (1995), pp. 165–188.

[139] Jean-Philippe Legier, Thierry Poinsot, and Denis Veynante. “Dynamically thickened flame LES model for premixed and non-premixed turbulent combustion”. In: *Proceedings of the summer program*. Vol. 12. Citeseer. 2000, pp. 157–168.

[140] KW Bedford and WK Yeo. “Conjunctive filtering procedures in surface water flow and transport”. In: *Large eddy simulation of complex engineering and geophysical flows* (1993), pp. 513–537.

[141] Akira Yoshizawa. “Statistical theory for compressible turbulent shear flows, with the application to subgrid modeling”. In: *The PoF* 29.7 (1986), pp. 2152–2164.

[142] Tobias Holzmann. “Mathematics, numerics, derivations and OpenFOAM®”. In: *Loeben, Germany: Holzmann CFD* (2016).

[143] Zhaoyang Xia et al. “VLES turbulence modelling for separated flow simulation with OpenFOAM”. In: *J. Wind. Eng. Ind. Aerodyn. J WIND ENG IND AEROD* 198 (2020), p. 104077.

[144] Fernando Luiz Sacomano Filho et al. “On the interaction between turbulence and ethanol spray combustion using a dynamic wrinkling model coupled with tabulated chemistry”. In: *Combust Flame*. 215 (2020), pp. 203–220.

[145] Tim Lieuwen, Yedidia Neumeier, and Ben T Zinn. “The role of unmixedness and chemical kinetics in driving combustion instabilities in lean premixed combustors”. In: *Combust. Sci. Technol.* 135.1-6 (1998), pp. 193–211.

[146] Hejie Li, Ahmed ElKady, and Andrei Evulet. “Effect of exhaust gas recirculation on NOx formation in premixed combustion system”. In: *47th AIAA Aerospace Sciences Meeting Including The New Horizons Forum and Aerospace Exposition*. 2009, p. 226.

[147] Lawrence Sirovich. “Turbulence and the dynamics of coherent structures. I. Coherent structures”. In: *Q. Appl. Math.* 45.3 (1987), pp. 561–571.

[148] Julien Weiss. “A tutorial on the proper orthogonal decomposition”. In: *AIAA aviation 2019 forum*. 2019, p. 3333.

[149] Christopher J Rutland. *Dynamic structure LES models*. Tech. rep. WISCONSIN UNIV-MADISON ENGINE RESEARCH CENTER, 2004.

[150] Hua Xiao et al. “3D simulation of ammonia combustion in a lean premixed swirl burner”. In: *Energy Procedia* 142 (2017), pp. 1294–1299.

[151] Bernhard Stiehl et al. “Numerical Simulation of an Axial-Staged Combustor at High Pressure”. In: *AIAA Scitech 2020 Forum*. 2020, p. 0630.

[152] Mohammed Abdulsada et al. “Effect of exhaust confinement and fuel type upon the blowoff limits and fuel switching ability of swirl combustors”. In: *Appl. Therm. Eng.* 48 (2012), pp. 426–435.

[153] Jaehoon Choi et al. “Modeling swirl decay rate of turbulent flows in annular swirl injectors”. In: *AIAA Journal* 56.12 (2018), pp. 4910–4926.

[154] Mohammad Shahsavari, Mohammad Farshchi, and Mohammad Hossien Arabnejad. “Large eddy simulations of unconfined non-reacting and reacting turbulent low swirl jets”. In: *Flow Turbul. Combust.* 98.3 (2017), pp. 817–840.

[155] Ying Huang and Vigor Yang. “Effect of swirl on combustion dynamics in a lean-premixed swirl-stabilized combustor”. In: *Proc Combust Inst.* 30.2 (2005), pp. 1775–1782.

[156] Stefan Dederichs et al. “Assessment of a gas turbine NOx reduction potential based on a spatiotemporal unmixedness parameter”. In: *J Eng Gas* 135.11 (2013).

[157] Bart Somers. “The simulation of flat flames with detailed and reduced chemical models”. PhD thesis. Gastec NV NL, 1994.

[158] Bo Zhang et al. “Thermoacoustic instability drivers and mode transitions in a lean premixed methane-air combustor at various swirl intensities”. In: *Proc Combust Inst.* 38.4 (2021), pp. 6115–6124.

[159] Kilian Oberleithner et al. “Formation and flame-induced suppression of the precessing vortex core in a swirl combustor: experiments and linear stability analysis”. In: *Combust Flame.* 162.8 (2015), pp. 3100–3114.

[160] Weijie Zhang et al. “Effect of differential diffusion on turbulent lean premixed hydrogen enriched flames through structure analysis”. In: *Int. J. Hydrogen Energy* 45.18 (2020), pp. 10920–10931.

[161] Balaji Muralidharan et al. “Application of a progress variable based approach for modeling non-premixed/partially premixed combustion under high-pressure conditions”. In: *JPC*. 2018, p. 4560.

[162] Tianwei Yang et al. “On the modeling of scalar mixing timescale in filtered density function simulation of turbulent premixed flames”. In: *PoF* 32.11 (2020), p. 115130.

[163] Norbert Peters. “Length Scales in Laminar and Turbulent Flames, Numerical Approaches to Combustion Modeling”. In: *Prog. Aerosp. Sci.* 135 (1991), pp. 155–182.

[164] Sébastien Ducruix, Daniel Durox, and Sébastien Candel. “Theoretical and experimental determinations of the transfer function of a laminar premixed flame”. In: *Proc Combust Inst.* 28.1 (2000), pp. 765–773.

[165] Seongpil Joo et al. “Thermoacoustic instability and flame transfer function in a lean direct injection model gas turbine combustor”. In: *Aerosp Sci Technol* 116 (2021), p. 106872.

[166] Alexis Giauque, Thierry Poinsot, and Franck Nicoud. “Validation of a flame transfer function reconstruction method for complex turbulent configurations”. In: *14th AIAA/CEAS Aeroacoustics Conference (29th AIAA Aeroacoustics Conference)*. 2008, p. 2943.

[167] Zhi X Chen et al. “Prediction of local extinctions in piloted jet flames with inhomogeneous inlets using unstrained flamelets”. In: *Combust Flame.* 212 (2020), pp. 415–432.

[168] R Cabra et al. “Lifted methane–air jet flames in a vitiated coflow”. In: *Combust Flame.* 143.4 (2005), pp. 491–506.

[169] PM Anacleto et al. “Swirl flow structure and flame characteristics in a model lean premixed combustor”. In: *Combust. Sci. Technol.* 175.8 (2003), pp. 1369–1388.

[170] Zhi X. Chen et al. “Large Eddy Simulation of a dual swirl gas turbine combustor: Flame/flow structures and stabilisation under thermoacoustically stable and unstable conditions”. In: *Combust Flame.* 203 (2019), pp. 279–300. ISSN: 0010-2180. DOI: https://doi.org/10.1016/j.combustflame.2019.02.013.

[171] Georg Baumgartner, Lorenz R Boeck, and Thomas Sattelmayer. “Experimental investigation of the transition mechanism from stable flame to flashback in a generic premixed combustion system with high-speed micro-particle image velocimetry and Micro-PLIF combined with chemiluminescence imaging”. In: *J. Eng. Gas* 138.2 (2016).

[172] Georg Baumgartner and Thomas Sattelmayer. “Experimental investigation on the effect of boundary layer fluid injection on the flashback propensity of premixed hydrogen-air flames”. In: *Turbo Expo: Power for Land, Sea, and Air*. Vol. 55102. American Society of Mechanical Engineers. 2013, V01AT04A011.

[173] 3af. *Home - Towards Sustainable Aviation Summit 2022 — 3af-tsas.com.* https://www.3af-tsas.com/home. [Accessed 04-Oct-2022]. 2022.

Appendices

A
TSAS2022 Paper

The main findings of this thesis report are summarized in the paper below. The paper was submitted for the Towards Sustainable Aviation Summit (TSAS2022) held October. 18-20, 2022, in Toulouse, France. The summit is organized by 3AF - Association Aéronautique et Astronautique de France, the French reference association for scientific and technological expertise in civil and military aerospace. The objective of the summit is to contribute to reach carbon neatrality by 2050 for the aviation ecosystem [173]. At the time of submission of this report (Oct. 18, 2022), the paper has not yet been peer reviewed.

LES ANALYSIS OF H2 ADDITION EFFECTS ON A CH4 SWIRL STABILIZED COMBUSTOR WITH AXIAL AIR INJECTION

Lennard Doodeman[1], **Gioele Ferrante**[1], **Ivan Langella**[1],
Arvind Gangoli Rao[1], **Georg Eitelberg**[1]
l.w.doodeman@student.tudelft.nl, g.ferrante@tudelft.nl, i.langella@tudelft.nl,
a.gangolirao@tudelft.nl, g.eitelberg@tudelft.nl

Abstract
Large eddy simulation (LES) paradigm is employed to analyse the internal flow field of a lean premixed swirl-stabilized combustor with axial air injection at both non-reacting and reacting conditions for a methane and a methane-hydrogen fuel mixture. The Thickened Flame combustion model (TFM) with the kinetic mechanism GRI 3.0 and the detailed chemical kinetics solver SAGE available in ConvergeCFD is employed to simulate the flow. An adaptive mesh strategy is used to maximise the mesh resolution in the flame and boundary layer regions. The numerical results are first validated against in-house experimental velocity measurements obtained via particle image velocimetry (PIV), and then leveraged to provide further insights on the flow behaviour. Significant reductions in CO_2, CO and NO_x emissions are observed when changing the fuel to the CH_4/H_2 mixture. From a POD analysis is observed that a Precessing Vortex Core (PVC) is present in both the reacting and non reacting conditions. Flashback is not observed during the simulated time.

Introduction
Hydrogen represents an attractive alternative fuel to tackle the problem of carbon-based emissions reduction in aeronautics. According to various studies, e.g.: [1], hydrogen combustion is among the most promising approaches for powering long-distance flight due to its high energy density, minimal carbon emissions and the possibility of producing it from water electrolysis through renewable energy. Nevertheless, its high flame temperature might cause substantial nitric oxides (NO_X) formation. This can be effectively decreased by using premixed lean-burn technology, taking advantage of hydrogen's wide flammability range to stabilize the flame under very lean conditions [2]. However, the risk of flashback due to the high flame speed and the possibility of instabilities caused by hydrogen's high diffusivity, pose design difficulties [3].

The present work aims to contribute to the development of a lean premixed hydrogen combustor for aeronautical applications with minimal NOx and carbon emissions. The laboratory-scale swirl stabilised combustor at TU Delft is numerically simulated to investigate turbulent swirling flow features, temperature field, flame stabilization and emissions. The combustor is composed of an axial swirler issuing into a mixing tube, where the fuel is injected and mixes with air before entering the combustion chamber. To prevent flashback, the stream-wise momentum component is increased by means of axial air injection [4], with the intended effect of achieving control on the stream-wise position of the flame stabilization point. In-house PIV velocity measurements of both reacting and non-reacting flow with a CH_4/air mixture are available for different power setting and operating equivalence ratio of the combustor. The numerical model is preliminary validated against this dataset and successively used to investigate the effects of hydrogen addition to the fuel mixture on the temperature and velocity field and on flame stabilization characteristics. Large Eddy Simulation (LES) is used for the numerical analysis of the combustor. In the LES approach, the reacting Navier-Stokes equations are filtered so that the large turbulent scales are resolved, while the effects of the smaller unresolved, sub-grid scale (SGS) motions, are modelled [5]. The capability of LES of accurately predicting unsteady reacting flow physical features with an affordable computational cost makes it a suitable tool to analyse the complex swirled and recirculating turbulent flow field inside the combustor. Many

[1]Faculty of Aerospace Engineering, Delft University of Technology, 2629 HS Delft, The Netherlands

combustion models have been proposed in the literature to mimic the interaction between turbulence, diffusion and reactions at the subgrid scale, and the reader can find a review in [6]. In the present study the combustor operates in a turbulent partially premixed regime. Therefore, an accurate prediction of the turbulent mixing processes between fuel and oxydizer is crucial, in order to identify the formation of inhomogeneous mixture spots in the mixing tube. The unclosed turbulence-diffusion-reaction interaction is modelled using the Thickened Flame Model (TFM), which predicts mixing in under resolved flame fronts by including numerical diffusion which artificially thickens the flame [7]. The TFM model is used together with detailed chemistry to properly account for the turbulence-flame interaction in presence of differential duffusion effects that can arise due to the presence of hydrogen in the fuel stream. In addition, an adaptive mesh refinement strategy based on the flame location and velocity gradient between cells is used to maximise the mesh resolution in the flame and boundary layer regions.

The objective of this work is to shed light on the effects of hydrogen addition on the operational characteristics of lean-burn swirled combustion devices. Numerical simulations of the TUDelft combustor operating with CH_4 under reacting and non-reacting conditions are carried out first. The results are compared to the experimental measurements to validate the numerical model and provide additional insights on the combustor internal turbulent flow field, temperature field and emissions. The analysis is then extended to another operating set point with the same power setting and air stream mass flow rate, but with a fuel mixture composed by 60% H_2 and 40% CH_4 in volume. A comparison between the two fuel conditions is carried out to assess the effects of hydrogen addition in terms of effectiveness of fuel/oxydiser mixing, flame anchoring and temperature field in relation to emissions level. Moreover, the effects on the turbulent swirling flow features are analysed, with focus on the description of the Precessing Vortex Core (PVC) through modal analysis of the predicted velocity fields.

Test Case

The laboratory-scale combustor designed at the TU Delft [8] illustrated in Fig. 1, is simulated in the present study. The design comprises an axial swirler with a geometric swirl number of 1.1, defined as in [9]. A mixing tube with a radius $R = 12$ mm and a length of 60 mm is present downstream of the swirler to ensure fuel/air mixing before issuing into the cylindrical combustion chamber. The total air mass flow rate is split into a part injected axially into the mixing tube and a part entering the swirler through four radial ports. The methane/hydrogen fuel is injected in the mixing tube through four radial ports with a diameter of 5.5 mm. The ratio between the combustion chamber and mixing tube diameter, often defined as confinement ratio, is equal to 6. The expansion of the cross section combined with the flow swirl causes a characteristic flow pattern with the formation of an outer recirculation zone (ORZ) and a central recirculation zone (CRZ) over which the flame stabilises, as illustrated in Fig. 1. Fuel and air are at a temperature of 288 K before entering the swirler. The combustion chamber is operated at atmospheric pressure.

The reacting flow fields resulting from the methane and methane/hydrogen blends are compared at the same power output and air mass flow rates. The power output of the combustor, calculated based on the fuel mass flow rate, fuel lower heating value (LHV) and density [10], and is set to 11 kW. The amount of axial air injection is defined as percentage of the total air massflow rate and is set to 5%. The value of the total mass flow rate is $\dot{m}_a = 5.061$ g/s. A summary of the operating conditions is given in Table 1.

The in-house experimental data consists of the velocity field on the combustor mid-plane for both non-reacting and reacting conditions (100% methane fuel only), which is determined using Particle Image Velocimetry (PIV). The measuring window ranges till 200 mm downstream of the combustor inlet [8].

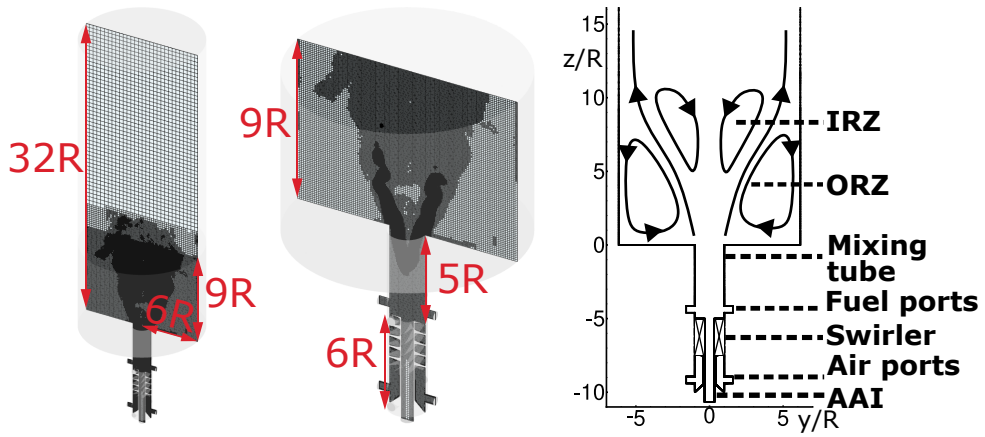

Figure 1: Sketch of combustor and mesh used for the LES. R is the radius of the mixing tube.

LES details

The Favre-filtered Navier Stokes equations including conservation of mass, momentum and energy are solved in the LES framework. A set of Favre-filtered transport equations is solved for each chemical species involved in the combustion process within the thickened flame model approach, to be described in the next paragraph. The sub-grid scale (SGS) stresses τ_{ij} in the filtered momentum equations are closed using the one-equation, dynamic structure model, as [11]:

$$\tau_{ij} = L_{ij}\left(\frac{2k_{\text{sgs}}}{L_{ii}}\right), \tag{1}$$

where L_{ij} and L_{ii} are the Leonard stress tensor and its trace respectively, and k_{sgs} is the sub-grid kinetic energy, which is modelled using a transport equation as in [11]. The filtered diffusion terms in all scalar equations are modelled using a gradient hypothesis, and a subgrid Schmidt number (Prandtl number in the case of the enthalpy equation) of 0.7. The turbulence-combustion interaction modelling at the subgrid level is discussed next.

Combustion model

The thickened flame model is employed in the present study for the closure of the filtered reaction rates in the species equations. In this approach the flame front is thickened with respect to its actual size while retaining the same laminar flame speed is retained. This is achieved by multiplying the thermal and molecular diffusivity by a factor F, and by dividing the reaction rate by the same factor [7]. In this project, F is determined such that, in conjucntion with the adaptive mesh refinement strategy, five or more cells are ensured across the flame front [12]. Subsequently, the thickened flame front can be resolved and stiffness of the problem caused by the broad range of time scales and strong gradients is eliminated [7]. To identify the reaction zone, a flame sensor is used to ensure that the thickening factor only affects the flame region [13]. The flame sensor S is determined according to the method in [14]. To ensure that the flame propagating speed is unaffected by the flame thickening, the diffusivity and reaction rate are multiplied with an efficiency function to correct the flame wrinkling [7]. The reaction rates for all the species including NO and NO_2 are computed using the multi-step kinetic mechanism

Table 1: Operating conditions of the investigated combustor.

Property	**Value**	**Units**	**Property**	**Value**	**Units**
Power	11	kW	Inflow temperature	288	K
Air mass flow rate	252.08	nlpm	Outflow pressure	101325	Pa
AAI%	5	%	Swirl number	1.1	-

GRI 3.0 [15] incorporated in the detailed chemical kinetic solver SAGE [16]. The rate of progress involves both a forward and a reverse rate coefficient, respectively determined using the Arrhenius form and an equilibrium coefficient.

Numerical details

The LES equations are resolved using the Pressure-Implicit with Splitting of Operators (PISO) algorithm for the pressure-velocity coupling [17] available in the commercial software ConvergeCFD [12]. A minimum of 2 and a maximum of 9 iterations are used to solve the velocity and pressure fields through predictor-corrector strategy, with a convergence criterion based on density.

An external loop is used to solve for the energy, species and other passives transport equations. A variable time step is used to guarantee a CFL number smaller than 0.5 everywhere in the domain. The temporal terms are discretised using an implicit Euler scheme, while second order central schemes are used for all the convective terms except for the subgrid kinetic energy transport equation, where an upwind scheme is used. No blended scheme or limiters are used.

Boundary conditions are assigned as follows. Flat velocity profile is specified at the inlets is specified according to the mass flow rates from the experimental data, while a zero-gradient condition is given at the outlet. At the walls the boundary layer is not entirely resolved within the computational grid, therefore wall functions are used along with the non-slip condition. Both the Werner and Wengle model [18] and the Law of the Wall model [19] were tested in preliminary simulations for sensitivity purposes, showing similar results. The former is computationally more efficient and is therefore used in this work. Temperature is assigned at the inlet using data from the experiments, and adiabatic condition is assumed at the walls. All scalars are zero at the inlet except for oxygen, nitrogen and fuel, which are specified according to their respective mass-flow rates. A zero-gradient condition is used for all scalars at the outlet and on wall, except for the subgrid kinetic energy, which is zero at the walls.

The mesh has been setup using the adaptive mesh refinement approach available in ConvergeCFD. A baseline mesh with a characteristic cell size of 5 mm in all directions is used for initialisation purposes. Subsequently, the mesh is refined based on sub-grid scale (SGS) velocity, wall distance values and the TFM thickening factor [20]. The total number of cells is limited to 6M cells with a max cell size in the flame front of 0.3 mm and of 1.25 mm in the region of interest (up to a downstream location of $9R$ in the combustion chamber). At the wall, the height of the first cell is limited to a maximum $y^+ = 15$, ensuring that it entirely contains the viscous sublayer. A typical mesh at a generic time step is shown in Fig. 1, it can be seen how the mesh gets refined near the wall, and in the regions where the flame front is expected. Pope's criterion [21] was used to evaluate the mesh quality in preliminary simulations. In the majority of the domain, the ratio between the modelled turbulent kinetic energy (k_{SGS}), and the total turbulent kinetic energy (resolved + SGS) was smaller than 0.2 [21], as displayed in Fig.3.

Each simulation is run for five flow-through times, defined as the time required for the flow to develop through the domain until a steady average mass flow rate at an axial location of z = 0.11 m (9R) is reached. Two flow-through times are used to guarantee the syeady state and three to collect the statistics. All simulations were run on the TU Delft HPC12 internal cluster using between 128-480 cores in parallel. This resulted in about $1.9 \cdot 10^5$ CPU hours per simulation on a wall-clock using 2.3 GHz AMD processors.

POD Analysis

The complex turbulent swirled dynamics in the combustor might hinder the presence of a precessing vortex core (PVC). Therefore a proper orthogonal decomposition (POD) method is used in this work to analyse the LES dataset with the method of the snapshots developed in [22]. In this method the flow is decomposed into a set of deterministic functions capturing portions of

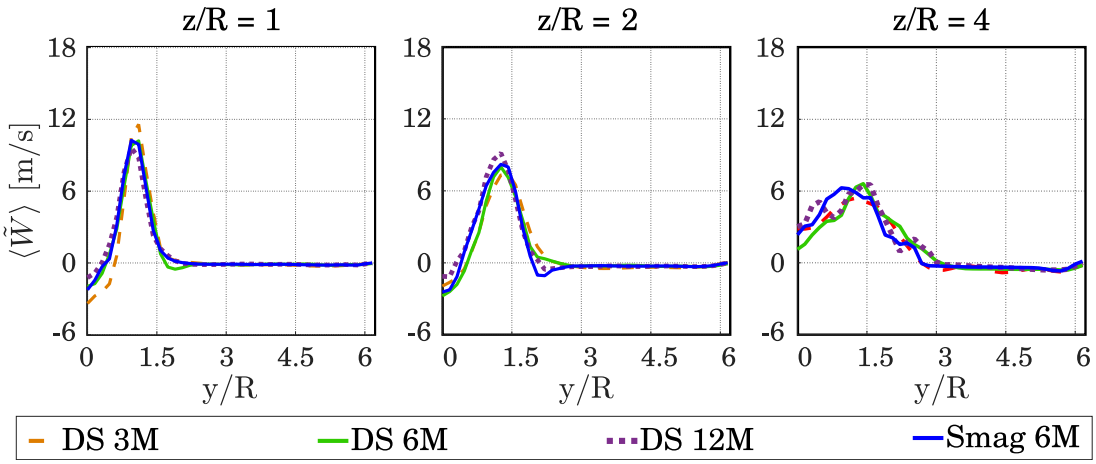

Figure 2: Radial profiles of mean axial velocity at different streamwise locations obtained from non-reacting methane/air LES, for different mesh size and two turbulence models: Dynamic Structure model (DS) and Smagorinsky model (Smag).

the total kinetic energy (TKE) of the flowfield. A correlation matrix ($\mathbf{C_s}$) is computed as

$$\mathbf{C_s} = \frac{1}{m-1}\mathbf{V}\mathbf{V}^T \tag{2}$$

where $\mathbf{V}$ is the velocity matrix in Y-direction and m is the total number of considered LES time steps [23]. The degree of correlation between the velocity fluctuations in Y-direction at various locations can subsequently be assessed by determining the eigenvalues of the correlation matrix. Therefore, it is possible to relate these eigenvalues (A_S) to the coherent structures found in a flow. By ordering the eigenvalues on size, the temporal modes are sorted based on their contribution to the TKE [23]. To compute the spatial coefficients ($\mathbf{\Phi_s}$) of the modes the transported Y-velocity matrix is projected onto the temporal modes.

Results and discussion

Sensitivity analysis

A preliminary analysis using different turbulence models and mesh sizes is carried out first for the non-reacting case with CH_4/air mixture. Time averaged axial velocity $\langle \tilde{W} \rangle$ profiles are computed along the radial direction in the combustion chamber at different stream-wise locations z, with $z = 0$ corresponding to the outlet of the mixing tube; and compared with the experimental measurements in [8]. The simulation is repeated using three different meshes composed of 3, 6 and 12 million elements respectively, combined with two turbulence models: the dynamic structure model (DS) and the Smagorinsky model (Smag). Fig. 2 shows that the predicted velocity field does not exhibit a strong dependence on the chosen mesh. Thus, the 6M elements mesh is retained for the following analysis, after verifying that Pope's criterion is satisfied everywhere in the domain, as shown in Fig. 3. Results obtained with different turbulence models are also very similar, with a relative error of the peak velocity that remains below 3% at any axial point. Since the dynamic structure model is suited for anisotropic turbulence effects [24] that may arise in the reacting case, the latter is used from now on to carry out the LES.

Validation

Averaged axial velocity profiles are compared with data from the experiments in Fig. 4 for both non-reacting and reacting (100% CH_4 fuel only) cases. For the non-reacting case, the value of the velocity peak appears to be predicted fairly well; nevertheless, its predicted position in the radial direction is underestimated due to a difference in the spreading rate of the jet. This is in turn associated to a larger inner recirculation zone observed in the experiments (not shown),

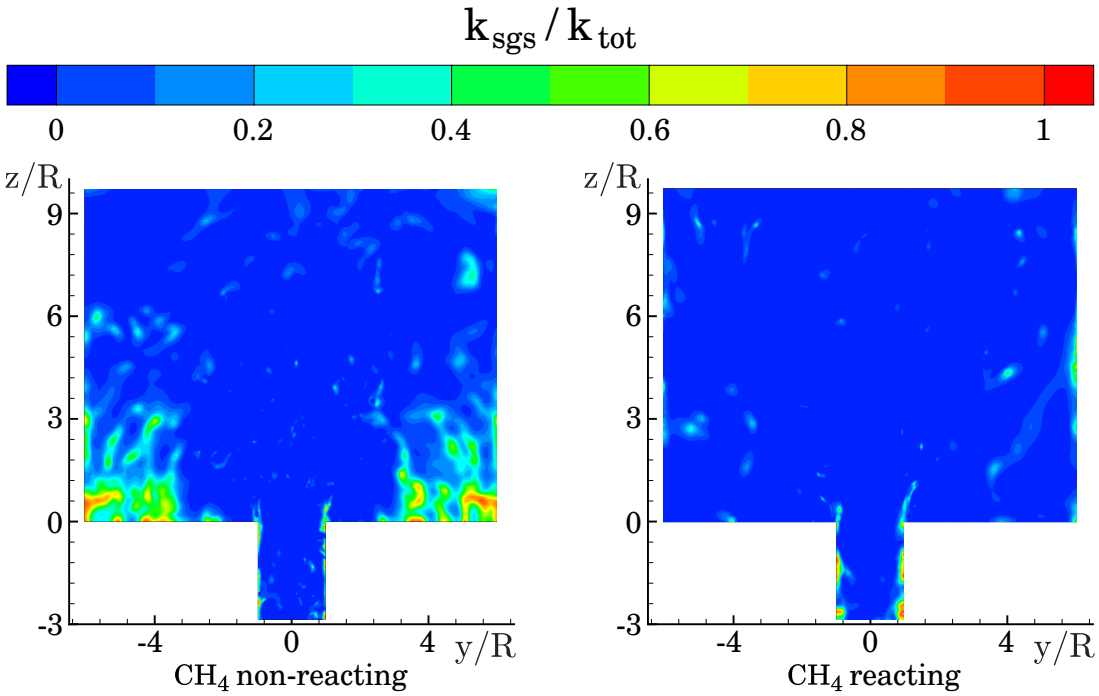

Figure 3: Pope's criterion: cell values of the subgrid to total turbulent kinetic energy.

extending up to $z/R = 4$ with stronger backflow velocity. Additional sensitivity analyses on wall models, CFL number and turbulence intensity were performed (not shown) to understand the causes of this difference, but with little effect on the computed data. On the other hand, a strong sensitivity of the spreading jet on the outlet boundary conditions was observed in the experimental campaign for the non-reacting case. Since such a sensitivity was not observed for the reacting simulations, no further investigation is conducted here, also considering the relatively good match between LES and measurements in the reacting case, to be shown next.

Comparisons between LES and experimental radial profiles of mean axial velocity for the reacting case shown in Fig. 4, indicate that the LES is able to predict the velocity peak and its radial location with good accuracy up to a downstream coordinate $z = 2R$. Further downstream, the LES still predicts the correct location of the peaks and overall velocity behaviour, indicating a correct spreading rate as compared to experiments; however, it over-predicts the peak velocity value at $z = 4R$. This over-prediction of the peak velocity could be caused by insufficient mixing in the SGS model [25], or to the presence of an exhaust confinement in the experimental case [26].

Due to the above analysis, we conclude that the LES predicts with relatively good accuracy the reacting flow field. Since velocity gradients increase due to the heat release from the flame, these comparisons further suggest that the correct flame shape and position is captured, although quantitative investigations on temperature and species could not be performed as this data was not available from experiments. Because of the above reasons, the LES setup with TFM and detailed chemistry is further used for the investigations in the next section.

Hydrogen blend simulations

The effects of H_2 addition in the fuel stream are investigated in this section for both non-reacting and reacting cases. The hydrogen blend mixture is composed by 40% methane and 60% hydrogen in volume, the and the fuel mass flow rate is adjusted to match the same power output as for the methane-only case, keeping the total air mass flow rate constant. This mixture results in an overall equivalence ratio of 0.7, which is lower than the 0.75 for the methane-only case. It is thus not obvious a-priori what the effect of hydrogen addition on thermochemical characteristics and emissions can be, and this is investigated next.

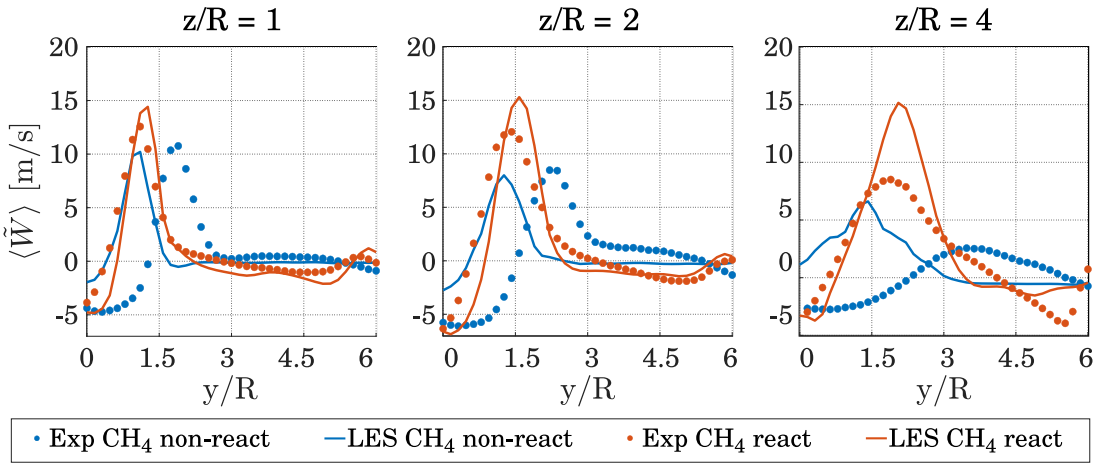

Figure 4: Comparison mean axial velocity profiles obtained from LES (solid lines) and experiments (symbols) at various axial locations, for the CH_4 non-reacting and reacting cases.

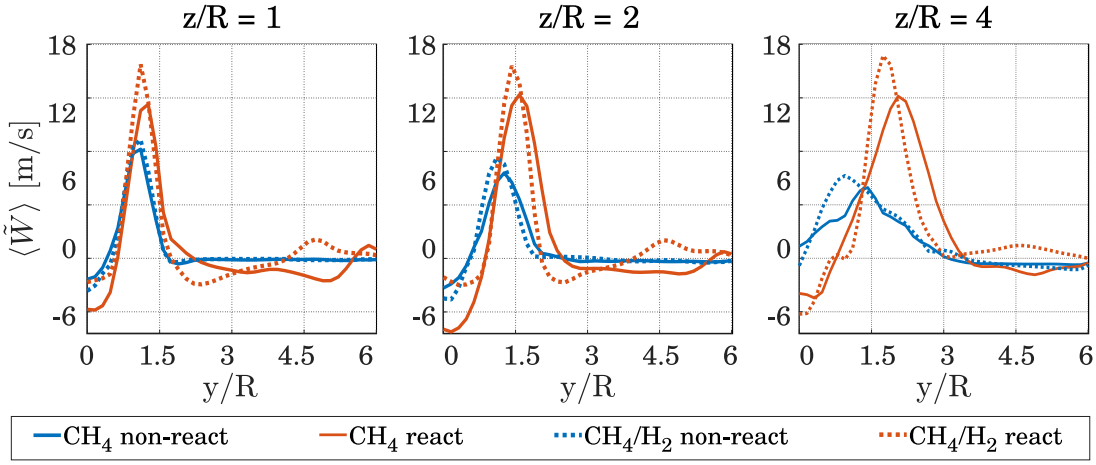

Figure 5: Mean axial velocity profiles from the LES for different fuel mixtures (reacting and non-reacting) are compared at different streamwise locations.

Mean axial velocity radial profiles at different streamwise locations are shown in Fig. 5. Overall, the addition of hydrogen shows little effect on the velocity field in the non-reacting case. Although this was somewhat expected (the fuel/air mixture is lean), this assessment was worth it given the high diffusivity and low density of hydrogen, and its possible effect on mixing properties. In the reacting case, the addition of H_2 results in a higher maximum velocity of the jet and in a shift of the peak closer to the axis ($y/R = 0$). This is due in turn to the fact that the flame anchoring point moves upstream, which can be observed in Fig 7. The mixing tube bounds the momentum increase in the radial direction, favouring the stream-wise momentum increase. In addition, the jet exhibits a wider opening jet angle in the reacting cases, which is the result of the combined effects of heat release and lower density of the products, which lead to an increased velocity in the normal direction of the M-shaped flame.

To better understand the flow in the combustion chamber, the evolution of swirl number SW, equivalence ratio ϕ, and its standard deviation σ through the mixing tube are further investigated in Fig. 6. The swirl number is computed in the LES following the methodology of [9]. At the outlet of the swirler vanes it corresponds to the geometric swirl number of 1.1. This effective swirl number increases in the mixing tube first ($z/R < -4.5$) to then re-decrease quickly at $z/R \approx -4.5$. This decrease is due the reduction of irregularities in the radial and tangential directions as the flow evolves in the mixing tube, consistently to previous studies [27], and is aided by the fuel injection between $z/R = -4.1$ and $z/R = -4.6$. In turn, this affects

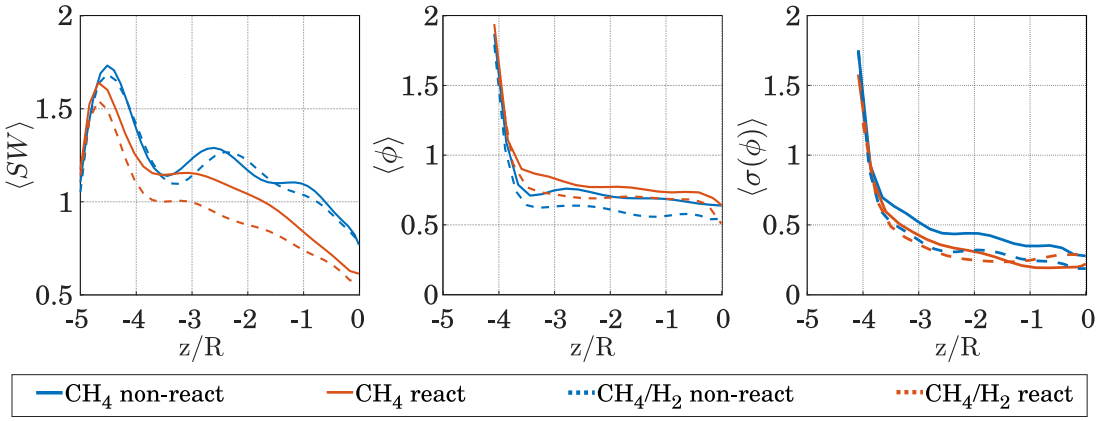

Figure 6: Axial profiles of mean swirl number (left), equivalence ratio (centre) and its standard deviation (right) in the mixing tube ahead of the combustor chamber. The region near the combustor entrance, indicated by the dashed rectangle is zoomed out in the top-right of the figures for clarity.

the viscous dissipation and radial flow divergence, thus the axial flux of angular momentum [28]. The resulting effective swirl number at the mixing tube outlet remains 0.77 for both the non-reacting cases, and it decreases to 0.61 and 0.57 respectively for the CH_4-only and the CH_4/H_2 blend reacting cases. This decrease as compared to the non-reacting case is caused by the increased axial velocity at the combustion chamber inlet [28], and this increase is of larger amount in the hydrogen blend case as was observed for Fig. 4. Also, the higher effective swirl number of the reacting CH_4 mixture results in a wider opening of the jet as compared to the CH_4/H_2 reacting case, which is visible in Fig 5 [29]. These differences could affect the mixedness of the flow downstream, causing variation of equivalence ratio in the flame region with a direct effect on the emissions [4, 30]. The level of unmixedness in the flame region is therefore quantified using the method of Li et al. [31]. By looking at the mean behaviour of equivalence ratio Φ and its standard deviation σ in Fig 6, one can notice that, while the mixture becomes substantially leaner when hydrogen is added to the mixture, no significant change occurs in terms of σ. This suggests that any change in emissions, to be analysed later, has to be attributed to variation in mean equivalence ratio, rather than turbulent mixing.

Further insights on the flow field behaviour between methane-only and hydrogen blend cases can be provided by looking at the mean temperature field in Fig 7. The main observation is that temperature is in general significantly higher in the CH_4 case, which is somewhat counter-intuitive. Nevertheless, lower temperatures in the hydrogen blend case are mainly driven by the overall leaner mixture in this case, which is consistent with flamelet calculations using CHEM1D [32]. This result has profound implications in the design of new-generation combusting devices employing swirl-stabilised flame systems. The above result, in fact, suggests that when operating at the same power, the use of hydrogen can be beneficial in terms of NOx emissions due to the lower temperatures, at least for the confiuguration investigated. A more quantitative assessment on emsissions is thus presented next.

Emissions insights

In Table 2, the mean mass fraction of CO_2, CO and NOx at the combustor outlet plane are given. The addition of hydrogen to the fuel results in a decrease in CO_2 and CO, as one would expect with a fuel mixture containing fewer carbon atoms. Moreover, consistently with the decrease of temperature peaks, an overall decrease of 88% of NO is observed. This is an important observation, since the use of hydrogen in lean burn combustors has to be assessed from the same power setting as done in this work.

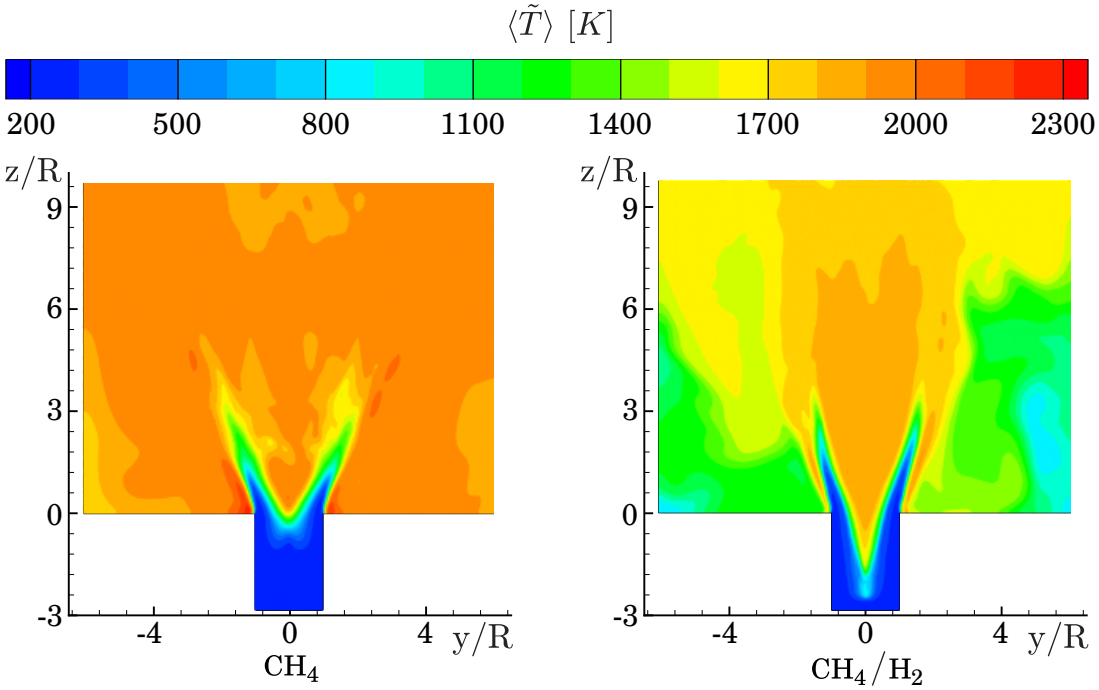

Figure 7: Midplane contours of mean temperature from LES for the methane-only and hydrogen enriched cases.

POD analysis

Pressure oscillations and heat release fluctuations caused by PVC may act as drivers for thermoacoustic instabilities [33]. The precession of a PVC is indicated by a spatial phase shift of 90° between two modes [34]. The eigenvalue of the spectrum of the POD modes represents the contribution of the PVC to the total fluctuating kinetic energy. According to this criterion, it can be determined that a PVC is present for both fuel mixtures for both the non-reactive and reactive CH_4 and CH4/H_2 cases, see Fig 8 and Fig 9. This is also in agreement with the study of Dellenback et al. considering the effective swirl number at the combustor inlet [35]. When hydrogen is added to the fuel the modes associated to the PVC tends to interest a more downstream location in the combustor. This behaviour may be associated to a later development of the helicoidal structure of the PVC, which may be caused by the increased flame wrinkling [36] and/or the lower effective swirl number at the combustor outlet [35].

From the TKE and frequency analysis of the POD analysis can be concluded that the TKE and the frequency are in the same order of magnitude for the non-reacting cases. Consistency in the simulation can be inferred from these macro features, which remain essentially the same. Furthermore, it is observed that the TKE increases for the reacting cases. This may indicate the presence of flame generated turbulence [37].

As final note, no flashback was observed during the simulation time when hydrogen was added to the mixture. On the other hand, from the temperature profiles in Fig 7 it can be seen that, for the CH_4/H_2 mixture, the flame has significantly moved upstream and within the

Table 2: Computed mass fraction of species at the outlet plane.

Species	CH4	CH4/H2	Difference %
CO2	0.113	0.080	-27%
CO	6.75E-04	3.05E-05	-95%
NO	4.91E-05	6.03E-06	-88%

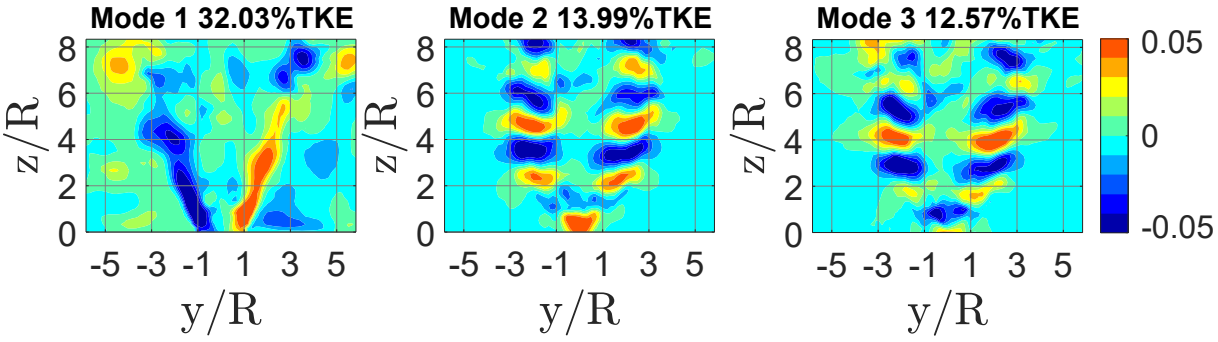

Figure 8: Midplane contours of the first three POD modes for the CH4 reacting case.

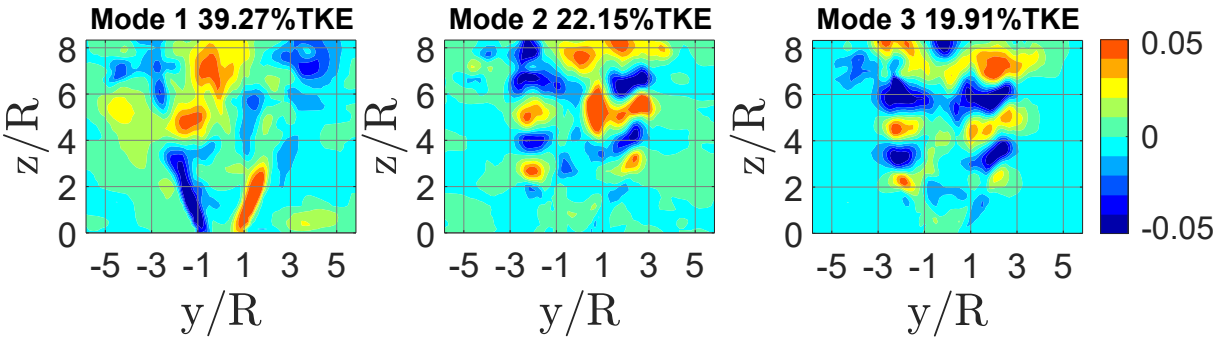

Figure 9: Midplane contours of the first three POD modes for the CH4/H2 reacting case.

mixing tube. This flame anchoring position is not ideal from practical perspectives as flashback could still be triggered at later times. Further research is needed to understand how to stabilise hydrogen-enriched flames for safe operations.

Conclusions

Methane and a hydrogen enriched methane mixtures have been studied in this work using LES paradigms and detailed chemistry with a thickened flame approach. Results have been first validated for the methane-only case against experimental measurements of axial velocity, showing that the LES is able to predict the reacting flow field with good accuracy. The effects of hydrogen addition on a methane swirl-stabilized combustor with axial air injection on the emissions and flame stability have then been analysed. Results indicate that, when keeping the power constant, CO emissions decrease by 95% and NO decreases of 69%. These significant reduction is observed to be driven by the fact that the flame burns locally at leaner equivalence ratios, implying lower local temperatures. The POD analysis of the fluctuating velocity field in the radial direction indicates the presence of a precessing vortex core (PVC) in the flow. The addition of hydrogen appears to cause a reduction in the PVC frequency. Finally, although no flashback was observed in the LES as consequence of the addition of hydrogen, the flame was observed to stabilise significantly upstream as compared to the methane-only case. This suggests that further research is needed in order to develop safe-operating burners fuelled with hydrogen or

Table 3: Turbulent kinetic energy (TKE) (in plane x: 0 m, y: -0.07 – 0.07 m, z: 0–0.1 m) and frequency of PVC from POD for the CH_4 and CH_4/H_2 LES cases. NR is non reacting and R is reacting

	CH_4 non-react	CH_4/H_2 non-react	CH_4 react	CH_4/H_2 react
Frequency [Hz]	253	257	377	217
TKE [m$\hat{2}$/s&2]	8726	9512	24051	23200

hydrogen blends.

Acknowledgement
This project has been financed by the Dutch Ministry of Economic Affairs and Climate under the TKIscheme (Grant number TKI HTSM/18.0170) along with SAFRAN Aircraft Engines and Airbus.

References

[1] van der Sman, E., Peerlings, B., Kos, J., Lieshout, R., Boonekamp, T., "Destination 2050: A route to net zero european aviation", (2021).

[2] Cho, E.S., Chung, S.H., "Improvement of flame stability and NOx reduction in hydrogen-added ultra lean premixed combustion", *J. Mech. Sci. Technol.* 23(3): 650–658 (2009).

[3] Beita, J., Talibi, M., Sadasivuni, S., Balachandran, R., "Thermoacoustic Instability Considerations for High Hydrogen Combustion in Lean Premixed Gas Turbine Combustors: A Review", *Hydrogen* 2(1): 33–57 (2021).

[4] Reichel, T.G., "Flashback prevention in lean-premixed hydrogen combustion", (2017).

[5] Pope, S.B., "Ten questions concerning the large-eddy simulation of turbulent flows", *New J. Phys.* 6(1): 35 (2004).

[6] Veynante, D., Vervisch, L., "Turbulent combustion modeling", *Prog. Energy Combust. Sci.* 28(3): 193–266 (2002).

[7] Colin, O., Ducros, F., Veynante, D., Poinsot, T., "A thickened flame model for large eddy simulations of turbulent premixed combustion", *Physics of Fluids* 12(7): 1843–1863 (2000).

[8] van den Bergh A., "Design and test of a swirl-stabilized methane combustor with axial air injection.", (2022).

[9] Beer J., C.N., "M. and chigier, na, combustion aerodynamics", *Appl. Sci. Publ. LTD* (1972).

[10] Warnatz, J., Maas, U., Dibble, R.W., Warnatz, J., *Combustion*, Springer (2006).

[11] Pomraning, E., "Development of large eddy simulation turbulence models", (2000).

[12] Tylczak, E., "Models on top of models: Thickened flames in converge - converge cfd software", (2020).

[13] Durand, L., Polifke, W., "Implementation of the thickened flame model for large eddy simulation of turbulent premixed combustion in a commercial solver", in *Turbo Expo: Power for Land, Sea, and Air*, vol. 47918, pp. 869–878 (2007).

[14] Mehl, C., Liu, S., Colin, O., "A strategy to couple thickened flame model and adaptive mesh refinement for the les of turbulent premixed combustion", *Flow, Turbulence and Combustion* 107(4): 1003–1034 (2021).

[15] Frenklach, M., Wang, H., Goldenberg, M., Smith, G., Golden, D., "Gri-mech: An optimized detailed chemical reaction mechanism for methane combustion. topical report, september 1992-august 1995", Tech. rep., SRI International, Menlo Park, CA (United States) (1995).

[16] Senecal, P., Pomraning, E., Richards, K., Briggs, T., Choi, C., McDavid, R., Patterson, M., "Multi-dimensional modeling of direct-injection diesel spray liquid length and flame lift-off length using cfd and parallel detailed chemistry", *SAE transactions* pp. 1331–1351 (2003).

[17] Issa, R.I., "Solution of the implicitly discretised fluid flow equations by operator-splitting", *J. Comput. Phys.* 62(1): 40–65 (1986).

[18] Werner, H., Wengle, H., "Large-eddy simulation of turbulent flow over and around a cube in a plate channel", in *Turbulent shear flows 8*, pp. 155–168, Springer (1993).

[19] Bradshaw, P., Huang, G.P., "The law of the wall in turbulent flow", *Proceedings of the*

Royal Society of London. Series A: Mathematical and Physical Sciences 451(1941): 165–188 (1995).

[20] Legier, J.P., Poinsot, T., Veynante, D., "Dynamically thickened flame les model for premixed and non-premixed turbulent combustion", in *CTR Summer Program*, vol. 12, pp. 157–168 (2000).

[21] Pope, S.B., Pope, S.B., *Turbulent flows*, Cambridge university press (2000).

[22] Sirovich, L., "Turbulence and the dynamics of coherent structures. i. coherent structures", *Q. Appl. Math.* 45(3): 561–571 (1987).

[23] Weiss, J., "A tutorial on the proper orthogonal decomposition", in *AIAA aviation 2019 forum*, p. 3333 (2019).

[24] Rutland, C.J., "Dynamic structure les models", Tech. rep., Wisconsin Univ-Madison Engine Research Center (2004).

[25] Stiehl, B., Worbington, T., Woodard, A., Ahmed, K.A., Velez, C., Martin, S.M., "Numerical simulation of an axial-staged combustor at high pressure", in *AIAA Scitech 2020 Forum*, p. 0630 (2020).

[26] Abdulsada, M., Syred, N., Bowen, P., O'Doherty, T., Griffiths, A., Marsh, R., Crayford, A., "Effect of exhaust confinement and fuel type upon the blowoff limits and fuel switching ability of swirl combustors", *Appl. Therm. Eng.* 48: 426–435 (2012).

[27] Choi, J., Jung, E., Kang, S., Do, H., "Modeling swirl decay rate of turbulent flows in annular swirl injectors", *AIAA J.* 56(12): 4910–4926 (2018).

[28] Shahsavari, M., Farshchi, M., Arabnejad, M.H., "Large eddy simulations of unconfined non-reacting and reacting turbulent low swirl jets", *Flow Turbul Combust* 98(3): 817–840 (2017).

[29] Huang, Y., Yang, V., "Effect of swirl on combustion dynamics in a lean-premixed swirl-stabilized combustor", *Proc Combust Inst.* 30(2): 1775–1782 (2005).

[30] Dederichs, S., Zarzalis, N., Habisreuther, P., Beck, C., Prade, B., Krebs, W., "Assessment of a gas turbine nox reduction potential based on a spatiotemporal unmixedness parameter", *J Eng Gas* 135(11) (2013).

[31] Li, H., ElKady, A., Evulet, A., "Effect of exhaust gas recirculation on nox formation in premixed combustion system", in *47th AIAA Aerospace Sciences Meeting Including The New Horizons Forum and Aerospace Exposition*, p. 226 (2009).

[32] Somers, B., "The simulation of flat flames with detailed and reduced chemical models", (1994).

[33] Zhang, B., Shahsavari, M., Rao, Z., Yang, S., Wang, B., "Thermoacoustic instability drivers and mode transitions in a lean premixed methane-air combustor at various swirl intensities", *Proc. Combust. Inst.* 38(4): 6115–6124 (2021).

[34] Oberleithner, K., Stöhr, M., Im, S.H., Arndt, C.M., Steinberg, A.M., "Formation and flame-induced suppression of the precessing vortex core in a swirl combustor: experiments and linear stability analysis", *Combust. Flame* 162(8): 3100–3114 (2015).

[35] Dellenback, P., Metzger, D., Neitzel, G., "Measurements in turbulent swirling flow through an abrupt axisymmetric expansion", *AIAA J.* 26(6): 669–681 (1988).

[36] Zhang, W., Wang, J., Lin, W., Mao, R., Xia, H., Zhang, M., Huang, Z., "Effect of differential diffusion on turbulent lean premixed hydrogen enriched flames through structure analysis", *Int. J. Hydrogen Energy* 45(18): 10920–10931 (2020).

[37] Langella, I., "Large eddy simulation of premixed combustion using flamelets", (2016).

B
Tecplot Macro

```
$!MACROFUNCTION NAME = "Test Macro Function"
$!EXTRACTFROMPOLYLINE
EXTRACTLINEPOINTSONLY = YES
EXTRACTTHROUGHVOLUME = YES
RAWDATA
4
# x y z coordinates
0 0 0.01
0 0 0.02
0 0 0.03
0 0 0.04
$!ENDMACROFUNCTION
```